University of Calabria

Ph.D. in Molecular Bio-pathology
(Disciplinary Fields: BIO18-Genetics, ING/INF04-Automation)

Mathematical modelling, system analysis and experimental study of the caspases activation in the extrinsic pathway of apoptosis

Candidate
Vincenza Pace

Supervisor
Prof. Luciano Carotenuto

Dott. Dina Bellizzi

Co-ordinator
Prof. Giovanna De Benedictis

2007

Table of contents

Sommario

L'apoptosi è un processo fisiologico caratteristico degli organismi pluricellulari. Esso gioca un ruolo essenziale sia durante lo sviluppo embrionale che nella vita dell'individuo adulto, poiché regola l'organogenesi ed il mantenimento dell'omeostasi organismale. Disfunzioni in tale processo spesso accompagnano gravi patologie fra cui alcune forme di cancro, malattie neurodegenerative ed immunodeficienze, inoltre è stata rilevata anche una correlazione con l'invecchiamento. L'importanza del fenomeno è evidenziata dal fatto che le molecole che intervengono nell'apoptosi si sono conservate nel corso dell'evoluzione. Il processo consiste di varie fasi ognuna delle quali è finemente regolata: segnali intrinseci ed estrinseci attivano una rete di interazioni molecolari nella cellula, in cui essenziale è il ruolo delle caspasi, una famiglia di proteine con funzione proteolitica. Esse, una volta attivate, innescano a loro volta specifiche reazioni a cascata che alla fine portano alla frammentazione del DNA e quindi alla morte della cellula. Ciascun evento del processo è caratterizzato da una serie di reazioni in cui sono coinvolte numerose proteine; ciascuna reazione è regolata da vari fattori che agiscono sia sulle forme attive che sulle forme inattive delle caspasi. Il quadro che emerge dall'analisi del processo è complesso. Proprio tale complessità, e l'esigenza di disporre di uno strumento interpretativo e predittivo, ha stimolato la costruzione di modelli matematici che descrivono le principali reazioni del pathway.

Nel presente lavoro abbiamo analizzato uno di questi modelli. Tale modello prende in considerazione le interazioni dinamiche tra procaspasi-8 e procaspasi-3, caspasi-8 attiva e caspasi-3 attiva e le proteine inibitrici BAR e IAP. Abbiamo dimostrato che il modello può avere uno, due o tre stati di equilibrio: in ogni caso uno degli stati di equilibrio è caratterizzato dall'assenza delle caspasi attive. Poiché tale stato è rappresentativo di una cellula in condizioni normali, esso è stato denotato col termine "equilibrio *life"*. Si sono analizzate, ottenendo risultati originali, le proprietà di stabilità e si è studiata la dipendenza dai parametri delle possibili configurazioni di stati di equilibrio. Successivamente, risolvendo numericamente le equazioni differenziali che caratterizzano il modello, è stata simulata l'evoluzione temporale delle proteine coinvolte nel pathway, in presenza di vari tipi di stimolo e per un ampio spettro di valori dei parametri. In particolare, abbiamo valutato l'effetto di uno stimolo transitorio e di uno stimolo continuo sull'evoluzione temporale dell'attivazione delle caspasi-3 ed -8. Entrambi i tipi di stimolo utilizzati forniscono una risposta qualitativamente simile, che

è caratterizzata da tre fasi distinte. Nella prima fase, la caspasi-8 attiva viene riconosciuta e legata dalla proteina BAR per formare un complesso; in questa fase la concentrazione di caspasi-3 attiva e del complesso che quest'ultima forma con la proteina inibitrice IAP è trascurabile. La seconda fase è caratterizzata da bassi valori della concentrazione delle caspasi -3 ed -8 attive e da un leggero incremento dei due complessi. Nella terza fase, a seconda dell'intensità dello stimolo, si può osservare o la transizione nello stato apoptotico (caratterizzato da alti livelli della concentrazione delle caspasi attive) o il ritorno del sistema allo stato di equilibrio *life*. La durata di questa fase è inversamente proporzionale all'intensità della perturbazione iniziale (o al livello dello stimolo persistente). Le simulazioni effettuate predicono una risposta in cui si verifica un rapido incremento della concentrazione delle caspasi attive, ritardato rispetto all'istante iniziale di applicazione dello stimolo. Infine è stato simulato un esperimento in cui si è modificato il tasso di produzione della proteina BAR. Un elevato valore di tale tasso, che corrisponde a un'elevata concentrazione di BAR all'equilibrio, causa un aumento del livello di stimolo necessario a indurre la transizione nello stato di equilibrio apoptotico, mentre un basso valore del tasso di produzione di BAR causa una risposta molto più rapida poiché il tempo di transizione diminuisce.

Nella seconda parte del presente lavoro abbiamo verificato sperimentalmente la validità biologica del modello mediante un'estesa analisi sperimentale su colture cellulari. Sono state scelte cellule di osteosarcoma 143B.TK$^-$. Preliminarmente si è cercato di rendere il più omogeneo possibile il sistema sperimentale sincronizzando le cellule nella fase G0/G1. Si è quindi definita sperimentalmente la concentrazione di Apo2L/TRAIL necessaria per ottenere livelli apprezzabili di apoptosi nelle colture. L'evoluzione nel tempo del fenomeno è stata seguita mediante varie tecniche. In particolare abbiamo evidenziato l'avvio del processo seguendo l'esposizione di fosfatidilserina sulla membrana delle cellule stimolate e abbiamo misurato, al variare della durata dello stimolo tra 15 minuti e 6 ore, i corrispondenti livelli di attivazione delle caspasi -3 ed -8 nelle stesse cellule. Inoltre abbiamo verificato l'avvenuta apoptosi mediante test di frammentazione del DNA e quindi l'avvenuta morte delle cellule mediante misure di mortalità cellulare. I picchi di attivazione delle caspasi sono successivi all'aumento dell'esposizione della fosfatidilserina sulla membrana cellulare. Inoltre, una frammentazione del DNA più marcata insieme ad un aumento della mortalità cellulare si osservano dopo il raggiungimento dei picchi delle due caspasi.

Nell'ultima fase del lavoro, per valutare l'effetto di BAR sul pathway apoptotico, è stato messo a punto un protocollo sperimentale che permettesse di evidenziare l'effetto dello stimolo apoptotico su cellule in cui fosse silenziato il gene *BAR*. Confrontando i livelli di espressione del gene *BAR* tra cellule silenziate e cellule non silenziate, trattate per differenti intervalli di tempo con Apo2L/TRAIL, si è osservato che l'espressione di *BAR* è direttamente modulata dall'Apo2L/TRAIL. L'attivazione della caspasi-3 è molto più rapida nelle cellule silenziate rispetto alle cellule non silenziate. Questo fenomeno potrebbe dipendere dal fatto che i livelli di espressione di *BAR*, e quindi della proteina BAR, nelle cellule silenziate sono bassi già all'inizio del trattamento. Inoltre, sia il test della frammentazione del DNA che le misure di mortalità cellulare hanno evidenziato una mortalità maggiore nelle cellule silenziate rispetto a quelle non silenziate, con riferimento al tempo di trattamento.

In conclusione, il confronto tra risultati *in silico* e risultati *in vitro* ha evidenziato una significativa concordanza, a livello qualitativo, tra le predizioni fornite dal modello e il comportamento nel tempo delle colture cellulari sottoposte a trattamento. Questo accordo suggerisce che il modello di fatto coglie e sintetizza gli aspetti essenziali del processo di attivazione delle caspasi, e può fornire un utile strumento per ulteriori indagini su aspetti non ancora approfonditi.

Summary

Apoptosis is a common physiological process that occurs in multi-cellular organisms. It plays an essential role both in fetal development and in adult organisms because it is essential for successful organogenesis and structuring of complex multi-cellular tissues. The importance of this phenomenon is further underlined by the presence in the apoptotic machinery of molecules highly conserved during the course of evolution. In recent years an increasing amount of data indicate that apoptosis, its activation or dysregulation have a role in either the etiology or the pathogenesis of several health disorders. Furthermore, a strong correlation has been found between altered apoptosis activity and aging. Apoptosis is modulated by extrinsic and intrinsic signals that activate complex intra-cellular signaling networks in which caspases play a pivotal role. The activation of these proteins starts up a complex network of processes whose outcome is the cell death. The complexity of the apoptotic process pushed researchers to assemble mathematical models that could help to identify the crucial steps of apoptosis.

We analyzed one of these mathematical models that considers the dynamical interactions between procaspases-8 and procaspase-3, active caspase-8 and caspase-3, and the inhibitor proteins BAR and IAP. We demonstrated that the model can have one, two or three equilibrium states: in any case one equilibrium state is characterized by the complete absence of active caspases, and we called this condition *life* equilibrium. This equilibrium is regarded as representative of the normal state of the cell. Furthermore the stability properties of the equilibria were analyzed, and the dependence of the equilibrium pattern on model parameters was investigated. We simulated the time evolution of the protein concentrations by solving the system differential equations for several sets of parameters, thus trying to mimic the quantitative cell response to external stimuli. In particular, we checked the effect of transient and persistent stimuli on the time evolutions of relevant proteins: active caspase-8 and 3. We observed that the time responses are similar in both conditions. In most of the tested models it was observed that the time evolutions of the protein concentrations are characterized by three distinct phases: a first phase in which active caspase-8 is captured by BAR to form the complex caspase-8÷BAR; the amount of caspase-3 and complex caspase-3÷IAP that is produced in this phase is negligible; a second phase, named *decision* phase, that is characterized by very low concentrations of active caspase-3 and -8, slow increase of the complex caspase-3÷IAP, and decrease of IAP concentration; a third phase in which, depending

on the perturbation and the model parameters, we observe either a very fast transition to a state with high concentrations of active caspase-3 and -8, or a return of the system to the *life* equilibrium. The duration of the *decision* phase is almost inversely proportional to the intensity of the initial perturbation (or the level of persistent stress) and may be very long. These simulation results predict that the increase of activity of caspase-3 and of caspase-8 occurs abruptly and is delayed with respect to the application of the stimulus. Finally we simulated experiments in which the production rate of BAR protein was modified. The increase of the level of BAR production causes an almost linear increase of the threshold perturbation needed to observe the transition to the *non-life* equilibrium within the simulation interval. The decrease of the level of BAR production produces much faster responses, because the transition time decreases.

The next step in our work was to check the biological reliability of the mathematical model. First, in order to obtain a homogeneous experimental system, we synchronized osteosarcoma 143B.TK$^-$ cells. Next, we tested the ability of recombinant Apo2L/TRAIL to induce extrinsic apoptosis in synchronized cells. Subsequently, we analyzed by flow-cytometry the time evolution of apoptosis activation by monitoring the exposition of posphatidylserine, the time evolutions of activation of both caspase-8 and caspase-3, DNA fragmentation and cell mortality. As regards the time course of events in the pathway, as resulting from the measurements taken on cell subpopulations after treatments with Apo2L/TRAIL for different time intervals (in the range 15 minutes-6 hours) we observed an increase of posphatidylserine exposition, followed by a subsequent increase of caspase-3 activity and caspase-8 activity. The fact that posphatidylserine exposition forestalls full activation of caspases is in line with the known mechanisms of the whole apoptotic process. Furthermore, we observed that a substantial DNA fragmentation is reached in correspondence of an increase of cell mortality after the full activation of caspases. In the last step of the experimental work we silenced the *BAR* gene in synchronized cells. We evaluated the effect of *BAR* silencing on Apo2L/TRAIL induced apoptosis by monitoring time evolution of caspase-3 activation, DNA fragmentation and cell mortality. We note that the expression of *BAR* is probably modulated by Apo2L/TRAIL. In fact, in non-silenced cells, the expression levels of *BAR* decrease with the time increase of treatment with Apo2L/TRAIL. As expected, the expression levels of *BAR* in silenced cells is low for all the duration of treatment. In silenced cells the peak of activation of caspase-3 is reached more rapidly

than in non-silenced cells. The DNA fragmentation test showed that in silenced cells the DNA at the end of treatment is completely degradated in small fragments; in non-silenced cells the typical pattern of fragmentation is observed. Also the mortality test showed that the fraction of dead cells is higher in silenced cells than in non-silenced cells from the beginning of the treatment.

The comparison of *in silico* results (simulations) with the results obtained in the experimental system has shown a consistent qualitative agreement between the time evolutions predicted by the model and the behavior of cell cultures. This proves that the model actually captures the essential features of the biological process, and could be a reliable tool in further studies of caspases activation.

List of abbreviation

PS Phosphatidyl Serine

Bp Bases Pairs

DNA Deoxyribonucleic Acid

PARP Poly (ADP-Ribose) Polymerase

CARD Caspase Recruitment Domain

DED Death Effector Domains,

DISC Death-Inducing Signalling Complex

TNF-R Tumor Necrosis Factor Receptor

ER Endoplasmic Reticulum

UPR Unfolded Protein Response

ATP Adenosine Triphosphate

OXPHOS Oxidative Phosphorilation

ROS Reactive Oxigen Species

Bcl-2 B-cell lymphoma 2,

cytc cytochrome *c*

APAF-1 Apoptosis Protease Activating Factor

TNF Tumor Necrosis Factor

TRAIL-R1 TNF-Related Apoptosis-Inducing Ligand Receptor 1

DR4 Death Receptor 4

TRAIL-R2 TNF-Related Apoptosis-Inducing Ligand Receptor 2

DR5 Death Receptor 5

DD Death Domain

FADD Fas-Associated Death Domain

DED Death Effector Domain

IAPs Inhibitor Apoptosis Proteins

BIR Baculoviral IAP Repeats

XIAP X-linked Inhibitor of Apoptosis Protein

BIR1 Baculoviral IAP Repeats 1

BIR2 Baculoviral IAP Repeats 2

Smac Second Mithocondrial Activator of Caspases

DcR Decoy Receptors

DcR1 Decoy Receptors 1

DcR2 Decoy Receptors 2

DcR3 Decoy Receptors 3

OPG Osteoprotegerin

c-FLIP FLICE-Like Inhibitory Protein

BAR Bifunctional Apoptosis Regulator

SAM S-Adenosyl Methionine

ODEs Ordinary Differential Equations

C8 procaspase-8

C8* active caspase-8

C3 procaspase-3

C3* active caspase-3.

1. Introduction

Apoptosis is a very important process that occurs in multi-cellular organisms. It plays a pivotal role both in fetal development and in adult organisms because it is essential for successful organogenesis and crafting of complex multi-cellular tissues (Steller, 1995). In adult organisms apoptosis is involved in the maintenance of normal cellular homeostasis and of efficiency of the immune system (Meyn et al., 1996; Williams, 1994). The importance of this phenomenon is further underlined by the presence in the apoptotic machinery of molecules highly conserved along evolution: genetic analyses in model organisms, most notably in the nematode *Caenorhabditis elegans,* have revealed a high level of functional and molecular conservation in the major components of the cell death pathway between invertebrates and mammals (Metzstein et al., 1998; Abrams, 1999). In recent years cumulative data indicate that apoptosis, its activation or dysregulation, has a role in different health disorders, either in the etiology or in the pathogenesis of diseases (Aloya et al., 2006). Enhanced or repressed apoptotic cell death contributes to developmental deficits, autoimmune diseases, cancer and neurological disorders (Meier et al., 2000; Yuan & Yankner, 2000). Furthermore, several data have revealed a strong correlation between altered apoptosis activity and aging (Zhang et al., 2003). Due to the role of apoptosis in crucial physiological and pathological processes, and taking advantage of an increasing knowledge of the molecular mechanisms occurring in this process, the number of studies focusing on apoptosis is exponentially increased in the past few years. The increasing is also due to the availability of a number of new tools of molecular biology to study this process. In a recent paper (Melino et al., 2001) it has been reported that apoptosis has been among the fastest growing research fields in the last decade. Indeed, the number of publications has increased from fewer than 100 in 1990 to over 13000 in 2000 (Melino et al., 2001). However, apoptosis is a typical field in which, despite the ever-increasing availability of data and the advancing of techniques to explore the “mechanics” of cellular components, the relationship between overall behavior of the cells regarded as biological systems, and the underlying molecular mechanism remains puzzling and elusive.

1.2 Physiology of Apoptosis

The term apoptosis was introduced by Lockshin in 1964 (Lockshin, 1964), who proposed that cell death during development is not of accidental nature but follows a sequence of controlled steps leading to locally and temporally defined self-destruction. Apoptosis was originally described by Kerr and co-workers in 1972 (Kerr et al., 1972) who observed by electron microscopy the peculiar changes in cells undergoing organized cell death. They noticed a characteristic, identical sequence of events in many different types of cells leading to controlled cellular self-destruction.

Today the term apoptosis defines a genetically encoded cell death program which is morphologically and biochemically distinct from necrosis or accidental cell death. The first characteristic morphological signs of apoptosis appear at the cell membrane level. The plasma membrane loses its typical asymmetry because phospholipids translocate from the inner leaflet to the outer leaflet of the plasma membrane to allow phagocytic recognition. The presence of the phospholipid phosphatidylserine (PS) on the outer leaflet of the plasma membrane acts as a signal for removal (Schlegel & Williamson 2001). Other signs of apoptosis are the increase of membrane permeability and alterations of cytosolic and mitochondrial proteins which produce nuclear changes. The ultimate morphological changes of apoptosis are nuclear condensation and an orderly form of intranucleosomal DNA fragmentation (180–200 bp) (Wyllie et al., 1980). At last the contents of dead cells are packaged into apoptotic bodies, which are recognized by neighbouring cells or macrophages and cleared by phagocytosis. From an experimental point of view two morphological events are particularly important during this phenomenon: changes in membrane asymmetry (exposition of PS) and DNA fragmentation. These last two events allow to follow the apoptotic process from the beginning to the end. Behind the morphological changes there are multiple biochemical complex processes. Each process in turn is a sub-network of other processes converging at various levels. The most relevant are: caspase activation that causes the induction of a proteolitic cascade (protein cleavage); activation of endonucleases (DNA breakdown); activation of DNA repairing systems (PARP); expression of surface markers on the apoptotic cells (phagocytic recognition). However, because the biochemical hallmarks of apoptosis are initiation of caspase cascade and DNA fragmentation, both these phenomena require to be demonstrated to establish if a cell has undergone apoptosis.

We shall see that the activation of caspases is a crucial point of induction, transduction and amplification of intracellular apoptotic signals.

1.2.1 Caspases

Caspases are central initiators and executioners of apoptosis. The term caspases is derived from cysteine-dependent aspartate-specific proteases. The catalytic activity of caspases depends on a critical cysteine-residue within a highly conserved pentapeptide motif in the active site. The caspases specifically cleave their substrates after aspartate residues. In humans caspases are ubiquitously expressed. They are cytosolic proteases produced as inactive proenzimes awaiting an appropriate activation stimulus (Denault & Salvesen, 2002). To date, 14 caspases have been found in mammals. Categorization of caspases based on their structure, function and substrate results in different classification systems. The structural classification divides the caspases into two main categories: long prodomain and short prodomain. caspase-1, caspase-2, caspase-4, caspase-5, caspase-8, caspase-9, caspase-10, caspase-11 and caspase-12 belong to the first category. caspases-3, caspase-6, caspase-7 and caspase-14 fall into the latter category. These caspases have short prodomains and are activated upon proteolytic cleavage by other caspases (Ho & Hawkins, 2005). Classification of caspases based on their function divides the caspases into two main categories: inflammatory and apoptotic caspases. caspase-1, caspase-4, caspase-5, caspase-11 and caspase-12 are inflammatory caspases (Martinon & Tschopp, 2007). The remaining caspases are involved in apoptotic signalling pathways and are subdivided into two subgroups: initiator and effector. caspase-2, caspase-9, caspase-8 and caspase-10 belong to the first group of caspases; caspase-3, caspase-6, caspase-7 and caspase-14 belong to the second group. These two methods of classification yield a close structure–function relationship among the caspases: all initiator apoptotic caspases contain a large prodomain whereas all effector caspases have a short prodomain.

In the apoptotic caspases three distinct regulatory domains have been characterized consisting of a caspase recruitment domain (CARD), a death effector domains DEDs, and a short N-peptide. Caspases-8 and 10 contain death effector domains (DED) in the N-terminal region of the pro-enzyme. The DED confers homomeric binding ability to adaptor proteins in the death-inducing signalling complex (DISC) at the cytoplasmic region of TNF-R family members known as Death Receptors. Caspase-2 and -9 contain the caspase recruitment domain (CARD). The CARD appears to confer homomeric

binding capabilities between caspases and their specific regulatory complexes. Both the CARD and the DED are members of the Death Domain Family of adapters and are responsible for the recruitment of the initiator caspases to their respective activation complexes. The effector caspases (caspases -3, -6 and -7) contain truncated N-terminal sequences without known regulatory function.

The mechanisms which activate initiator caspases are not completely clear. However, once initiator caspases are activated, they are capable of activating downstream caspases (effector caspases) either directly, through proteolysis, or indirectly via a secondary messenger mechanism. The mechanism by which this occurs is a specific intrachain cleavage that increases the catalytic activity of effector caspases by several order of magnitude. Upon activation by an initiator caspase, effector caspases are immediate "executioners" of the apoptotic program, cleaving certain cellular substrates to cause demolition of the cell.

There are essentially three ways through which the caspases can be activated. One way involves the endoplasmatic reticulum; another way involves the mitochondrion; the third way involves some membrane receptors.

1.2.2 Endoplasmic Reticulum-mediated procaspase-activation pathway

The endoplasmic reticulum (ER) is a cellular compartment in which the appropriate folding of new proteins occurs. Some conditions such as excess of proteins that must be folded, starvation of nutrients, anoxia, ischemia and virus infections can interfere with proper maturation of cellular proteins (Ma & Hendershot 2004, Feldman et al. 2005, Wu & Kaufman 2006). In these cases, the folding capacity of the organelle is perturbed, and the entire cell needs to adapt to the new condition. To cope with and adapt to ER stress, an intracellular ER-to-nucleus signal transduction pathway evolved (Cox et al., 1993; Mori et al., 1993; Cox et al., 1996; Mori et al., 1996). This pathway, termed unfolded protein response (UPR), increases the amount of ER membrane and its components, including chaperones and protein-modifying enzymes needed to fold proteins. The UPR also decreases translation and loading of proteins into the ER and enhances the targeting of unfolded proteins in the ER for degradation. If an acute UPR persists for a prolonged time, the cell commits apoptosis. The mechanisms by which UPR induces apoptosis are still not well understood. However, a combination of signals from UPR at last causes the Ca^{2+} release from ER. The Ca^{2+} release causes the

activation of Calpain and caspase-12 and then leads to apoptosis (Scorrano et al., 2003; Zong et al., 2003).

1.2.3 Mitochondrion-mediated procaspase-activation pathway

Mitochondria is an essential organelle whose primary function is the synthesis of ATP, the energy required for the biological activities of the cell. Mitochondrial energy is generated by oxidative phosphorylation (OXPHOS) that creates an electrochemical gradient across mitochondrial membranes. Internal and external stimuli such as DNA damage, reactive oxigen species (ROS) and radiations can interfere with this process and cause the dissipation of mitochondrial transmembrane potential. The lost of the mitochondrial transmembrane potential marks the point-of-no-return of the cell death process (Green et al., 1998; Kroemer et al., 1998; Zamzami et al., 1995; Zamzami et al., 1996; Green & Reed, 1998). The mechanisms by which this occurs is not completely clear. However, when the mitochondrial transmembrane potential is lost cytochrome *c* (*cytc*) and several other pro- and anti-apoptotic factors are released from the mitochondrial intermembrane space into the cytosol. Then, permeability of the mitochondrial membrane is regulated by the ratio between these pro-apoptotic and anti-apoptotic proteins. Bcl-2 protein family members are implicated in this process (Sharpe et al., 2004). In particular, family members Bax, Bak, and Bok are proapoptotic proteins; Bcl-2, Bcl-xL, Bcl-w and Mcl-1 are antiapoptotic proteins (Sharpe et al., 2004). The Bcl-2 family members control the mitochondrial membrane permeability through three distinct mechanisms: formation of protein channels within membranes, interaction with pre-existing mitochondrial membrane pores, and alteration of membrane lipids to produce lipidic pores. Once released, *cytc* forms an "apoptosome" in conjunction with apoptosis protease activating factor (APAF-1) and procaspase-9 (Zou et al., 1999). This complex promotes the activation of procaspase-9, which in turn activates effector caspases (caspases 3, 6, and 7) that collectively orchestrate the execution of apoptosis and then the cell collapse.

1.2.4 Death receptor-mediated procaspase-activation pathway

The death receptor- or extrinsic apoptotic pathway involves membrane receptors and other regulator proteins named adaptor proteins. To date several death receptors and relative adaptor proteins have been characterized. The best known death receptors belong to the tumor necrosis factor (TNF) super family, which trigger apoptosis upon

ligand binding: they are Fas (CD95/Apo1) (Dhein et al., 1995), TNF-R1 (p55) (Tartaglia et al., 1993), TRAMP (WSL-1/Apo3/DR3/LARD) (Kitson et al., 1996; Bodmer et al., 1997), TRAIL-R1 (DR4) (Pan et al., 1997) and TRAIL-R2 (DR5/Apo2/KILLER) (MacFarlane et al., 1997). Fas Ligand (CD95 ligand) binds Fas, TNF and lymphotoxin A bind to TNF-R1 (Ashkenazi & Dixit, 1998), TWEAK (Apo3 ligand) binds to TRAMP (Marsters et al., 1998) and TRAIL (Apo2 ligand) is the ligand for both TRAIL-R1 (Pan et al., 1997) and TRAIL-R2 (Walczak et al., 1998).

The molecular mechanism by which a death receptor induces caspases activation and then apoptosis needs further investigations; however the general aspects of the initial phases of this process are well known. Death receptors contain an intracellular death domain (DD) able to generate protein-protein interactions. Generally the death receptors are expressed as pre-associated homotrimers. When the preassociated receptor is bound by specific ligand, it becomes competent to bind an adaptor protein called Fas-associated death domain (FADD) to form a complex at the death receptor level named DISC. The link between receptor and ligand is due to an homotipic interaction between the DD of FADD and DD of the receptor. In addition to its DD, FADD contains another protein–protein interaction domain at its N-terminus termed death effector domain (DED). This domain is required for the recruitment of caspases containing these DED domains to the DISC. In particular, FADD interacts with procaspase-8, an initiator caspase that contains a DED domain. Once procaspase-8 associates with FADD, the high local concentration of procaspase-8 is believed to lead to its autoproteolytic cleavage and activation (Medema et al., 1997; Salvesen et al., 1999). The mechanism by which procaspase-8 is activated is not completely clear. However the formation of the DISC complex is followed by proteolitic processing and activation of the receptor-associated proteases (Medema et al., 1997). Then, active caspase-8 is released from the DISC, thereby initiating a subsequent cascade of additional processing and activation of downstream effector caspases (caspase-3, 6, 7) that at last cause cell death (Srinivasula et al., 1996; Muzio et al., 1997).

1.2.5 Caspases regulation

Because caspases play a crucial role in apoptotic machinery, their function must be tightly regulated. This is achieved by different mechanisms which exert control at various checkpoints within the cell. Once expressed, caspases can be regulated by several endogenous inhibitors by different mechanisms. Among these, the mechanism

used by inhibitor apoptosis proteins (IAPs) to suppress cell death remains debated. IAP family members are characterized by one or more Baculoviral IAP repeats (BIR) domain. The BIR domain consists of approximately 70 amino-acids residues and was found for the first time in Baculoviruses where it is involved in suppressing the host cell death response to viral infections (Yang & Li, 2000). Many IAPs have a RING finger domain, defined by seven cysteines and one histidine that can coordinate two zinc-finger atoms (Borden KL, 2000). Among IAPs, c-IAP1, c-IAP2 and XIAP have three BIRs in the N-terminal portion of the molecule and one RING finger domain at the C-terminus (Kurakin & Bredesen, 2007). IAP family members suppress apoptosis through direct physical association with the activated caspases. The interaction is mediated by the BIRs domains of IAPs and/or the linker region connecting BIR1 and BIR2 domains (Chai et al., 2001). They can directly bind the activated caspase-3 and caspase-7 and caspase-9 and inhibit their activities by ubiquitination (Roy et al., 1997). It has been suggested that the ubiquitination activity of IAPs is mediated by the RING domain and is regulated by BIR domain interactions. Another way to inhibit apoptosis by IAPs is obtained through the link between IAP-BIR domain and Smac/Diablo (Second Mitochondrial Activator of Caspases) which is released from mitochondrion after an apoptotic stimulus.

Because the caspases cascade represents a central point in the apoptotic pathway, its initiation is tightly regulated by a variety of other factors. Among these, the Decoy receptors (DcR) of the TNF superfamily inhibits death signalling through the sequestration of ligand. DcR include DcR1, DcR2, osteoprotegerin (OPG) and DcR3, DcR1, DcR2 and OPG bind to TRAIL; DcR3 binds Fas ligand (Ashkenazi & Dixit, 1999).

Death receptor signalling is also regulated by cellular FLICE-like inhibitory protein (c-FLIP), an endogenous inhibitor that interacts with FADD to antagonise apopotosis (Irmler et al., 1997).

Communication between intrinsic and extrinsic apoptosis can occur at various stages. For example, activation of procaspase-8 results in stimulation of Bid which leads to release of *cytc* and apoptosome activation. Moreover, the active caspase-3 exerts a positive feedback on procaspase-8 to produce active caspase-8. For these reasons at the intersection of the two ways there are other important apoptosis regulators. Among these a major role is played by the Bifunctional Apoptosis Regulator (BAR) protein. In fact, BAR protein contains a SAM domain that is needed for its interactions with Bcl-2,

Bcl-Xl and for suppression of Bax-induced cell death. In addition, because BAR is anchored in intracellular membranes where Bcl-2 resides, it can bridge procaspase-8 and Bcl-2 into a protein complex. Furthermore, BAR contains a DED domain needed for the interaction with initiator procaspases containing the DED domain (procaspase-8, 10). In any case BAR protein causes apoptosis inhibition. Thus BAR represents a protein at the intersection of two major pathways controlling apoptosis.

1.3 Mathematical modelling of apoptotic pathways

The mechanisms of apoptosis activation, which correspond to specific morphological and biochemical cell changes, differ depending on the cell type, the vital state and the conditions in which the cell grows. The network is made even more intricate by the existence of alternative ways that often converge at various levels and that share molecules implied in others cellular pathways. Furthermore, this complexity is increased by the presence of multiple levels of regulation by which the process can be stopped, increased or switched to another way.

In the past few years mathematical modelling has been proposed as useful tool to study complex biological systems (Di Ventura et al., 2006). Indeed, with the advancement of molecular biology techniques that allow to investigate the dynamical properties of a biological system in a quantitative and rational way, model predictions have become testable, thus providing new insights about various aspects of biological processes.

Because of the complexity of the apoptotic pathway, in recent years mathematical modelling has been used to understand different aspects of this process. In particular, some of these focused on the initial step of apoptosis: the caspase activation in extrinsic or intrinsic way. Fusseneger et al (Fussenegger et al., 2000) proposed a model of thirteen ordinary differential equations (ODEs) that describes the temporal evolution of caspase activation during extrinsic apoptosis pathway. In this paper, authors focused attention on analysis of inhibitory strategies by a simulation approach. A simulative approach was also used by Stucki et al. (Stucki & Simon, 2005) mainly to study the regulation of activation and degradation of caspase-3. Two models of the extrinsic pathway were proposed by Eissing and co-workers. (Eissing et al., 2004). The models consist of six or eight ODEs, respectively: the emphasis is on the property of bistability, considered as a fundamental condition to describe properly the caspase activation pathway. In a successive paper Eissing et al. (Eissing et al., 2005) studied the robustness of bistability with respect to parameter variations. Bistability property was considered

also in Bagci et al (Bagci et al., 2006), who proposed a mathematical model of the mitochondrial apoptotic pathway in which kinetic cooperativity in formation of the apoptosome ensured bistability. Rehm et al (Rehm et al., 2006) proposed a computational model of the extrinsic apoptotic pathway, focusing on the activation process of caspase-3 and its control by inhibitory proteins. In particular, the model showed a major inhibitor role of XIAP on active caspase-3 with respect to smac/DIABLO. These results were demonstrated by *in vitro* experiments carried out in HeLa cells (Rehm et al., 2006).

Bentele et al (Bentele et al., 2004) proposed a complex model of the extrinsic apoptotic pathway. In this paper a comparison between *in silico* and *in vitro* data was carried out and the existence of a threshold in the intensity of the external stimulus was showed.

1.4 Plan of the thesis

The thesis consists of three main parts. In the first part the eight order model proposed by Eissing and co-workers (Eissing et al., 2004) is studied in depth from several points of view:

-Theoretical analysis of the equilibrium states and respective stability properties

-Numerical analysis of the equilibrium and stability patterns on a very large sample of models with randomly generated parameters. The aim is to correlate parameter values with equilibrium patterns

-Numerical simulations of the time evolution of relevant chemical concentrations, (especially caspase-3*) in response either to a transient or to a persistent stimulus. The aim is to reveal the salient features of the responses (f.i. existence and intensity of a peak of caspase-3* concentration, delay between the start of stimulation and the peak) and to correlate them with static properties and parameter values. These topics are discussed in the two annexed papers (Carotenuto et al.; 2007a, b).

In the second part of the thesis an extensive experimental activity is described and the results are reported. The experiments aim at measuring the time evolutions of both caspase-3* and caspase-8* concentrations, of specific morphological indicators (expositions of phospatidylserine and DNA fragmentation) and of cell mortality.

A first set of experiments was carried out on osteosarcoma 143B.TK$^-$ cell populations in controlled conditions with respect to the cell cycle.

Since there is much debate about the regulatory role of inhibitor proteins, a second set of experiments was carried out on synchronized osteosarcoma 143B.TK$^-$ cell populations in which the *BAR* gene was silenced.

In the last part of the thesis the results from the model simulation and from *in vitro* experiments are discussed and compared, emphasizing the original aspects of the work.

2. Model description, analysis and simulation

This section reports the detailed analysis of the mathematical model, proposed by Eissing et al., of the biochemical processes leading to procaspase-3 activation through the extrinsic pathway of apoptosis. Results are reported in the manuscript entitled "Equilibrium, stability and dynamical response of a model of caspases activation in apoptosis", published on Journal of Biological Systems, vol. 15, pp. 261-285, September 2007.

2.1 Biological basis and formulation of the Model

The network of caspase activation pathways during apoptosis was described in the Introduction.

In Figure 2.1 the main reactions that characterize the extrinsic pathway are depicted. For ease of notation let C8=procaspase-8; C8*=caspase-8*=active caspase-8; C3=procaspase-3; C3*=caspase-3*=active caspase-3.

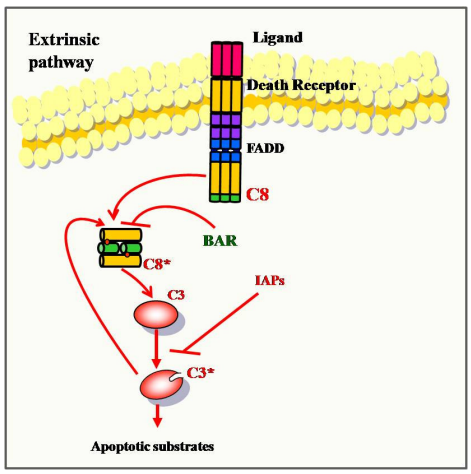

Figure 2.1 Extrinsic pathway of apoptosis.

In particular the Figure 2.1 shows:

- the DISC complex formation, by the recognition between ligand and its receptor;
- procaspase-8 recruitment and its activation by intra-chain cleavage of its pro-domain (Graf et al., 2007; Riedl and Salvesen, 2007), to produce caspase-8*;
- action of caspase-8* on procaspase-3 to produce caspase-3* by direct interaction;

- positive feedback of caspase-3* on procaspase-8 to produce caspase-8* (Soler et al., 2007);
- inhibition of caspase-8* by BAR, through formation of the complex caspase-8*÷BAR (Roth et al., 2003);
- inhibition of caspase-3* by IAP, through formation of the complex caspase-3*÷IAP (Hunter et al., 2007).

Other processes, not explicitly shown in the Figure 2.1, will be kept into account: natural production of procaspase-3, -8, IAP, BAR, and degradation of procaspase-3, -8, IAP, BAR, caspase-3*, caspase-8*, and of the complexes caspase-3*÷IAP and caspase-8*÷BAR.

This current knowledge is translated into mathematical form to create a model able to describe the relevant aspects of the biochemical behaviour of the components of the extrinsic apoptotic pathway.

The model considers the following reactions:

$$\text{Caspase}-8^{*}+\text{Procaspase}-3 \overset{k_1}{\Rightarrow} \text{Caspase}-8^{*}+\text{Caspase}3^{*}$$

$$\text{Procaspase}-8+\text{Caspase-}3^{*} \overset{k_2}{\Rightarrow} \text{Caspase-}8^{*}+\text{Caspase-}3^{*}$$

$$\text{Caspase-}3^{*}+\text{IAP} \underset{k_{-3}}{\overset{k_3}{\Leftrightarrow}} \text{Caspase-}3^{*}\div\text{IAP}$$

$$\text{Caspase-}8^{*}+\text{BAR} \underset{k_{-11}}{\overset{k_{11}}{\Leftrightarrow}} \text{Caspase-}8^{*}\div\text{BAR}$$

$$\text{Cleavage of IAP by Caspase-}3^{*}$$

For each reaction the rates v_i were deduced according to the law of mass action and are here reported:

- caspase-3* production: $v_1=k_1[C8^*]\cdot[C3]$;
- caspase-8* production: $v_2=k_2[C3^*]\cdot[C8]$;
- caspase-3*÷IAP production: $v_3=k_3[C3^*]\cdot[IAP]-k_{\_3}[C3^*\div IAP]$;
- caspase-8*÷BAR production: $v_{11}=k_{11}[C8^*]\cdot[BAR]-k_{\_11}[C8^*\div BAR]$;
- cleavage of IAP by caspase-3*: $v_4=k_4[C3^*]\cdot[IAP]$.

We assume linear rates for degradation of proteins and complexes, and constant rates for productions of procaspase-8, -3, BAR, IAP:

- caspase-8* degradation: $v_5=k_5$[C8*]
- caspase-3* degradation: $v_6=k_6$[C3*]
- caspase-3*÷IAP degradation: $v_7=k_7$[C3*÷IAP]
- IAP production and degradation: $v_8=k_8$[IAP]$-k_{\_8}$
- Procaspase-8 production and degradation: $v_9=k_9$[C8]$-k_{\_9}$
- Procaspase-3 production and degradation: $v_{10}=k_{10}$[C3]$-k_{\_10}$
- BAR production and degradation: $v_{12}=k_{12}$[BAR]$-k_{\_12}$
- caspase-8*÷BAR degradation $v_{13}=k_{13}$[C8*÷BAR]

From the reactions rates a system of eight ODEs was derived and is here reported: the solution of the ODEs gives the time evolution of the concentrations and is expected to simulate the behaviour of chemicals in a cell. Let x_i, i=1,2,..8 denote the concentration of the relevant chemical species above mentioned: x_1=[C8], x_2=[C8*], x_3=[C3], x_4=[C3*], x_5=[IAP], x_6=[C3*÷IAP], x_7=[BAR], x_8=[C8*÷BAR]. The units *molecules per cell (mol/cell)* for the concentrations, *minutes* (*min*) for the time are used.

$$\frac{dx_1}{dt} = -v_2 - v_1 = -k_2 x_1(t) x_4(t) - k_9 x_1(t) + k_{-9} \quad (1)$$

$$\frac{dx_2}{dt} = v_2 - v_5 - v_{11} = k_2 x_1(t) x_4(t) - k_5 x_2(t) - k_{11} x_2(t) x_7(t) + k_{-11} x_8(t) \quad (2)$$

$$\frac{dx_3}{dt} = -v_1 - v_{10} = -k_1 x_2(t) x_3(t) - k_{10} x_3(t) + k_{-10} \quad (3)$$

$$\frac{dx_4}{dt} = v_1 - v_3 - v_6 = k_1 x_2(t) x_3(t) - k_3 x_4(t) x_5(t) + k_{-3} x_6(t) - k_6 x_4(t) \quad (4)$$

$$\frac{dx_5}{dt} = -v_3 - v_4 - v_8 = (-k_4 - k_3) x_4(t) - k_3 x_6(t) - k_8 x_5(t) + k_{-8} \quad (5)$$

$$\frac{dx_6}{dt} = v_3 - v_7 = k_3 x_4(t) x_5(t) - k_{-3} x_6(t) - k_7 x_6(t) \quad (6)$$

$$\frac{dx_7}{dt} = -v_{11} - v_{12} = -k_{11} x_2(t) x_7(t) + k_{-11} x_8(t) - k_{12} x_7(t) + k_{-12} \quad (7)$$

$$\frac{dx_8}{dt} = v_{11} - v_{13} = k_{11} x_2(t) x_7(t) - k_{-11} x_8(t) - k_{13} x_8(t) \quad (8)$$

When necessary, we shall use the compact vector notation $\underline{x}=[x_1,\ldots,x_8]^T$ to denote the "state" of the system.

The model is characterized by nineteen parameters (k_1,...,k_{13}, k_{-3}, k_{-8},..,k_{-13}), whose numerical values shown in Table 2.1 are reproduced from Eissing et al (2004).

Table 2.1 Model parameters. The numerical values in the third column are from *Eissing et al.*

Parameter	Physical dimension [C]: concentration [t]: time	Nominal value [C]: molecules/cell [t]: minutes	Reaction where the parameter appears
k_1	$[C]^{-1}[t]^{-1}$	5.8×10^{-5}	C3+C8*→C3*+C8*
k_2	$[C]^{-1}[t]^{-1}$	1.00×10^{-5}	C8+C3*→C8*+C3*
k_3	$[C]^{-1}[t]^{-1}$	5.00×10^{-4}	C3*+IAP→C3*÷IAP
k_4	$[C]^{-1}[t]^{-1}$	3.00×10^{-4}	cleavage of IAP
k_5	$[t]^{-1}$	5.8×10^{-3}	decay of C8*
k_6	$[t]^{-1}$	5.8×10^{-3}	decay of C3*
k_7	$[t]^{-1}$	1.73×10^{-2}	decay of C3*÷IAP
k_8	$[t]^{-1}$	1.16×10^{-2}	decay of IAP
k_9	$[t]^{-1}$	3.90×10^{-3}	decay of C8
k_{10}	$[t]^{-1}$	3.90×10^{-3}	decay of C3
k_{11}	$[C]^{-1}[t]^{-1}$	5.00×10^{-4}	C8*+BAR→C8*÷BAR
k_{12}	$[t]^{-1}$	1.0×10^{-3}	decay of BAR
k_{13}	$[t]^{-1}$	1.16×10^{-2}	decay of C8*÷BAR
k_{-3}	$[t]^{-1}$	2.10×10^{-1}	C3*÷IAP→C3*÷IAP
k_{-8}	$[C]^{-1}[t]^{-1}$	$4.64 \times 10^{+2}$	production of IAP
k_{-9}	$[C]^{-1}[t]^{-1}$	$5.07 \times 10^{+2}$	production of C8
k_{-10}	$[C]^{-1}[t]^{-1}$	$8.19 \times 10^{+1}$	production of C3
k_{-11}	$[t]^{-1}$	2.10×10^{-1}	C8*÷BAR→C8*+BAR
k_{-12}	$[C]^{-1}[t]^{-1}$	$4.00 \times 10^{+1}$	production of BAR

Such values will be taken as the nominal ones, and the corresponding model will be said nominal.

The effect of a transient external stimulus applied through the cell membrane is modeled by imposing the instantaneous conversion, at time t=0, of a number of procaspase-8 molecules into caspase-8*. In this way the initial state of the model is

affected. The effect of a stress acting continuously on the receptors is modeled by transforming $q(t)>0$ *mol/cell/min* of procaspase-8 into an equal number of caspase-8* molecules on a given time interval: this representation requires to modify the equations 1 and 2 in the model:

$$\frac{dx_1}{dt} = -v_2 - v_1 = -k_2 x_1(t) x_4(t) - k_9 x_1(t) + k_{-9} - q(t)$$
$$\frac{dx_2}{dt} = v_2 - v_5 - v_{11} = k_2 x_1(t) x_4(t) - k_5 x_2(t) - k_{11} x_2(t) x_7(t) + k_{-11} x_8(t) + q(t)$$

2.2 Equilibrium and stability analysis in the presence of a transient stimulus

2.2.1 Equilibrium states: theoretical results

In a "normally living" cell the values of concentrations of caspase-3*, -8* should be negligible, as well as the concentrations of complexes. At the level of our model this condition is represented by the corresponding state variables to be equal to 0. We recall that an equilibrium state of the model is a constant solution of equations 1-8: $\underline{x}(t)=\underline{x}_E$, and is characterized by the condition $d\underline{x}/dt=0$: then its components satisfy the system of algebraic equations:

$$-k_2 x_1 x_4 - k_9 x_1 + k_{-9} = 0 \quad (9)$$
$$k_2 x_1 x_4 - k_5 x_2 - k_{11} x_2 x_7 + k_{-11} x_8 = 0 \quad (10)$$
$$-k_1 x_2 x_3 - k_{10} x_3 + k_{-10} = 0 \quad (11)$$
$$k_1 x_2 x_3 - k_3 x_4 x_5 + k_{-3} x_6 - k_6 x_4 = 0 \quad (12)$$
$$(-k_4 - k_3) x_4 x_5 + k_{-3} x_6 - k_8 x_5 + k_{-8} = 0 \quad (13)$$
$$k_3 x_4 x_5 - k_{-3} x_6 - k_7 x_6 = 0 \quad (14)$$
$$-k_{11} x_2 x_7 + k_{-11} x_8 - k_{12} x_7 + k_{-12} = 0 \quad (15)$$
$$k_{11} x_2 x_7 - k_{-11} x_8 - k_{13} x_8 = 0 \quad (16)$$

From equations 9-16 it is apparent that if the concentration of active form of pro-apoptotic proteins and of complexes are equal to zero: $x_2(t)= x_4(t)= x_6(t)= x_8(t)=0$, and we set, $x_1=k_{-9}/k_9$, $x_3=k_{-10}/k_{10}$, $x_5=k_{-8}/k_8$, $x_7=k_{-12}/k_{12}$, the system displays an equilibrium state:

$$\underline{x}_{EL} = [x_{L1}\ 0\ x_{L3}\ 0\ x_{L5}\ 0\ x_{L7}\ 0]^T = \left[\frac{k_{-9}}{k_9}\ 0\ \frac{k_{-10}}{k_{10}}\ 0\ \frac{k_{-8}}{k_8}\ 0\ \frac{k_{-12}}{k_{12}}\ 0\right]^T$$

This equilibrium will be called the "*life*" equilibrium, because it is characterized by the absence of active caspases both free and in complex form.

It is relevant to investigate the existence of other equilibrium states, possibly characterized by non-zero concentrations of active caspases, which may represent different physiological conditions of the cell. The equilibrium states are the non-negative real solutions of the algebraic equations 9-16. Appropriate definition of dimensionless state variables and manipulations of the equilibrium equations allow us to obtain from the initial system of ODEs a single 5-th degree algebraic equation in the variable x_4. One solution is x_4=0, which corresponds to the *life* equilibrium above mentioned. The other equilibrium states are obtained as the real positive roots of a 4-th degree equation. Due to extremely intricate explicit expressions of the coefficients of this equation the existence of positive roots is difficult to investigate. However it was proved that three cases can occur: either no positive solution, or one, or two positive solutions (Carotenuto et al., 2007b). Therefore ***the model 1-8 may have one, two or three equilibrium states one of which is the life equilibrium state.*** For ease of discussion models with one, two, three equilibrium states will be called type 1, type 2, type 3 models, respectively.

2.2.2 Local stability of equilibrium states: theoretical results

The stability of an equilibrium state refers to the behavior of the system trajectories (solutions of the differential equation) when they start from an initial state belonging to a neighborhood of the equilibrium: all trajectories starting from states sufficiently "close" to a *stable* equilibrium remain "close" to the equilibrium; all trajectories starting from states sufficiently "close" to an *asymptotically stable* equilibrium ultimately converge to the equilibrium; if an equilibrium state is *unstable*, some trajectories, although starting "infinitely close" to the equilibrium, attain a finite distance from the equilibrium in a finite time. In our problem, for example, if the "*life*" equilibrium state is asymptotically stable, then "sufficiently small" perturbations of the initial state produce trajectories which converge to the equilibrium. If the "*life*" equilibrium state is unstable, then there exist extremely small perturbations of the initial state which produce trajectories which get the state "far" from "*life*" equilibrium. It is important to note that even if an equilibrium state is asymptotically stable, "large" perturbations of the initial state may produce trajectories which do not converge to that equilibrium.

Denoting by $\underline{\varphi}(t, x_0)$ the solution of the differential equations $\frac{d\underline{x}}{dt} = \underline{f}(\underline{x})$ which represent the dynamical system, satisfying the initial condition $\underline{x}(0) = \underline{x}_0$, the formal definition of an asymptotically stable equilibrium state is:

an equilibrium state $\underline{x}_E$ is *asymptotically stable* if $\forall \varepsilon > 0 \quad \exists \delta(\varepsilon) > 0$ such that, for any initial state x_0 which satisfies $\|x_0 - x_E\| \leq \delta$, it results

$$\|\varphi(t, x_0) - x_E\| \leq \varepsilon \ , \forall t \geq 0 \quad and \quad \lim_{t \to \infty} \|\varphi(t, x_0) - x_E\| = 0$$

Asymptotic stability or instability of an equilibrium state can be checked by linearization. The procedure requires:

- constructing the Jacobian matrix $J(x) = \left[\frac{\partial f_i}{\partial x_j} \right]_{i=1,...n,\, j=1,..n}$
- evaluating the matrix at $\underline{x}=\underline{x}_E$,
- computing the eigenvalues of $J(x_E)$, i.e. the roots of its characteristic polynomial.
- if all the eigenvalues of $J(x_E)$ have negative real part, then x_E is asymptotically stable; if at least one eigenvalue has positive real part then x_E is unstable.

Therefore, the stability analysis of the "*life*" equilibrium was carried out in terms of eigenvalues of the Jacobian matrix obtained from equations 1-8. A criterion for asymptotic stability of the "*life*" equilibrium (Carotenuto et al., 2007b) has been proved:

$$Let\ S = \frac{(k_{-11}k_5 + k_{13}k_5 + k_{13}k_{11}x_{L7})(k_{-3}k_6 + k_7k_6 + k_7k_3x_{L5})}{x_{L1}x_{L3}(k_{-11} + k_{13})(k_{-3} + k_7)}; \qquad (17)$$

if $k_1k_2 < S$***, then the "life" equilibrium state is asymptotically stable; if*** $k_1k_2 > S$***, then the "life" equilibrium state is unstable because of one real positive eigenvalue of the Jacobian matrix.***

The proof uses the special structure of the Jacobian matrix, the Hurwitz criterion and "root-locus" analysis.

It is important to notice (Carotenuto et al., 2007b) that there exists a connection between stability of the "*life*" equilibrium state and number of equilibrium states: ***if the life equilibrium is unstable, then there exists a unique non-life equilibrium; when the life equilibrium state is asymptotically stable, then either no non-life equilibrium exists, or we have two non-life equilibria.***

Looking at equation (17) we note that:

- k_4 (rate of cleavage of IAP by C3*) does not affect the stability of the *life* equilibrium;
- an increase [decrease] of k_1 (production of C3*), k_2 (production of C8*) destabilizes [stabilizes] the *life* equilibrium;
- an increase [decrease] of k_5 (degradation of C8*), k_6 (degradation of C3*) stabilizes [destabilizes] the *life* equilibrium.

As regards *non-life* equilibrium states their stability as been checked by numerically evaluating the appropriate Jacobian matrix and its eigenvalues.

2.2.3 Equilibrium and stability of the nominal model

Direct computation of the equilibrium states of the nominal model has revealed the existence of three equilibrium states, their values are reported in Table 2.2. On the basis of the values of the state variables we defined this state as *life* equilibrium states (E_L), *non-life* equilibrium state 1 (E_{NL1}) and *non-life* equilibrium state 2 (E_{NL2}). E_{NL1} and E_L states are very close, sharing very low concentrations of C8*, C3*, C8*÷BAR and C3*÷IAP. The other *non-life* equilibrium state (E_{NL2}) is characterized by high concentrations of active caspases and complexes caspase-3*÷IAP, caspase-8*÷BAR. We called this equilibrium state *apoptosis* equilibrium.

Table 2.2 Equilibrium states of the nominal model.

Variables	**E_L (*life*) asymptotically stable**	**E_{NL1} unstable**	**E_{NL2} (*apoptosis*) asymptotically stable**
	(*mol/cell*)	(*mol/cell*)	(*mol/cell*)
[C8]	130000	129870	9132
[C8*]	0	0	74380
[C8*÷BAR]	0	44	3447
[BAR]	40000	39492	21
[C3]	21000	20848	19
[C3*]	0	0	5162
[C3*÷IAP]	0	34	3000
[IAP]	40000	39546	264

The analysis of the stability of these equilibrium states has revealed a bistability pattern: E_L is asymptotically stable, E_{NL1} is unstable, E_{NL2} is asymptotically stable. This pattern suggests that to move from the *life* to the *apoptosis* equilibrium a transient stimulus must be applied which exceeds some threshold. This result is consistent with the normal behaviour of a cell, which is resistant against negligible and accidental stimuli, but irreversibly undergoes apoptosis when the entity of the stimulus is appropriate. In addition, several lines of evidence suggest that some signal transduction pathways governing cell fate decisions display a bistable behaviour (Ferrell & Xiong, 2001; Xiong & Ferrell, 2003).

2.2.4 Numerical experiments

Experiment 1) In this section we analyze the dependence of the equilibrium states and of their stability from the model parameters. For each parameter k_i let us define the interval $I_i(a)=[k_i^{nom}(1-a), k_i^{nom}(1+a)]$, where a is an index of the size of the interval. 50 values of a, logarithmically scaled in the interval [0.01, 0.9], were considered; for each a, a sample consisting of 10000 parameter vectors, with components $k_1,\ldots.k_{13}$, k_{-11}, k_{-3}, randomly generated in the respective intervals $I_i(a)$, was created, and the corresponding equilibrium states and eigenvalues of the associated Jacobian matrix were computed. The parameter k_{-8}, k_{-9}, k_{-10}, k_{-12} of the reactions involving C3, C8, IAP and BAR were computed from k_8, k_9, k_{10}, k_{12} in such a way that the *life* equilibrium state was the same as the *life* equilibrium of the nominal model. This procedure simulates the production of populations of cells characterized by parameters whose average values are the nominal ones; the value of a determines how much the cells are similar to each other. The constraints on k_{-8}, k_{-9}, k_{-10}, k_{-12} impose that all the cells of the population, in normal conditions, have the same concentrations of procaspase-8, procaspase-3, and of inhibitors IAP, BAR.

Figure 2.2a shows the relative frequencies of type 1, type 2, type 3 models in the samples, as a function of the size parameter a.

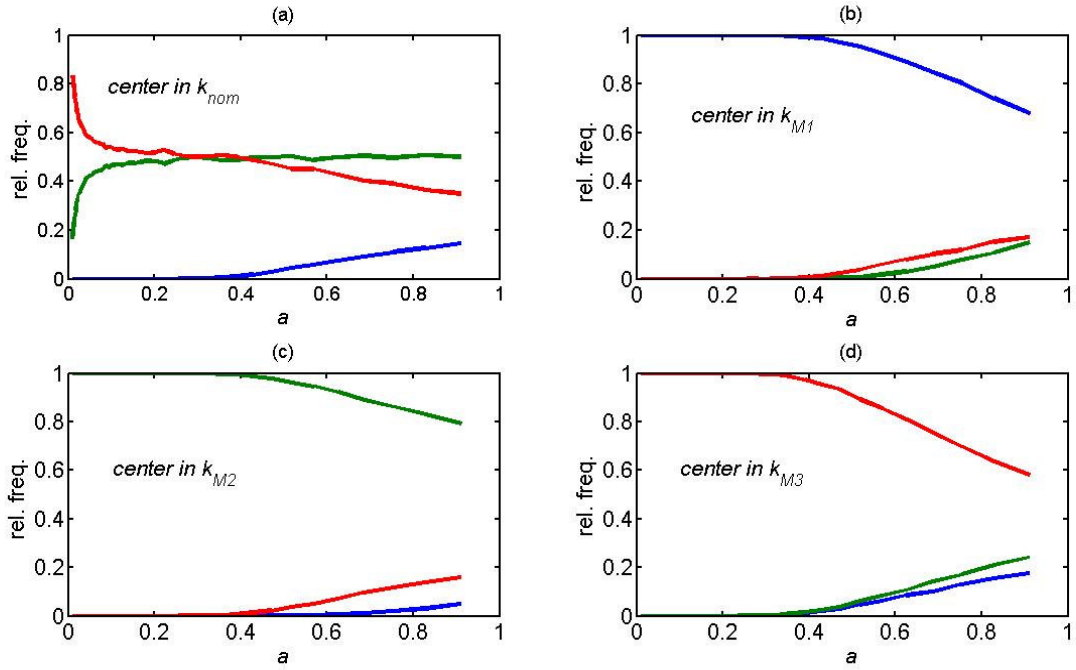

Figure 2.2 Relative frequencies of type 1 (blue), type 2 (green), type 3 (red) models in samples belonging to regions R(a, $\underline{k}^{\mathrm{nom}}$) (panel a), R($a$, $\underline{k}_{M1}$) (panel b), R(a,$\underline{k}_{M2}$) (panel c), R(a,$\underline{k}_{\mathrm{M3}}$) (panel d) as a function of the size parameter a. For each centre $\underline{k}_{\mathrm{c}}$ ($\underline{k}_{\mathrm{c}}$= $\underline{k}^{\mathrm{nom}}$, $\underline{k}_{M1}$, $\underline{k}_{M2}$, $\underline{k}_{M3}$) and for each a (50 logarithmically scaled values in [0.01, 0.9]) a sample consisting of 10000 parameter vectors was generated, with the components k_i, i=1,...,13,-3,-11 pseudorandom numbers uniformly distributed on the intervals I(a,k_{ci})=[k_{ci} (1−a), k_{ci} (1+a)] . The parameters k_{-8}, k_{-9}, k_{-10}, k_{-12} were computed from k_8, k_9, k_{10}, k_{12} in such a way that the life equilibrium state was the same as the life equilibrium of the nominal model.

Clearly, if a is very small, almost all the tested models behave as the nominal one. When a is increased, the fraction of models with two equilibrium states increases, and for even larger a values also models with the sole life equilibrium are present. In a wide range of a values, the fraction of models with two equilibrium states is almost constant at the value 0.5, and the increase of the fraction of models with one equilibrium state corresponds to a decrease of the fraction of models with three equilibrium states. This property is explained by the fact that the nominal model is very close to the "surface" of the parameter space which "separates" type 3 from type 2 models: then for a>0.3 (Figure 2.2a) the volume in which models are sampled is split into almost equal parts by the "separation surface". When the volume is increased, the region where the life equilibrium is stable contains more and more models with only one equilibrium.

Experiment 2) In this section we analyze equilibrium and stability patterns in a sample of 100000 models, with parameter vectors randomly generated according to the rules described in *Experiment 1*, setting a=0.9. This sample is denoted by S_{nom}.
Several different patterns have been observed:

- 14678 models with one, asymptotically stable equilibrium (type 1 models, sub-sample S_1);
- 50566 models with two equilibria (type 2 models, sub-sample S_2): the *life* equilibrium (unstable) and one *non-life* equilibrium which is asymptotically stable in most cases (50263 models) and unstable in a few cases (303 models);
- 34756 models with three equilibria (type 3 models, sub-sample S_3): the life equilibrium (asymptotically stable), one "low" *non-life* equilibrium E_{NL1}, one "high" *non-life* equilibrium E_{NL2} (the terms "low" and "high" refer to the values of [C3*] at the respective equilibria: $0<[C3^*]_{NL1}<[C3^*]_{NL2}$). The "low" equilibrium is unstable in all models, the "high" equilibrium is asymptotically stable in most cases (34659 models), but there exist a few models (97) in which it is unstable.

The vectors of the median values of parameters in each sub-sample S_1, S_2, S_3 were calculated and they are reported in the Table 2.3.

Table 2.3 Median values of parameters belonging to sets S_1, S_2, S_3. S_i: subset of S_{nom} comprising the parameter vectors for which the model has *i* equilibrium state(s).

Parameter	**median on S_1** $\underline{k}_{M1}$	**median on S_2** $\underline{k}_{M2}$	**median on S_3** $\underline{k}_{M3}$
k_1	4.92×10^{-5}	6.88×10^{-5}	4.34×10^{-5}
k_2	6.70×10^{-6}	1.19×10^{-5}	8.32×10^{-6}
k_3	6.87×10^{-4}	3.90×10^{-4}	5.52×10^{-4}
k_4	2.37×10^{-4}	3.01×10^{-4}	3.27×10^{-4}
k_5	5.92×10^{-3}	5.78×10^{-3}	5.69×10^{-3}
k_6	5.78×10^{-3}	5.79×10^{-3}	5.80×10^{-3}
k_7	2.31×10^{-2}	1.39×10^{-2}	1.89×10^{-2}
k_8	1.45×10^{-2}	1.16×10^{-2}	1.01×10^{-2}
k_9	3.74×10^{-3}	3.93×10^{-3}	3.94×10^{-3}
k_{10}	2.07×10^{-3}	3.90×10^{-3}	4.62×10^{-3}
k_{11}	5.60×10^{-4}	3.91×10^{-4}	6.10×10^{-4}
k_{12}	1.18×10^{-3}	1.00×10^{-3}	9.10×10^{-4}
k_{13}	1.28×10^{-2}	9.21×10^{-3}	1.40×10^{-2}
k_{-3}	1.08×10^{-1}	2.46×10^{-1}	1.97×10^{-1}
k_{-8}	$5.81 \times 10^{+2}$	$4.62 \times 10^{+2}$	$4.04 \times 10^{+2}$
k_{-9}	$4.87 \times 10^{+2}$	$5.10 \times 10^{+2}$	$5.12 \times 10^{+2}$
k_{-10}	$4.35 \times 10^{+1}$	$8.19 \times 10^{+1}$	$9.71 \times 10^{+1}$
k_{-11}	1.88×10^{-1}	2.48×10^{-1}	1.59×10^{-1}
k_{-12}	$4.72 \times 10^{+1}$	$4.00 \times 10^{+1}$	$3.64 \times 10^{+1}$

Using $\underline{k}_{Mi}$ values as centers, and applying the same procedure as in *experiment 1*, regions of the parameter space containing only type 1, or type 2 or type 3 models were defined and are shown in Figures 2.2 b, c, d. The maximum values of *a* for which only type 1, or type 2 or type 3 models are obtained are 0.27, 0.24, 0.22, respectively. Observing the three parameters vectors ($\underline{k}_{Mi}$ Table 2.2) that characterize the three corresponding type of models, some important considerations emerge. Compared to type 1 and type 3 models, type 2 models are characterized by higher values of k_1, k_2, that affect the feedback loop between C8* and C3*, lower values of k_3, k_{11} (rates of formation of the complexes C3*÷IAP, C8*÷BAR), and higher values of k_{-3}, k_{-11} (rates

of dissociation of the complexes C3*÷IAP, C8*÷BAR). This is consistent with the instability of the *life* equilibrium of type 2 models.

It is important to analyze the values of the concentration of C3* at the asymptotically stable *non-life* equilibrium (denoted as $[C3^*]_{NLA}$) since this value is representative of a pro-apoptotic condition of the cell. Figure 2.3 shows the relative frequency distributions of $\log_{10}([C3^*]_{NLA})$ in type 2 and type 3 models. The median values of the distributions are 6117 *mol/cell* and 7330 *mol/cell*, respectively; note that 28% of the type 3 and 26.6% of the type 2 models have $[C3^*]_{NLA}$<1000 *mol/cell*.

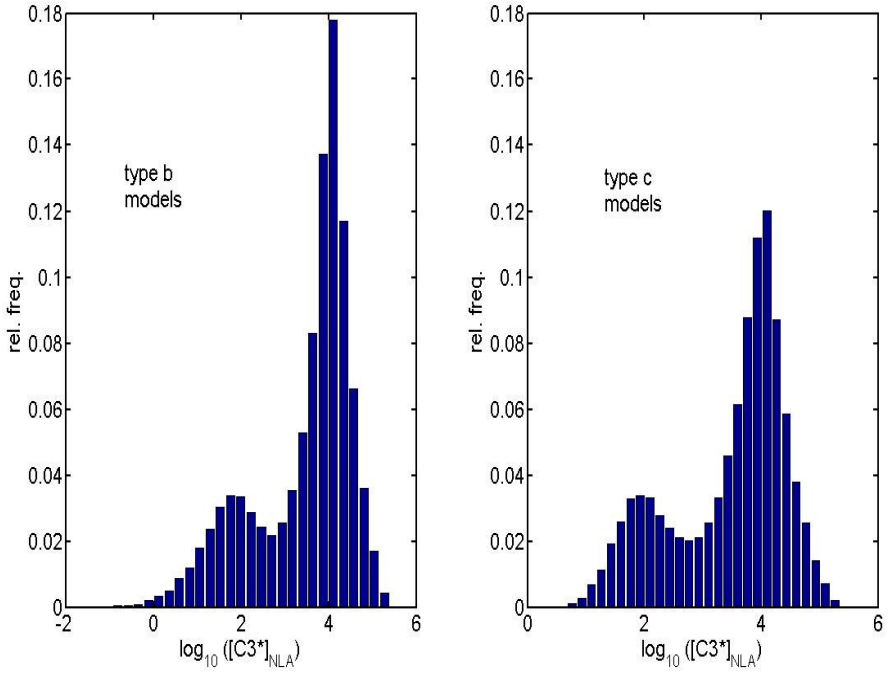

Figure 2.3 Relative frequencies distributions of the concentration of C3* at the asymptotically stable *non-life* equilibrium ($[C3^*]_{NLA}$) in the subsamples of S_{nom} characterized by two or three equilibrium states. S_{nom} is a sample of 100000 models whose parameters are generated as in Figure 2.2, with a=0.9.

2.3 Equilibrium and stability in the presence of a persistent stimulus

As expected, the presence of a persistent stimulus modifies the equilibrium and stability patterns. Equations 9, 10 become:

$$-k_2 x_1 x_4 - k_9 x_1 + k_{-9} - q = 0 \qquad (18)$$

$$k_2 x_1 x_4 - k_5 x_2 - k_{11} x_2 x_7 + k_{-11} x_8 + q = 0 \qquad (19)$$

From equation 18 it is clear that $k_{-9}-q$ must be non-negative, that is $q \le q_{MAX}=k_{-9}$.

The equation that characterizes the equilibrium is more complex, and the only analytical result is that there exists at least one equilibrium state (Carotenuto et al., 2007a). The

obvious difference with the case $q(t)=0$ is that no equilibrium with $x_2(t)= x_4(t)= x_6(t)= x_8(t)=0$ may exist: then it does not make sense to speak of *life* equilibrium. With reference to the nominal model, numerical computation shows that the nominal model loses its bistability for $q=5 \times 10^{-6} k_{-9}$; above this value it has a unique asymptotically stable equilibrium, with [C3*]≅5162 *mol/cell*, almost independently of q.

Furthermore equilibrium and stability of the 100000 models analyzed in *Experiment 2* were considered, in the presence of high and low values of the persistent stimulus: $q=0.8k_{-9}$, and $q=0.01k_{-9}$, respectively. The results are shown in Table 2.4 where models are again classified according to the number of equilibria when $q=0$, as belonging to the subsample S_1, S_2, S_3 (subsamples of type 1, 2, 3 models).

Table 2.4 Equilibrium and stability patterns of randomly generated models.

q	**S_1 (14678)**	**S_2 (50566)**	**S_3 (34756)**
0	one equilibrium a.s. 14678*	one equilibrium -	one equilibrium -
	two equilibria -	two equilibria a.s. – u. 50263 u. – u. 303	two equilibria -
	three equilibria -	three equilibria -	three equilibria a.s. – u. – a.s. 34659 a.s. – u. – u. 97
$0.01k_{-9}$	one equilibrium a.s. 14072 u. 22	one equilibrium a.s. 50440 u. 126	one equilibrium a.s. 18878 u. 7
	three equilibria a.s. – u. – a.s. 541 a.s. – u. – u. 41 u.u.u. 1	three equilibria -	three equilibria a.s. – u. – a.s. 15827 a.s. – u. – u. 44
$0.8\ k_{-9}$	one equilibrium a.s. 14671 u. 5	one equilibrium a.s. 50566	one equilibrium a.s. 34756
	three equilibria a.s. – u. – a.s 1 a.s. – u. – u. 1	three equilibria -	three equilibria -

* number of models that exhibit the specific pattern;
a.s.: asymptotically stable equilibrium; u.: unstable equilibrium;
S_k: set of models having k equilibrium states when $q=0$.

The other relevant feature of the static behaviour of the models is the value of [C3*] at an asymptotically stable equilibrium, selecting the largest value in case of bistability.

It is again denoted by $[C3^*]_{NLA}$, and its frequency distributions in the sets S_1, S_2, S_3 are shown in Figure 2.4.

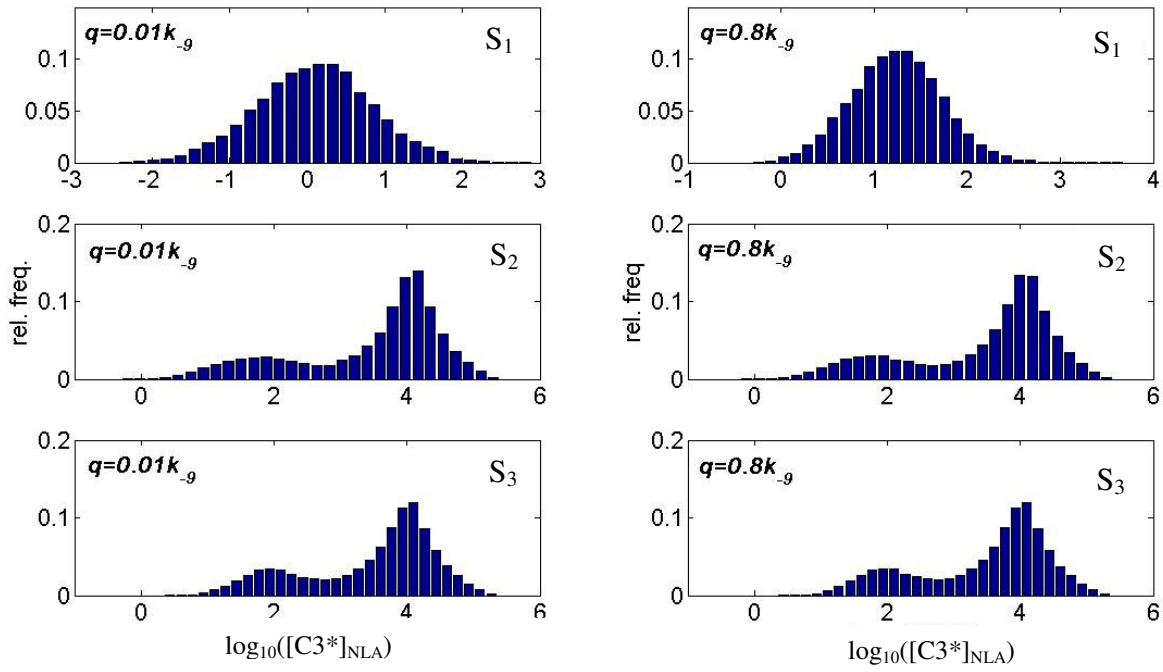

Figure 2.4 Distributions of the relative frequencies of the values of $[C3^*]_{NLA}$ in models belonging to S_1, S_2, S_3, subjected to low-level (q=0.01k_{-9}) and high-level (q=0.8k_{-9}) persistent stress.

The main features of the equilibrium patterns and of the distributions of $[C3^*]_{NLA}$ are:

- when q>0 models with two equilibria do not exist: this is a striking difference from the case q=0;
- in type 2 models the unstable life equilibrium disappears when a persistent input is applied; the value of [C3*] at the unique asymptotically stable equilibrium is nearly independent of q: then the static behaviour is essentially determined by model parameters;
- a relevant fraction of models in S_2 has a low level of $[C3^*]_{NLA}$ (f.i. $[C3^*]_{NLA}$<1000 *mol/cell* in about 27% of cases with q=0.8q_{MAX}): in view of this result it is simplistic to associate the models of S_2 with proneness to apoptosis;

- most of the models belonging to S_1 have a unique asymptotically stable equilibrium also when exposed to persistent stress; the exceptions occur with the low-level input: few models (4.0%) have three equilibria and very few have a single unstable equilibrium. Concentrations of C3* at equilibrium are small: with q=0.8q_{MAX} only 26 (0.18%) of the models have $[C3^*]_{NLA}$>1000 *mol/cell*;
- models belonging to S_3 partly retain the bistable pattern with the low-level stress; on the contrary the high-level stress "destroys" any track of the life equilibrium and of its unstable partner;
- for type 3 models the distribution of the values of $[C3^*]_{NLA}$ is almost the same for $q=0$, q=0.01q_{MAX}, q=0.8q_{MAX}. Also in this case the steady-state concentrations are determined essentially by model parameters.

In conclusion we note that a wide variety of patterns is present: some patterns are rare, but their existence is evidence of the complexity of possible model behaviours. As for the case where $q=0$, numerical simulation have shown that models with only unstable equilibria have periodic time evolutions.

2.4 Dynamical response analysis

This section reports the detailed analysis of the dynamical behaviour of the relevant proteins involved in the biochemical processes that lead to the apoptosis. A large number of simulations was carried out with the aim to reveal the characteristic features of the time evolutions of the concentrations in response to an external stimulus. The time evolutions were simulated by numerically solving equations (1)-(8). The MATLAB function *ode15s* has been used, with enhanced precision set by the function *odeset.* The effect of the external stimulus applied through the cell membrane is made acting on the *life* equilibrium value of C8*. Two different kinds of stimulus were considered: an instantaneous and a continuous stimulus. In the first case a number of C8 molecules is "instantaneously" converted into C8* molecules: after this the system evolves without external forcing; in the second case a number of C8 molecules is "continuously" converted into C8* molecules with a constant rate for a defined time interval.

2.4.1 Dynamical response of the nominal model

The instantaneous perturbation was simulated by imposing as initial state $\underline{x}(0) = \underline{x}_0 = [x_{L1}\ x_{02}\ x_{L3}\ 0\ x_{L5}\ 0\ x_{L7}\ 0]^T$ in which, besides C8, C3, BAR and IAP at the *life* equilibrium concentrations, a number of C8* molecules are present: $[C8^*]_{IN}=x_2(0)=x_{02}>0$.

From simulations of the response to such stimulus emerged the existence of a perturbation threshold reported also in Eissing et al. 2004 ($x_{20}\approx 75$ *mol/cell*) below which the evolution returns to the *life* equilibrium. Perturbations larger than this threshold are able to generate a transition from the *life* equilibrium to the *non-life* equilibrium E_{NL2}.

Figures 2.5a, b show the time evolution of [C8*], [C8*÷BAR] and [C3*], [C3*÷IAP] respectively.

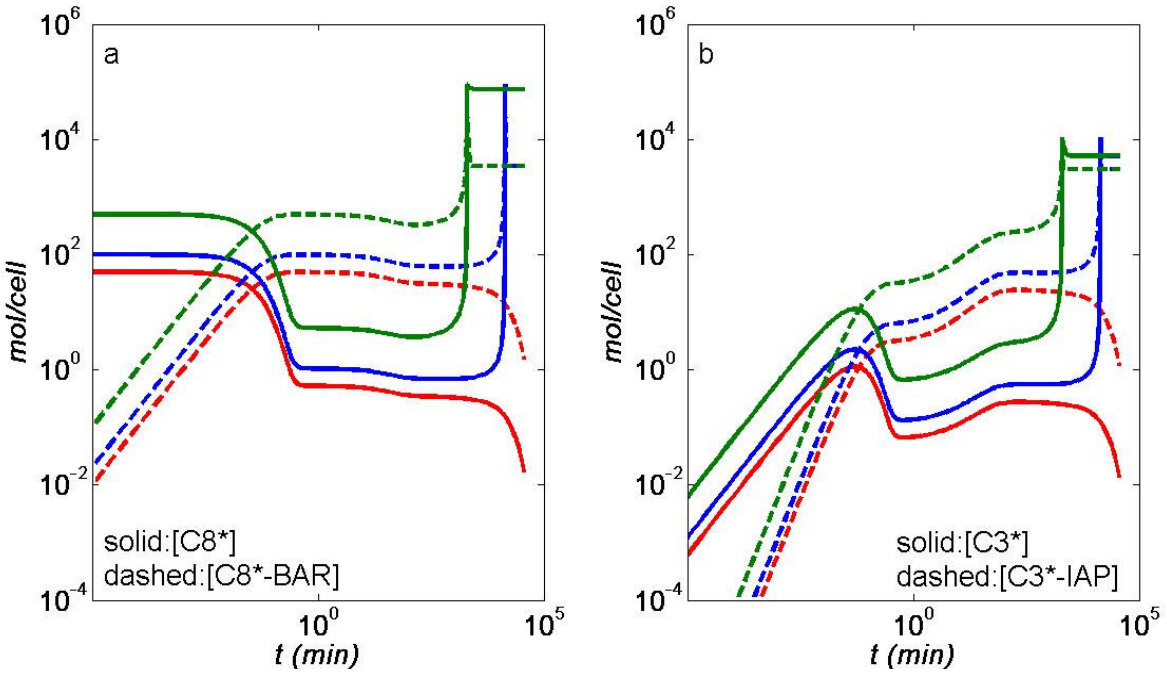

Figure 2.5 Time evolutions, in logarithmic scales, of [C8*], [C8*÷BAR] (a) and [C3*], [C3*÷IAP] (b) for the nominal model; initial perturbations: 50 *mol/cell* (red); 100 *mol/cell* (blue); 500 *mol/cell* (green).

The time evolutions of the protein concentrations are characterized by three distinct phases.

- a first phase in which C8* is rapidly captured by BAR to form the complex C8*÷BAR; the amount of C3* and complex C3*÷IAP that is produced in this phase is negligible.

- a second phase, named *decision phase*, that is characterized by very low values of [C3*] and [C8*], slow increase of [C3*÷IAP], and decrease of [IAP]. The duration of this phase (t_D) is almost inversely proportional to the intensity of the initial perturbation and when this perturbation is very close to the threshold this phase is very long.
- a third phase in which depending on the initial perturbation, we observe either the transition to apoptotic state with high values of [C3*] and [C8*], or a return of the system to the *life* equilibrium with low values of [C3*] and [C8*].

Figure 2.6 shows the transition corresponding to a perturbation of 100 *mol/cell*: the time evolution of the state variables of the model is restricted to the time interval [13400, 14000] minutes.

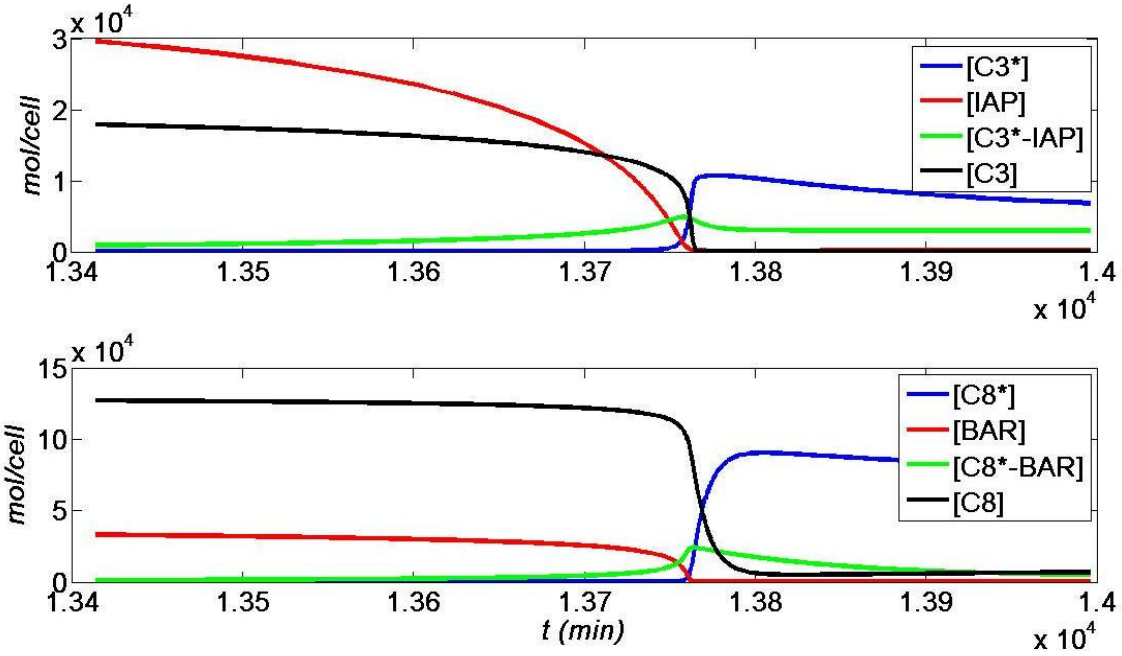

Figure 2.6 Time evolution of the state variables of the nominal model restricted to the time interval [13400, 14000] minutes; initial perturbation: 100 *mol/cell*.

From a biological point of view the observed trajectories of the state variables of the model suggest an important role played by the dynamical interactions between inhibitors (IAP and BAR) and active caspases in the cell fate decisions. In fact, the transition that leads to apoptosis seems to start when IAP is no more sufficient to bind new C3*, which causes a very fast increase of [C3*], followed by the increase of [C8*].

Simulations in which the initial perturbation exceeds the threshold from 100 to 10000 *mol/cell* have shown that only the time interval needed to reach the transition is affected by the intensity of the perturbation: the results are in Table 2.5.

Table 2.5 Relevant paramters of the time response of [C3*] to initial perturbations of various intensity. t_D: time, during the transition, at which the derivative of [C3*] attains its maximum; M_4=max[$x_4(t)$]: the peak value of [C3*]; t_R: time required for [C3*] to change from 10% to 90% of the peak value.

Initial stimulus (*c*) (*mol/cell*)	**t_D (*min*)**	**M_4 (*mol/cell*)**	**t_R (*min*)**
100	13787.9	10716	9.0
250	4036.2	10716	9.2
500	1983.6	10706	9.0
1000	988.7	10682	9.1
2000	479.8	10898	9.3
3000	311.2	11271	9.5
4000	229.1	11611	9.2
5000	181.0	11879	9.2
6000	149.5	12082	9.1
7000	127.3	12232	9.2
8000	110.8	12343	9.1
9000	98.0	12426	9.3
10000	87.7	12489	9.3

The continuous perturbation was simulated by imposing that a number of C8 molecules is "continuously" transformed into C8* at a constant rate $q(t)=q>0$ (*mol/cell/min*), for an interval of T minutes.

From simulations with this kind of stimulus an important result was observed. As for the case of an instantaneous stimulus, the transition time is almost inversely proportional to the rate of perturbation. In addition, no threshold seems to exist. In fact, the transition between the life equilibrium and the death equilibrium states is observed provided that the perturbation is applied for a sufficiently long time. From a biological point of view both types of perturbation: intense pulse, or else a constant level of external stimulus are plausible. Choosing either model depends on the experimental

setup that is simulated: in the experiments that we performed, to be described in the next sections, the inductor acts continuously on the cell culture. Figure 2.7 shows the time evolutions of [C3*] corresponding to different types of stimulus.

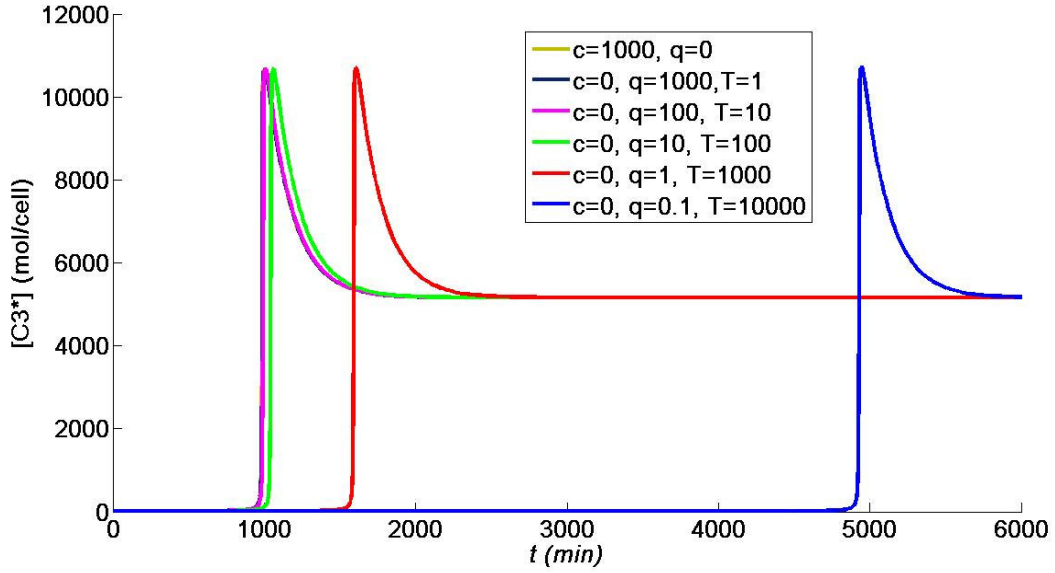

Figure 2.7 Time evolutions of [C3*] corresponding to different types of stimulus applied to the nominal model. *c*: intensity of the initial perturbation; *q*,*T*: level and duration of the continuous action. The curves for *c*=1000, *q*=1000, *q*=100 are indistinguishable

2.4.2 Response of randomly generated models

A detailed analysis of the dynamic behavior of the models in the sample S_{nom} defined in *Experiment 1* was carried out. An instantaneous (*section a*) and a continuous (*section b*) stimulus will be considered.

Section a) A large initial perturbation was used and the attention was focused on the time evolution of [C3*].

As parameters that quantitatively characterize the features of the time responses were chosen:

- the *delay time* (t_D), measured as the time at which the derivative of [C3*] attains its maximum;
- the *peak value* of [C3*];
- the time at which the *peak value* of [C3*] is attained (t_P).

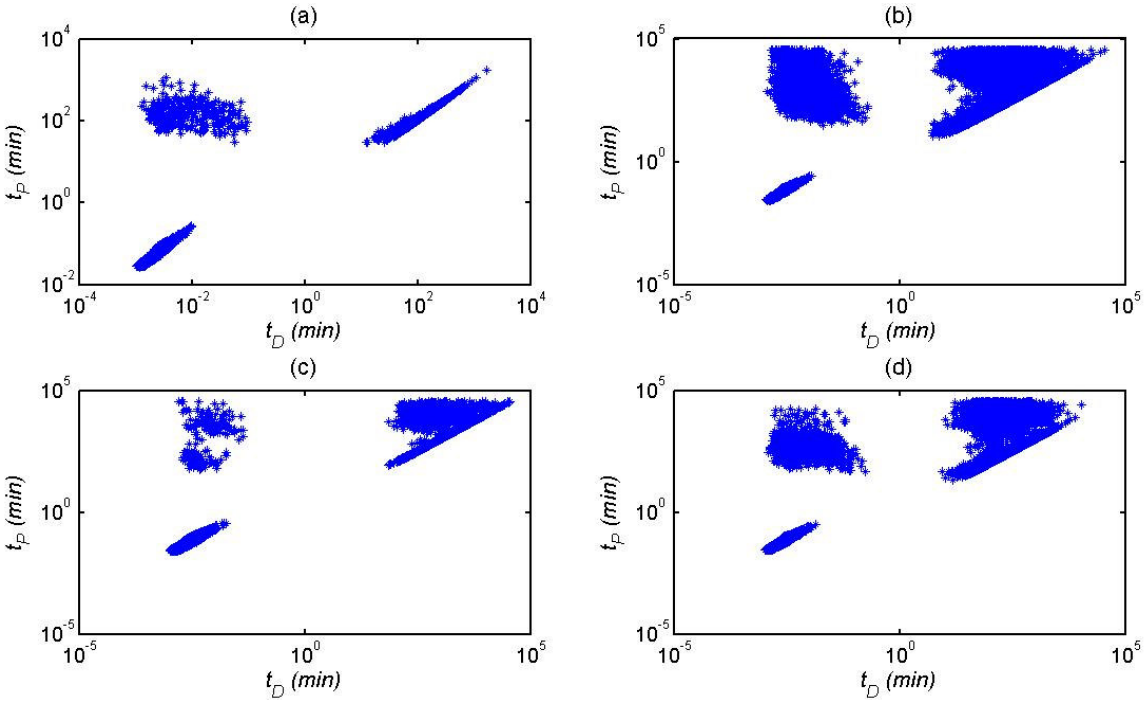

Figure 2.8 Features of the responses of type 1 (panel a), type 2 with asymptotically stable *non-life* equilibrium (panel b) and type 3 models (panels c and d). For each model the pair t_P (time at which [C3*] attains the maximum)- t_D (time at which the slope of the graph of [C3*] attains the maximum) is plotted. The simulation interval is [0, 36000] min. The initial perturbations are: type 1 models: $[C8^*]_{IN}$=10000 *mol/cell*; type 2 models: $[C8^*]_{IN}$=1000 *mol/cell*; type 3 models (panel c): $[C8^*]_{IN}$=1000 *mol/cell*; (panel d): $[C8^*]_{IN}$=10000 *mol/cell*.

Type 1 models. The 14678 models (with the unique, asymptotically stable life equilibrium) were simulated with an initial perturbation $[C8^*]_{IN}$=10000 *mol/cell*. In Figure 2.8a is shown t_D and t_P of [C3*] in type 1 models. From this figure it is clear that the population can be subdivided into three subgroups:

- 13133 models (type 1a) characterized by very small transition time and peak times; in these models $[C3^*]_{Max}$ ranges from 13 to 1372 *mol/cell*;
- 307 models (type 1b) characterized by a very small transition time and a large peak time (>20 min); in these models $[C3^*]_{Max}$ is almost uniformly distributed in the interval 50– 8000 *mol/cell*;
- 1238 models (type 1c) characterized by a large transition time (>10 min) and a slightly larger peak time; in these models $[C3^*]_{Max}$ ranges from 542 to 18407 *mol/cell*, and 800 models (65% of the group) have $[C3^*]_{Max}$>8000 *mol/cell*.

Typical time responses of models in the three groups are shown in Figure 2.9.

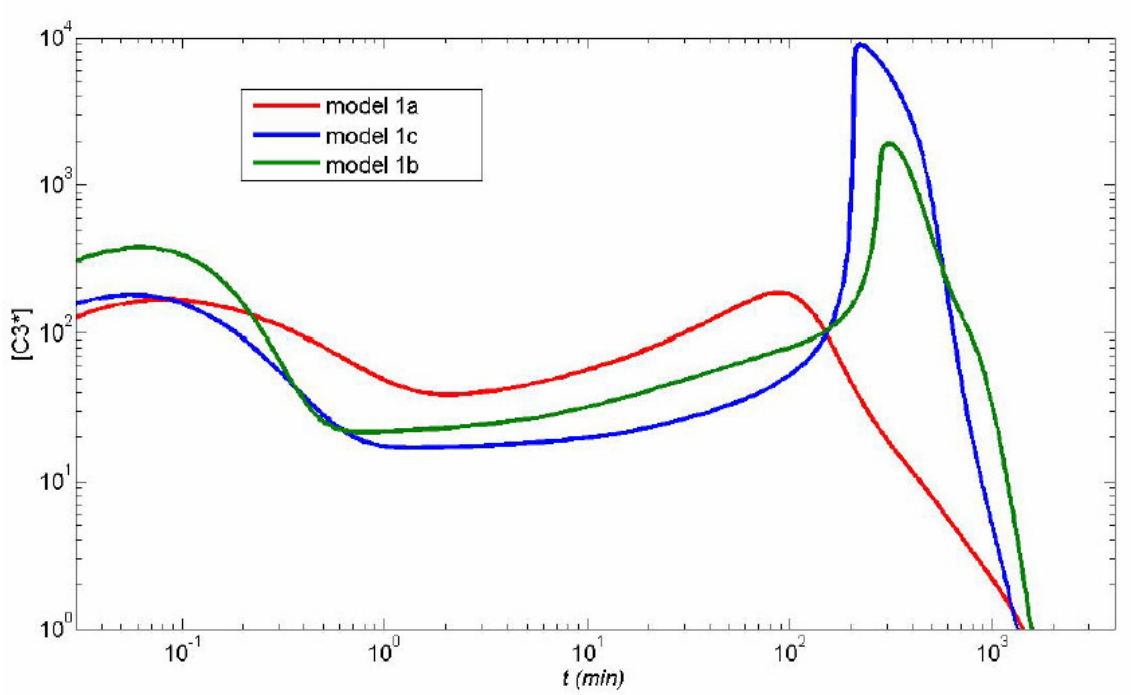

Figure 2.9 Characteristic evolutions of [C3*] in type 1 models.

Type 2 models. Among the 50566 models with two equilibrium states, 303 models have an unstable non-life equilibrium. As expected, such models have periodic evolutions: Figure 2.10 shows a typical plot of [C3*], consisting of sequences of spikes.

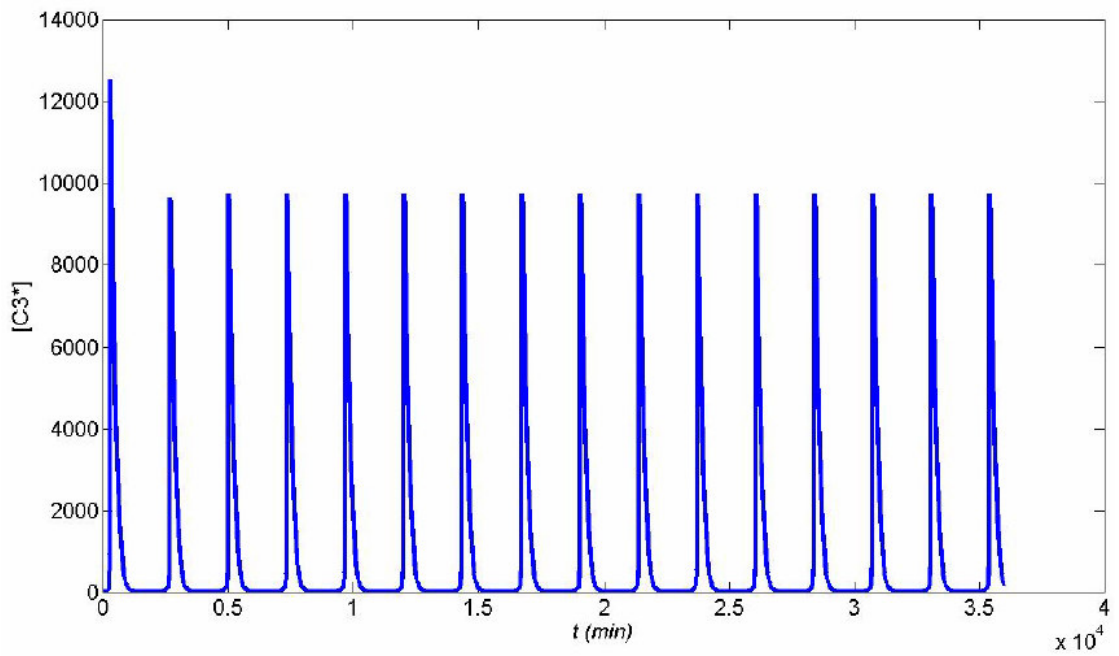

Figure 2.10 Time evolution of [C3*] in a model with unstable *life* and *non-life* equilibria.

Experiments with several values of $[C8^*]_{IN}$ in the range 100-10000 *mol/cell* have shown that the steady-state period and amplitude do not depend on the stimulus intensity. On the whole the amplitudes of [C3*] range from few tens to more than 10000 *mol/cell* and periods from hours to days.

Apart from these 303 cases, type 2 models have unstable *life* and asymptotically stable *non-life* equilibria.

Looking at the Figure 2.8b it is apparent that the models in S_2 consist of four classes:

- type 2a (characterized by small t_D and small t_P)
- type 2b (characterized by small t_D and high t_P)
- type 2c (characterized by almost equal values of t_D and t_P)
- type 2d (characterized by high value of t_P with respect to t_D)

Typical time responses of models in the four groups are shown in Figure 2.11.

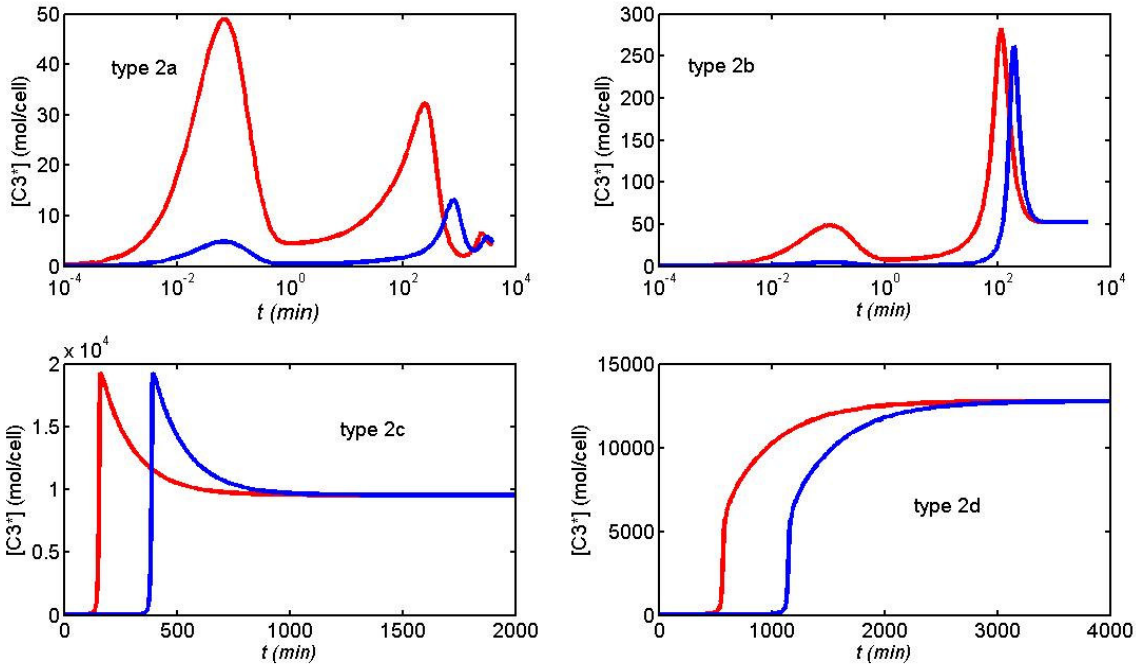

Figure 2.11 Characteristic time evolutions of [C3*] in type 2 models, for $[C8^*]_{IN}$=100 *mol/cell* (blue) and $[C8^*]_{IN}$=1000 *mol/cell* (red).

Type 3 models. These models, with the exception of 97 cases that behave like type 1 models, show the typical pattern of bistability: here are presented the main results of simulations with $[C8^*]_{IN}$=1000 *mol/cell* and $[C8^*]_{IN}$=10000 *mol/cell*, because now the intensity of initial stimulus is essential in triggering the activation phase. A fundamental point is that in both cases the models can be classified according to same criterion as for models of type 2 (see Figure 2.8c, d). The graphs are not reported for the sake of

brevity, because are very similar to those of Figure 2.11. The increase (decrease) of the sizes of groups 3c, 3d (3a, 3b) with the increase of the initial perturbation means that more models attain the activation phase in the simulation interval, although a substantial fraction (about 50%) still does not commute. As we can see, a variety of behaviours is found in a set of models whose parameters may vary at most by a factor of twenty.

Section b) For each model of the sample S_{nom} the time response due to a constant input over a time interval of 36000 minutes was computed, both at low-level ($q(t)=0.01k_{-9}$) and high level ($q(t)=0.8k_{-9}$), with the life equilibrium as initial state ($x_2=0$).

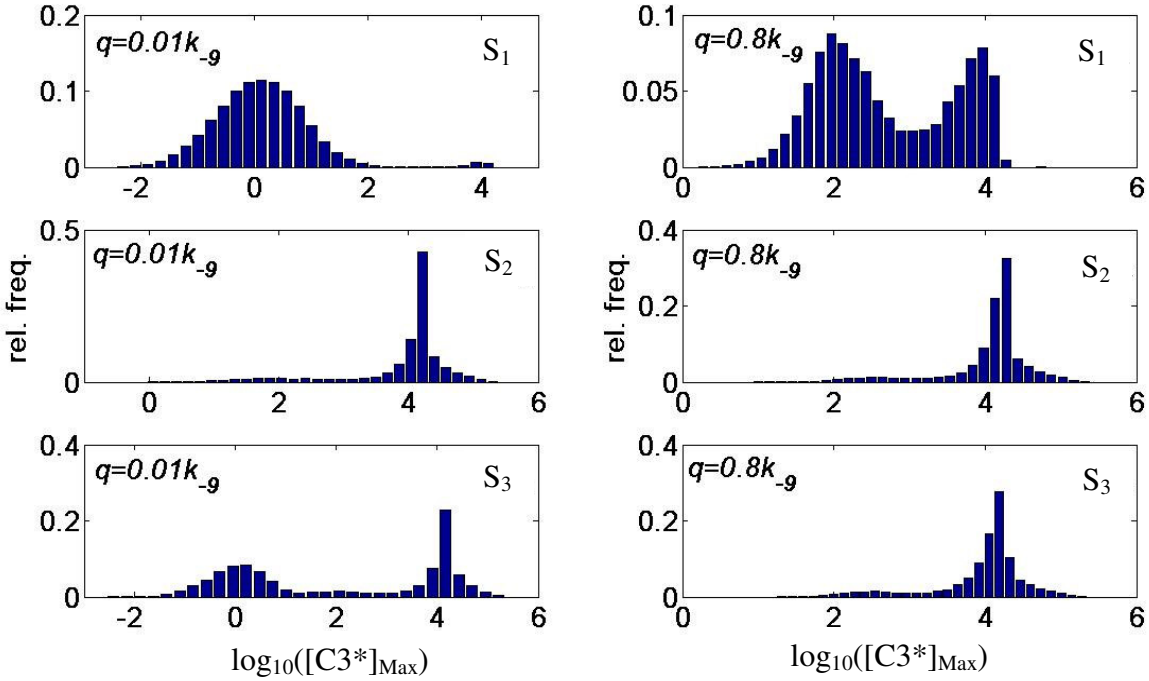

Figure 2.12 Distributions of the relative frequencies of the peak values of [C3*] responses in models belonging to S_1, S_2, S_3 subjected to low-level ($q=0.01k_{-9}$) and high-level ($q=0.8k_{-9}$) persistent stress.

Table 2.6 Relevant parameters of the time responses of [C3*] to continuous stimulus stresses for randomly generated models.

Models and input[a]	$\mathbf{t_D}$ (***min***)[b]	$\mathbf{[C3^*]_{Max}}$ (***mol/cell***)[b]	$\mathbf{t_R}$ (***min***)[b]
S_1 (*l-l*)	0.07-52.8-35510	0.004-1.30-17128	5.10-428-35230
S_1 (*h-l*) ()	0.18-8.28-2894	1.57-297-66102	3.20-38.1-2863
S_2 (*l-l*) ()	14.4-277-18293	0.93-15917-248930	3.03-16.5-12100
S_2 (*h-l*)	0.25-50.2-1013	8.48-15947-248930	3.07-16.5-3799
S_3 (*l-l*)	0.07-447-35977	0.003-118-223110	2.78-404-35674
S_3 (*h-l*)	0.31-86.0-1660	17.7-13284-223110	2.98-22.0-3824

[a] S_1, S_2, S_3: sets of models defined in *section 2.6*; (l-l) low-level input, (h-l) high-level input.
[b] minimum-median-maximum of the delay times, peak values, rise times.

Figure 2.12 and Table 2.6 summarize the results of this numerical experiment, with the exception of the models showing periodic behaviour. The evolution of [C3*] shows either a monotone increase to the equilibrium value or a sharp maximum followed by a decrease to equilibrium; the monotone increase is found in about 50% of the cases with low-level input, 21% with high-level input.

For models in S_2 both shape and peak value of the responses are almost independent of the input level, which affects only the delay. For the bistable models of S_3 the effect of increasing the input level is to increase the number of models which undergo the transition in the simulation interval: indeed [C3*] is still increasing at the end of the simulation interval for many models in S_3 with $q=0.01k_{-9}$. Models in S_1 are the most sensitive to the input level: when $q=0.01k_{-9}$ only 172 (1.2%) peak values exceed 5000 *mol/cell*, versus 3378 (27.1%) when $q=0.8k_{-9}$.

The numerical experiment mimics the application of a persistent stress to a population of cells. It is clear from the results that the dynamical behaviour cannot be overlooked: the application of a constant input may produce a response with high overshoot with respect to the steady state value, depending on the model parameters. Laboratory experiments should clarify if the death of the cell can be triggered by a short intense pulse of [C3*], or else a high constant level of [C3*] must be maintained.

2.4.3 Mortality curves in a population

Let us consider now a sample S consisting of 4471 bistable models with parameter vectors characterized by $[C3^*]_{NLA}$>3607 *mol/cell*. Since each model may be regarded as representative of a cell, the set S may represent a rather homogeneous populations of cells that in normal conditions have the same concentrations of relevant proteins because the *life* equilibrium is the same for all models. The integration of the model equations over an interval [0, t_F] for all parameter vectors in S, starting from the same initial condition is representative of a laboratory experiment in which the population is uniformly exposed to a instantaneous stimulus, and is monitored in the subsequent t_F minutes to measure the time evolution of active caspases and the number of dead cells.

The time evolutions of the models in S were computed over an interval of 3600 minutes, for initial perturbations in the range $[C8^*]_{IN}$=1000-7000 *mol/cell*. The distribution of the delay times t_D strongly depends on the intensity of the perturbation. Rather than showing the frequency distribution of the delay times we provide an equivalent representation which can be interpreted as mortality functions of the cell population. Figure 2.13 shows, for the various perturbations, the cumulative distribution F(d) of the delays, taken with respect to the whole population consisting of 4471 *cells*: F(d)=(n° of *cells* where transition occurred with $t_D \leq$d)/(total n° of *cells*). The curves of Figure 2.13 can be interpreted as cumulative mortality curves of the *cell population*: if we assume that a cell dies when [C3*] attains the maximum value (which is larger than the assumed threshold) then the fraction of times the delay is lower than, say, 1000 minutes is equal to the fraction of cells dead in a time interval of 1000 minutes from the application of the stimulus.

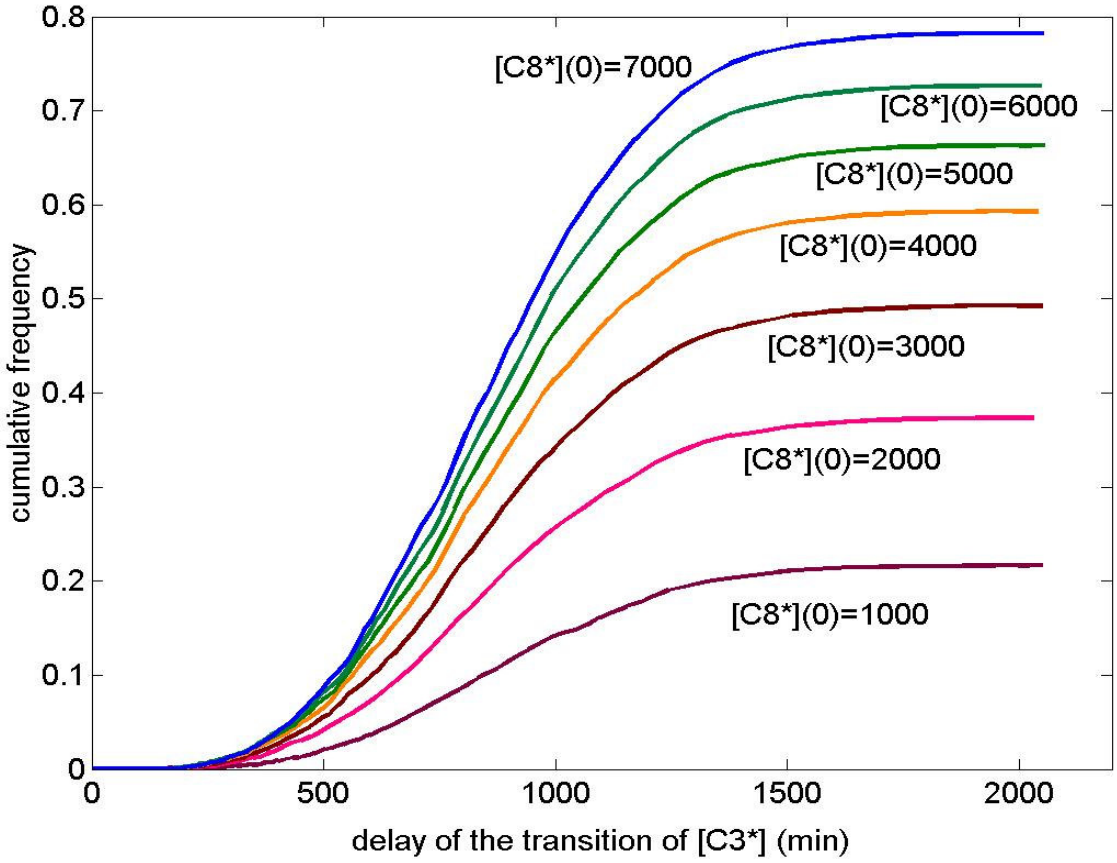

Figure 2.13 Cumulative frequency distribution of the delay of the transition of $x_4(t)$ for different initial perturbations.

2.4.4 Active caspase-3 concentration in a population

This numerical experiment simulate what the results of a measurement of [C3*] on an heterogeneous population of cells may look like. The experiment is as follows:

seven sets of models were generated with the procedure described in section 2.2.4: eac set consists of 5000 parameter vectors belonging to a neighborhood of the median parameter vector of bistable models;

for all models of the *i-th* set the responses to a persistent stimulus of duration T_i minutes, i=1,2,..,7 and intensity q= 400 *mol/cell/min* were computed (T=[15 30 60 120 180 240 360]);

the mean of the final values of [C3*] and of [C8*] in each group, say $[C3^*]_{mean}(T_i)$, $[C8^*]_{mean}(T_i)$ were computed.

Figure 2.14 shows the results of this experiment: it is clear that the specific features of single cell experiments (peak of concentration with fast rise time, after an interval of low value) are present also in the population averages.

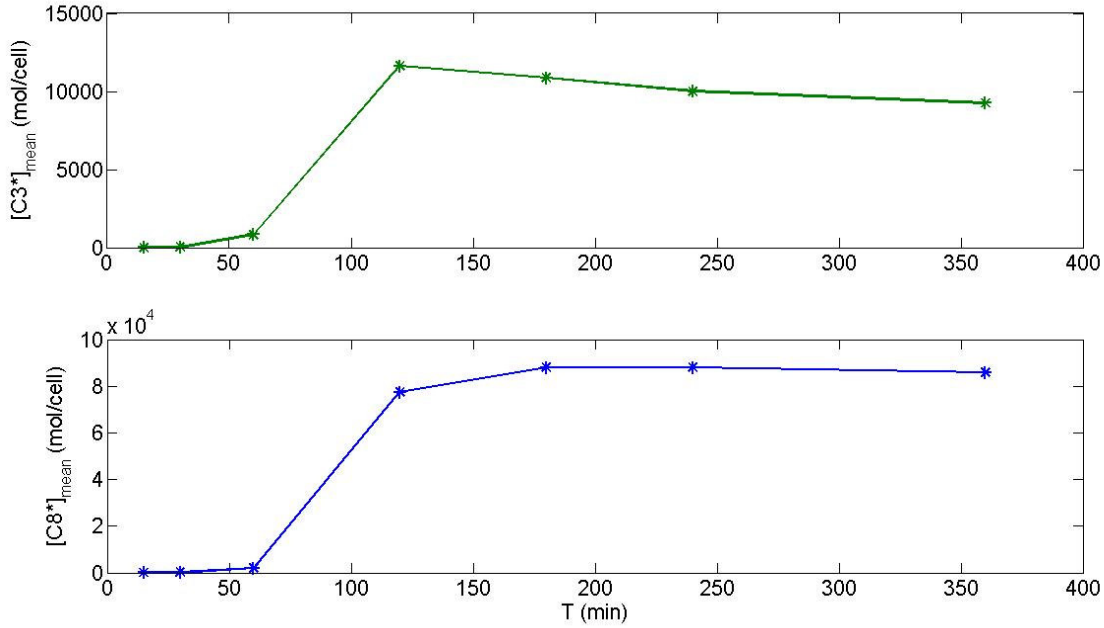

Figure 2.14 Collective response of sets of models to persistent stimuli. Each set consists of 5000 randomly generated models of type 3. $[C3^*]_{mean}$ ($[C8^*]_{mean}$): average values of [C3*] ([C8*]) at the end of intervals of length T where a constant stimulus (q=400 *mol/cell*) is applied.

2.5 Caspase regulation

The crucial point of the pathway leading to activation of procaspase-3 is represented by the regulatory mechanisms. In this section a detailed analysis of the model predictions about such regulatory mechanisms is reported. Note that the role of IAP's protein family is still debated in the literature, whereas little attention has been devoted to BAR. For this reason only the discussion on BAR is reported; an analysis of the model sensitivity to IAP changes is in (Carotenuto et al., 2007a).

In order to analyze the effect of the concentration of BAR inhibitor protein on the static and dynamic behaviour of the model, we modified the source term k_{-12} in equation 1-8. The nominal value of this parameter is k_{-12}=40 *mol/cell/min*. Note that the most obvious effect of changing the parameter is to change the concentration of BAR at the *life* equilibrium: $[BAR]_{EL}=k_{-12}/k_{12}$.

Equilibrium, stability, and dynamical response to external stimulus for k_{-12} that changes from 4 to 80 were considered. The other parameters were not changed from the nominal values.

A slight decrease of the level of production of BAR below the nominal value (k_{-12}<39.371) changes the equilibrium pattern from bistability to instability of the *life* equilibrium, together with one asymptotically stable *non-life* equilibrium. For k_{-12}>39.371 the model shows the bistable pattern. The same pattern was observed when the IAP source was modified.

Variation of k_{-12} does not affect the value of $[C3^*]_{NLA}$ that remains at about 5160 *mo/lcell*.

As to the dynamical response of models characterized by the bistable behaviour, the increase of the level of BAR production causes an almost linear increase (Figure 2.14) of the threshold perturbation needed to observe the transition to the *non-life* equilibrium within the simulation interval.

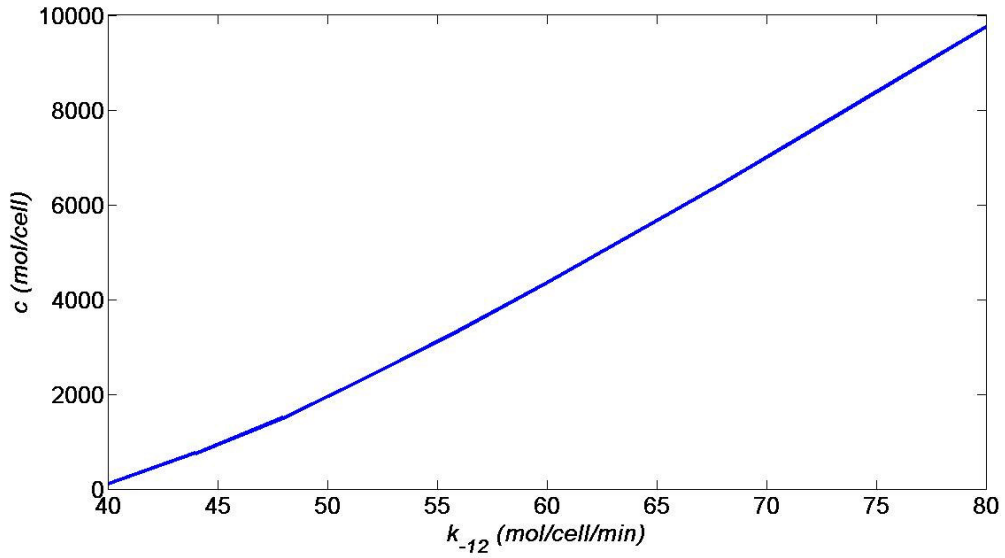

Figure 2.14 Dependence of the threshold perturbation on the BAR source k_{-12}.

Finally, the effect of BAR source variation on the transition time and peak value of [C3*] at different stimulus intensity has been analyzed. A negative power law ($t_D = \alpha c^{-\beta}$, Figure 2.15) dependence was found between the transition time and the intensity of the external stimulus with parameters α and β that increase with k_{-12}. This

implies that low values of BAR concentration produce much faster responses, because the transition time decreases.

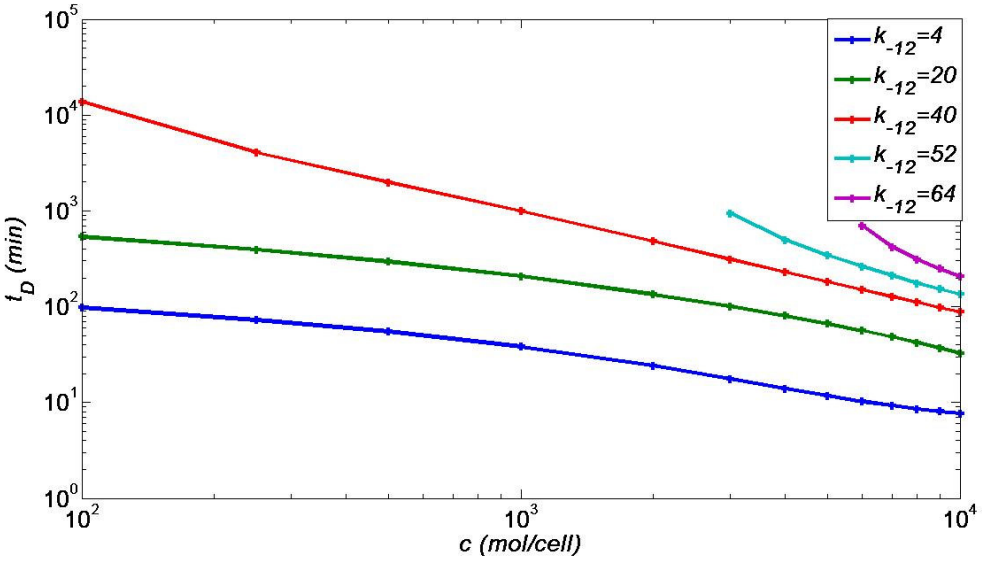

Figure 2.15 Dependence of the delay time t_D on the perturbation intensity c and on the BAR source k_{-12}.

Consistently with the insensitivity of the *non-life* equilibrium value of [C3*] to changes of k_{-12}, also the peak value *of* [*C3**] is only slightly affected by k_{-12}.

From a biological point of view the dependence of both the threshold perturbation and the time of transition on the rate of production of BAR confirms the important role played by this protein in the regulation of the extrinsic apoptotic pathway. It is also important to note that the model predicts a stronger effect on the timing of the phenomenon, than on the levels of C3* concentrations.

The analysis of the model and the dynamical simulation reported in this section have been as guidelines for designing *in vitro* experiments which will be described in the next sections.

3. Laboratory experiments

3.1 Aim of the experiments and experimental design

The model introduced and analyzed in *chapter 2* considers the dynamical interactions between crucial proteins that lead to the activation of procaspase-3 and procaspase-8. The objective of the experimental activity was to compare the predictions of the model with the behavior of populations of cells exposed to an appropriate external stimulus. The stimulus must elicit the extrinsic apoptotic pathway, and must be applied to a set of cells as homogeneous as possible. To satisfy the last requirement not only the same type of cells must be used but also these cells must be in the same phase of the cell cycle (synchronized cells). The achievement of such a uniform state, which is important in the study of any biological pathway, is particular relevant in apoptosis because it has been shown (Hsu et al., 2006) that the level of active caspase-3 undergoes periodic changes during the different phases of cell cycle. Therefore a preliminary set of experiments was devoted to choose the best synchronization procedure and to characterize the type and the concentration of the inductor which triggers the apoptotic pathway. A first set of main experiments aimed at measuring the time evolution of:

- active caspase-3 concentration
- active caspase-8 concentration
- parameters recognized as independent indicators of the apoptotic states
- fraction of dead cells

both in cell populations exposed to the apoptotic stimulus and in undisturbed populations taken as controls. A second set of experiments aimed at addressing the role of the inhibitor protein BAR, already numerically tested on the model. To this purpose a population of cells in which the *BAR* gene is silenced was produced. A further series of preliminary experiments was required to evaluate degree of silencing and status of the cells. The same main experiments as before were carried out: measurement of caspase-3 activity, measurement of the indicators of apoptosis and of the dead cells fraction both in the presence and in the absence of the apoptotic stimulus. In this case, the interest is not only on the effect of the stimulus on cells where *BAR* was silenced, but also on the effect of silencing on unperturbed cells.

An overall view of the experimental procedure is given in the flow chart of Figure A.

Figure A

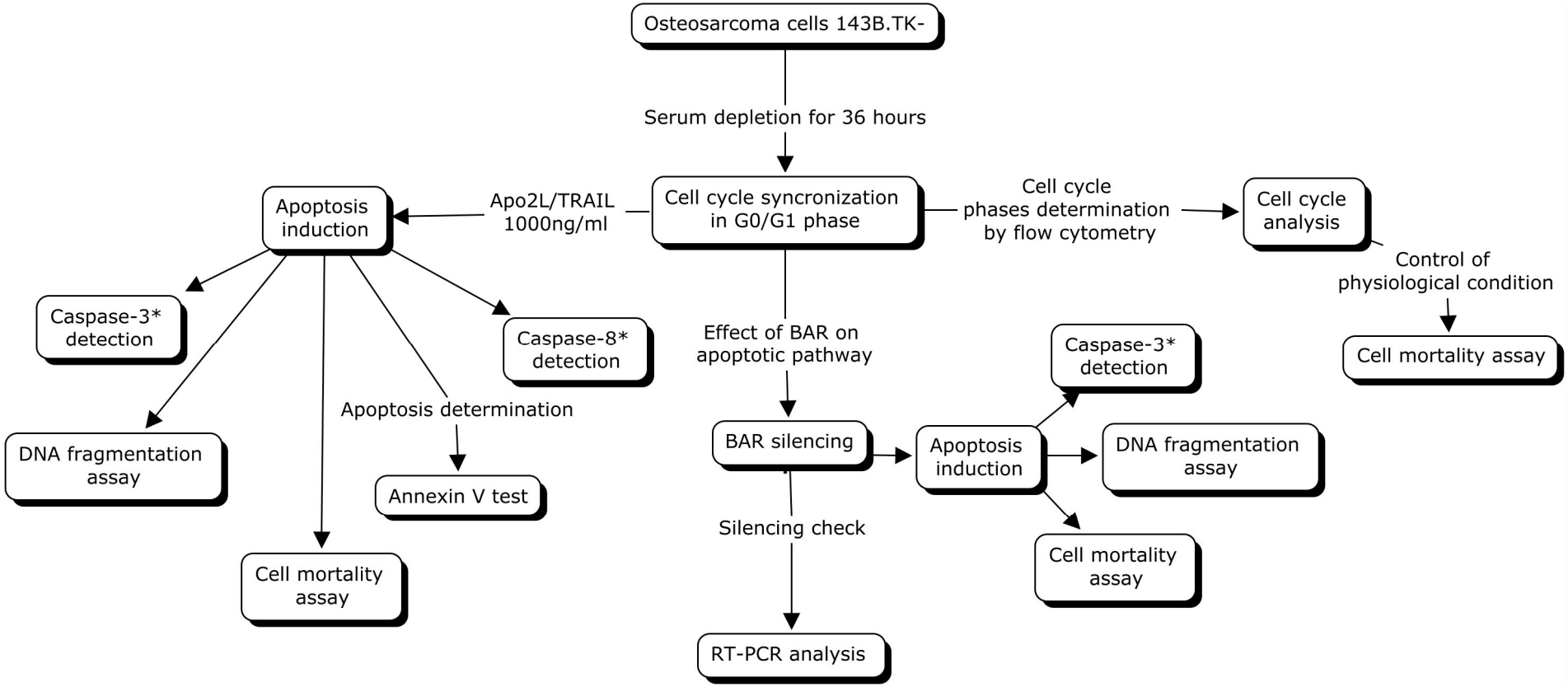
Osteosarcoma cells 143B.TK-
Serum depletion for 36 hours
Cell cycle syncronization in G0/G1 phase
Apo2L/TRAIL 1000ng/ml
Apoptosis induction
Caspase-3* detection
Caspase-8* detection
DNA fragmentation assay
Apoptosis determination
Annexin V test
Cell mortality assay
Cell cycle phases determination by flow cytometry
Cell cycle analysis
Control of physiological condition
Cell mortality assay
Effect of BAR on apoptotic pathway
BAR silencing
Silencing check
RT-PCR analysis
Apoptosis induction
Caspase-3* detection
DNA fragmentation assay
Cell mortality assay

3.2 Materials and Methods

3.2.1 Cell Culture and reagents

143B.TK$^-$ osteosarcoma cells were maintained in DMEM (Dulbecco's Modified Eagle Medium) (Gibco) containing 4.5 g/L glucose and 110 µg/mL pyruvate, supplemented with 10% FBS (Fetal Bovine Serum) (Gibco), 100 µg/mL 5-bromo-2′-deoxy uridine (Sigma) and 50 µg/mL gentamicin (Gibco). 143B.TK$^-$ were cultured in a water-humidified incubator at 37 °C in 5% CO_2/95% air.

3.2.2 Cell Synchronization

Four different protocols were tested for cell cycle synchronization: 1) and 2) serum deprivation of growth medium for 24 and 36 hours respectively; 3) treatment with Aphidicolin for 16 hours; 4) treatment with Aphidicolin for 16 hours followed by serum deprivation and subsequent cell culture for 48 hours.

With regard to protocols 1 and 2, 1 x 10^6 cells were cultured in DMEM into 100-cm^2 plates for 12 hours. Then the medium was replaced with medium without serum and the cells were cultured in this condition for 24 or 36 hours (Protocols 1 and 2). With regard to protocols 3 and 4, 1 x 10^6 cells were cultured in DMEM into 100-cm^2 plates for 12 hours. Then, the cells were cultured after adding of 5.9 µM Aphidicolin for 16 hours. For protocol 4, cell culture was maintained for 48 hours in serum deprivation condition. At the end of above mentioned treatments each sample was stained with propidium iodide and the level of synchronization was revealed by flow cytometry.

3.2.3 Apoptosis induction

3 x 10^5 synchronized cells were seeded in 60 cm^2 well plates and allowed to adhere to the plate over night. Then cells were treated for time intervals of different length (from 15 minutes to 6 hours) with 1000ng/ml of recombinant Apo2L/TRAIL.

3.2.4 Measurement of caspase-3 and caspase-8 activities

Active caspase-3 (caspase-3*) was assayed by using the caspase-3 Detection Kit from Calbiochem. The assay utilizes a specific molecule DEVD-FMK that is recognized by caspase-3*. DEVD-FMK is conjugated to FITC as the fluorescent *in situ* marker. The complex FITC-DEVD-FMK is cell permeable, non toxic and irreversibly binds caspase-3* in living cells. This complex generates fluorescence. The measurement of

fluorescence intensity by flow cytometry gives the measure of caspase-3* concentration. For the analysis 3 x 10^5 Apo2L/TRAIL treated cells and non-treated cells were incubated at 37°C with 5% CO_2 for time intervals of different length. FITC-DEVD-FMK was added at 0.3 ml of each cell sample. Then the cells were incubated at 37°C with 5% CO_2 for 45 minutes, collected, washed and analyzed by flow cytometry. The signal generated was proportional to the amount of caspase-3* in the cells. In all analyses a minimum of 1×10^4 cells per sample was acquired in list mode and analyzed with Cell Quest software.

Caspase-8* was assayed by using a fluorescent substrate containing the IETD sequence (Red-IETD-FMK), that is recognized by the active form of procaspase-8. This fluorescent marker is a labeled, cell-permeable, non toxic that binds irreversibly caspase-8* in living cells. This substrate is able to generate fluorescence when is recognized by active caspase-8. The Red-IETD-FMK was purchased from Calbiochem. For the analysis, 3 x 10^5 cells untreated and treated with Apo2L/TRAIL 1000ng/ml were incubated at 37°C with 5% CO_2 for time intervals of different length. Red-IETD-FMK was added at 0.3 ml of each sample (stimulated e non-stimulated cells). Then the cells were incubated at 37°C with 5% CO_2 for 45 minutes, collected, washed and analyzed by flow cytometry. In all analyses a minimum of 1×10^4 cells per sample were acquired in list mode and analyzed with Cell Quest software.

3.2.5 Annexin V assay

Annexin V assay is based on the observation that during induction of apoptosis, phosphatidyl serine (PS) is translocated from the inner leaflet to the outer leaflet of the plasma membrane. The exposition of phosphatidyl serine enables phagocites to recognizes the apoptotic cells which are removed without cell proteolytic enzyme leakage. PS is preferentially bound by Annexin V. On the other hand Annexin V, conjugated with fluorochromes FITC, allows to follow the time of exposition of PS and then the timing of the apoptotic process by flow cytometry. For the analysis 5 x 10^5 Apo2L/TRAIL treated and non-treated cells were incubated at 37°C with 5% CO_2 for variable time intervals. The cells were washed in Phosphate Buffered Saline (PBS) and diluted in a binding buffer. Annexin V-FITC was added to 0.195 ml of cell suspension and then was incubated at room temperature for 10 min. Successively the cells were washed in PBS and were resuspended in 0.190 ml of binding buffer. Each sample was treated with propidium iodide and then was analyzed by flow cytometry. Annexin V is

used in conjunction with propidium iodide because in this way apoptotic cells can be distinguished from necrotic cells. The signal generated is proportional to the amount of PS present on the external plasma membrane. Annexin V-FITC Kit was purchased from Bender MedSystems. In all analyses a minimum of 1×10^4 cells per sample were acquired in list mode and analyzed with Cell Quest software.

3.2.6 Cell mortality assay

Treated and untreated cells were assayed for viability by Trypan Blue exclusion assay. The cell membrane of dead cells becomes permeable and can be stained. In contrast, the intact plasma membrane of viable cells is impermeable to stain. Then viable and-non-viable cells can be distinguished by light microscopy as dead (blue-stained) and viable (non-stained) cells. Floating and adherent cells were collected and 200 µl of cellular suspension were added to an equal volume of 0.4% Trypan Blue solution (Sigma). Successively the cells were counted on a hemocytometer with an inverted light microscope using a 20× magnification.

3.2.7 DNA laddering

The DNA fragmentation test is based on the activation of cellular endonucleases that is a typical phenomenon of apoptotic cells. In fact, apoptotic cells shown a typical ladder of small fragments of double-stranded DNA. The fragments are multiples of approximately 180 bp, reflecting the preferential accessibility of inter-nucleosomal linker DNA to endonucleases.

Treated and untreated cells were trypsinized and centrifuged at 2500 g for 5 minutes. The pellet was incubated on ice for 20 minutes in 400 µl of lysis buffer (10 mm Tris-HCl pH 8, 20 mm EDTA, 0.2% Triton-X100). After a 12000 g centrifugation for 20 minutes, an equal volume of phenol/chloroform was added to the supernatant. Then, after a new 12000 g centrifugation for 5 minutes, an equal volume of chloroform was added to supernatant and centrifuged again. The supernatant was collected and stored at −20 °C overnight after adding 0.1 volume of 3 m sodium acetate pH 5.2 and 2 volumes of ethanol to precipitate DNA. DNA was pelleted by centrifugation at 12000 g per 20 minutes, rinsed with 70% ethanol and then resuspended in a buffer containing 100 mg/mL RNase. After 2 hours of incubation at 37 °C, the DNA samples were loaded on a 1.5% agarose gel, electrophoresed in TAE (Tris/Acetate/EDTA) buffer and stained with ethidium bromide.

3.2.8 Gene silencing by siRNA treatment

siRNA are double-stranded RNAs of 21-23 nucleotides that induce the sequence-specific degradation of homologous RNAs. They are the molecular mediators of RNA interference that is a natural mechanism of post-trascriptional gene-silencing.

For our analyses siRNA specific for *BAR* gene was purchased from Qiagen.

siRNA transfection was performed in osteosarcoma cells as recommended by standard protocol. Cell plating and transfection are performed on the same day. Briefly, 2.5 x 10^5 cells were seeded in 6-well plates containing complete medium. 5nM siRNA were added to 3 µl of HiPerFect Reagent (Qiagen) and the mix was incubated at room temperature for 10 min. Then, the cells were treated with silencing mixture and incubated at 37°C for 72 hours. The successive step is: *RNA extraction and Reverse Transcriptase-PCR*. In order to confirm the silencing of *BAR* gene, total RNA was extracted from untreated and treated by using RNeasy Mini Kit (Qiagen). The RNA concentration of each sample was measured by biophotometer Bio-Rad at 260/280 nm absorbance ratio.

RT-PCR (Reverse Transcriptase-PCR) reactions were carried out by using the ImPromII Reverse Transcription System kit (Promega). The RT-reaction consist of two steps: in a first step, a mix containing 500 ng of total RNA and 500ng of Oligo(dT)15 Primer (0.5mg/ml) was pre-heated at 70° C for 5 minutes; in a second step, the reaction was carried out in a 40 µl of final volumes containing 1X ImProm-II 5X Reaction Buffer; 300 µM of MgCl2 (25 mM); 125 µM of each dNTP of dNTP mix (10mM each of 4 dNTPs); 20 U of Recombinant RNasin Ribonuclease Inhibitor (20 U/ µl); 0,15 µl of Reverse Transciptase. The final reaction mix was incubated at 25° C for 5 minutes, at 37° C for 60 minutes and finally at 95° C for 10 minutes to inactivate the Reverse Transcriptase enzyme.

The primers for *BAR* gene were designed by using "AutoPrime" program available on the web site (http://www.autoprime.de/AutoPrimeWeb). We designed also the primers for housekeeping *GAPDH* gene, used as PCR internal control.

The PCR mixture was in 25 µl of final volume and contained:

- 1 µl of cDNA, 0.25 U/µl of Taq polymerase,
- MgCl2 4 mM,
- Reaction Buffer 1X,

- dNTP 1.25 mM,
- BAR Primer Forward 0,4 μM (Table 3.1),
- BAR Primer Reverse 0,4 μM (Table 3.1),
- GAPDH Primer Forward
- GAPDH Primer Reverse

Table 3.1

Primers	Forward primer 5'-3'	Reverse primer 5'-3'
BAR	TCTGCCGTCACTGCCTTGGCT	ACACGTTCTAGCTCCATGAG
GAPDH	GACAACTTTGGTATCGTGGA	TACCAGGAAATGAGCTTGAC

The PCR method consisted of a pre-denaturation step at 92° C for 1 minute, followed by 30 cycles at 92° C for 1 minute, 62° C for 1 minute and 72° C for 1 minute. The final step was incubation at 70°C for 10 minutes. PCR products were analyzed on 2% agarose gel containing 0.5mg/ml ethidium bromide. Fluorescence intensity of the bands was calculated by using a densitometer analysis (Kodak Electrophoresis Documentation and Analysis System 290, EDAS 290) and normalized respect to *GAPDH* band intensity ("Relative Band Intensity").

3.3 Results of the experiments

3.3.1 Cell-cycle synchronization

Recall that the experimental system consists of cultures of human osteosarcoma cells 143B.TK$^-$. A standardized protocol to synchronize the cell-cycle of the cells in a culture does not exist because some synchronization procedures can interfere with the normal vitality of the cells or can show a cell-specificity. The efficiency of synchronization of four different protocols (see *Materials and Methods*) was tested on the experimental system. Table 3.2 shows the percentage of cells in the different phases of the cell-cycle at the end of the synchronization treatment.

Table 3.2. Percentage of cells in the different phases of the cell-cycle obtained by cytofluorimetric analysis. In brackets hours of treatment are indicated.

	Cell cycle phases		
Treatment	**G0/G1**	**S**	**G2/M**
Untreated (control cells)	42.1%	38.7%	19.2%
Serum deprivation (24 hours)	39.3%	44.1%	16.6%
Serum deprivation (36 hours)	**82.2%**	9.5%	8.3%
Aphidicolin 5.9 uM (16 hours)	52.8%	36.9%	10.3%
Aphidicolin 5.9 uM (16 hours) plus serum deprivation (48 hours)	29.1%	45.7%	25.2%

From this table it is clear that three protocols provided low levels of synchronization (lower than 50%). The highest rate of synchronization (>80%) was obtained by using serum depletion for 36 hours, and cells were blocked in G0/G1 phase. Since the synchronization treatment is in any case a stress for the cells, its effect on cell viability was tested. The fraction of dead cells in the synchronized population was measured at different times in a total interval of 28 hours after the synchronization treatment. As

shown in Figure 3.1, the fraction of dead cells remains at about 30% in the first 12 hours after synchronization. Only after 24 hours from the synchronization treatment the fraction of dead cells increases up to about 60%.

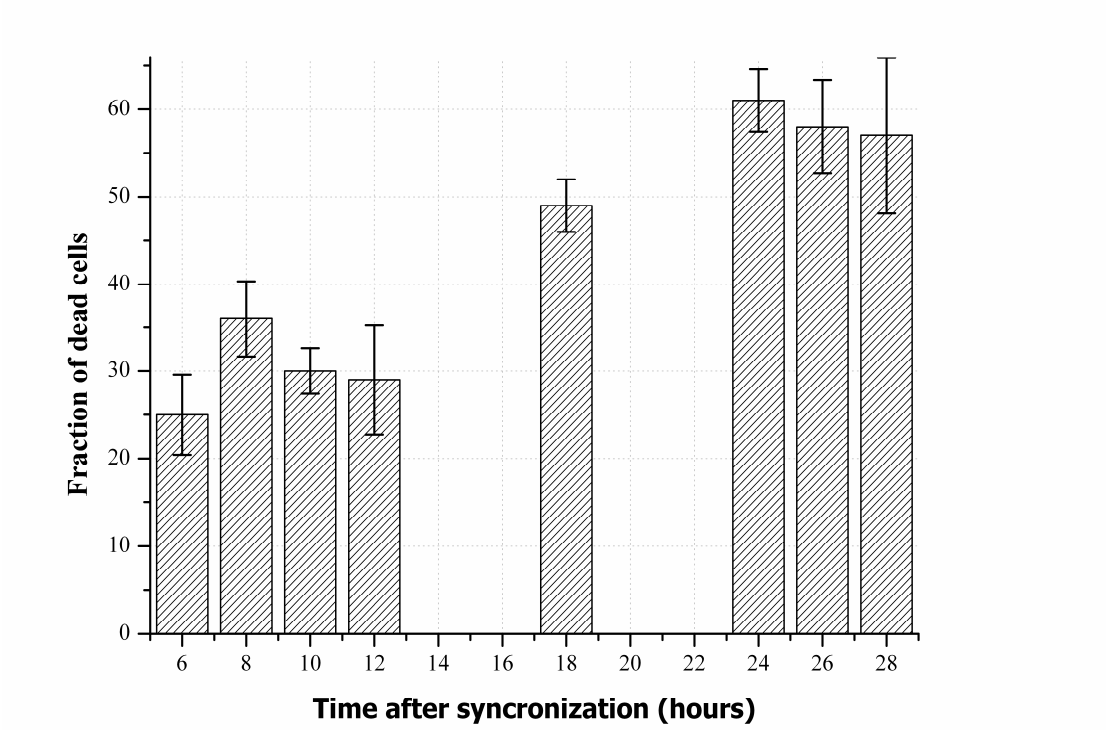

Figure 3.1. Time evolution of the fraction of dead cells after synchronization by serum starvation. Cells were seeded in 6-well plates, allowed to adhere for 12 hours, washed in PBS, and incubated in serum-free medium for 36 hours. Successively, cell death for each time point was assessed by counting living versus dead cells by trypan blue exclusion assay. The values represent the average of three independent experiments. Bars: one standard deviation.

We concluded that the procedure guarantees that a large fraction of synchronized cells is in good health and can give a uniform response to stimuli, at least on time intervals consistent with the earlier stages of apoptosis.

Thus, all the subsequent experiments were carried out by synchronizing osteosarcoma 143B.TK$^-$ cells with serum deprivation for 36 hours.

3.3.2 Sensitivity of osteosarcoma cells 143B.TK$^-$ to recombinant soluble Apo2L/TRAIL

It must be recalled that a level of apoptosis is anyway present in a synchronized cell culture. To determine the concentration of Apo2L/TRAIL able to induce a level of apoptosis significantly above the background, we carried out a dose/response

experiment in which osteosarcoma cells 143B.TK$^-$ were exposed to various doses of Apo2L/TRAIL. Since the fluorocytometric measurement of caspase-3*, described in *section 3.2.4* does not provide an absolute value of concentration, we compute the ratio between the measurement of caspase-3* in stimulated cells and the measurement of caspase-3* in non stimulated cells. This ratio, that we call *caspase-3 activity* and denote with the symbol α_{C3}, is used here and in the following as a measure of the excess of caspase-3* concentration in perturbed cells with respect to unperturbed cells. Figure 3.2 shows the *caspase-3 activity* after 12 and 24 hours of treatment, as a function of the concentration of Apo2L/TRAIL.

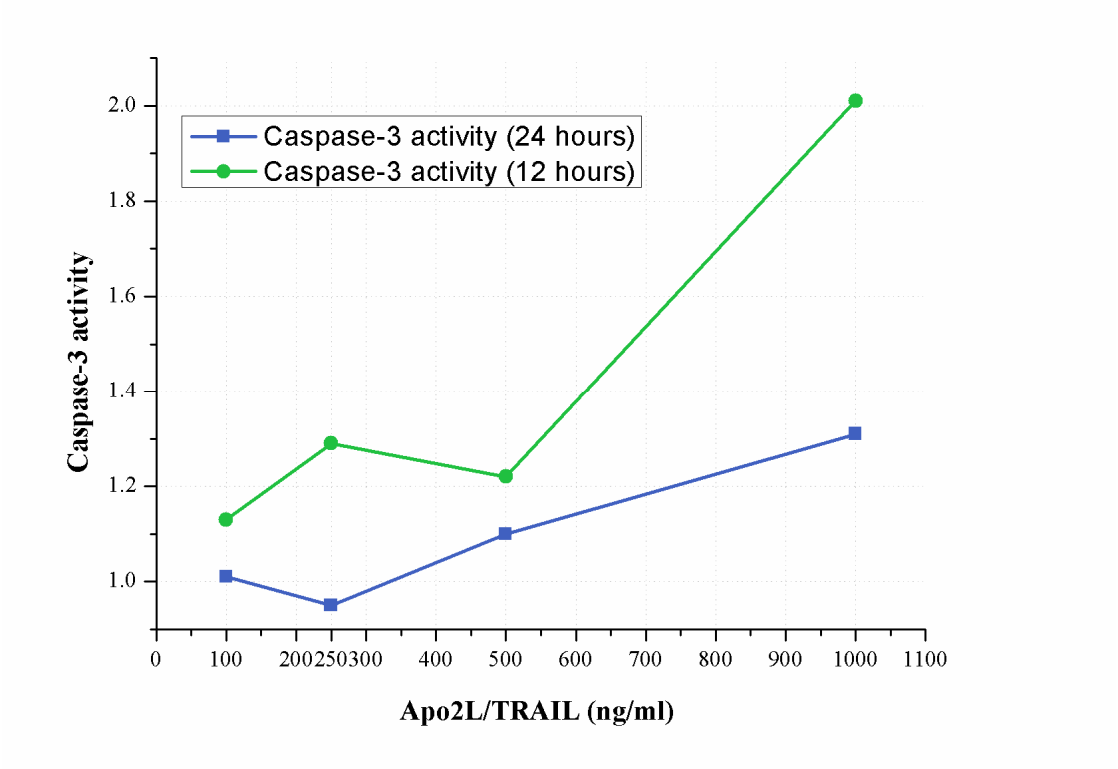

Figure 3.2 Response of synchronized cells to Apo2L/TRAIL. After synchronization the cells were stimulated for 12 and 24 hours with Apo2L/TRAIL at 100, 250, 500, 1000 ng/ml concentrations. For each concentration of Apo2L/TRAIL the *caspase-3 activity* α_{C3} was computed as the ratio between the concentration of caspase-3* in stimulated cells and the concentration of caspase-3* in non stimulated cells as described in *Materials and Methods*.

Since the characteristic times of apoptotic processes do not exceed 12 hours, it is clear that the 2-fold maximal activity reached at 1000ng/ml of Apo2L/TRAIL suggests that such concentration is sufficient to elicit a significant response. Then in all subsequent

experiments the cells were stimulated with recombinant soluble Apo2L/TRAIL 1000ng/ml.

3.3.3 Time evolution of caspase-3 activity

The time evolution of the model concentration of caspase-3*, computed by numerical integration of the model equations, shows several characteristic features, that have been pointed out in *section 2.6*. To obtain the time response of a population of real cells subjected to a stimulus we should, in principle, set up an experiment in which the amount of caspase-3* is measured at successive time instants on the ***same*** cell population. This experiment is unfeasible: however the assumption of homogeneity of synchronized cells allows to obtain an equivalent result by analyzing several sub-populations, each subjected to the Apo2L/TRAIL treatment for a specific time interval. At the end of the time interval the *caspase-3 activity* (α_{C3}) is computed as described before. Figure 3.3 shows α_{C3} as a function of the time length of treatment with Apo2L/TRAIL: α_{C3} remains nearly constant for the first 120 minutes of treatment. A rapid increment occurs between 120 and 180 minutes, reaching the maximum value of α_{C3}=3.5. From 180 to 240 minutes the activity decreases maintaining nearly constant values for the next times of treatment. On the basis of the above equivalence, we interpret the graph as representative of the time evolution of caspase-3* concentration in a population of stimulated cells.

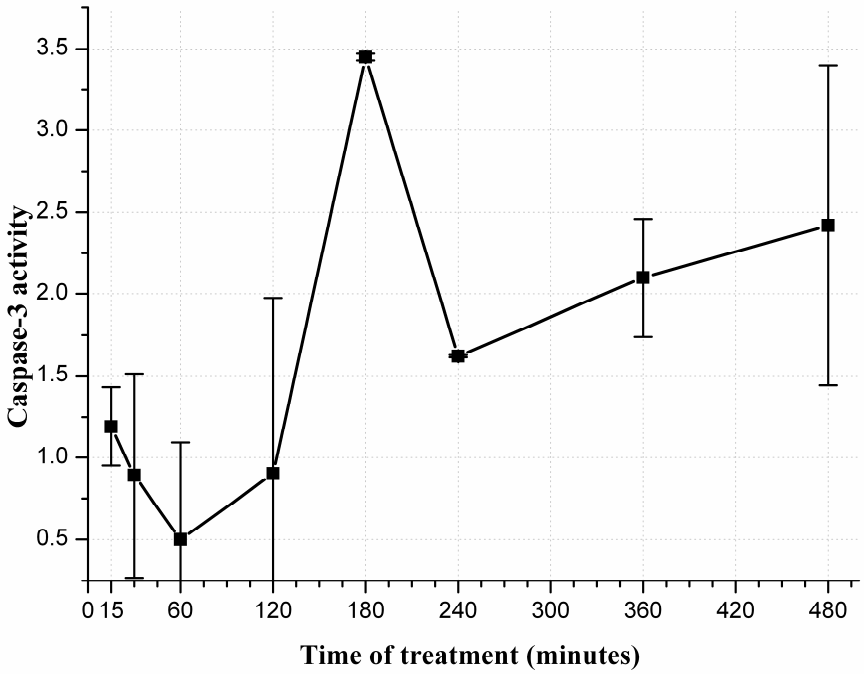

Figure 3.3 Time course of the pro-apoptotic effect of Apo2L/TRAIL in osteosarcoma cells 143B.TK$^-$. 3 x 10^5 cells were incubated for the shown time points with 1000ng/ml Apo2L/TRAIL. α_{C3}: *caspase-3 activity* was computed as the ratio between the measurements of caspase-3* concentration in stimulated cells and in non stimulated cells, at the end of the indicated time intervals of incubation. The values represent the average of three independent experiments. Bars: one standard deviation.

3.3.4 Time evolution of caspase-8 activity

We measured the time evolution of caspase-8* concentration following the same procedure described in *section 3.3.3* for caspase-3*. Figure 3.4 shows the *caspase-8 activity* α_{C8} as a function of the time length of treatment with Apo2L/TRAIL: α_{C8} remains nearly constant for the first 120 minutes of treatment. An increment occurs between 120 and 240 minutes, reaching the maximum value of α_{C8}=2.1. From 240 to 480 minutes the activity decreases maintaining nearly constant values for the next times of treatment. On the basis of the above equivalence, we interpret the graph as representative of the time evolution of caspase-8* concentration in a population of stimulated cells.

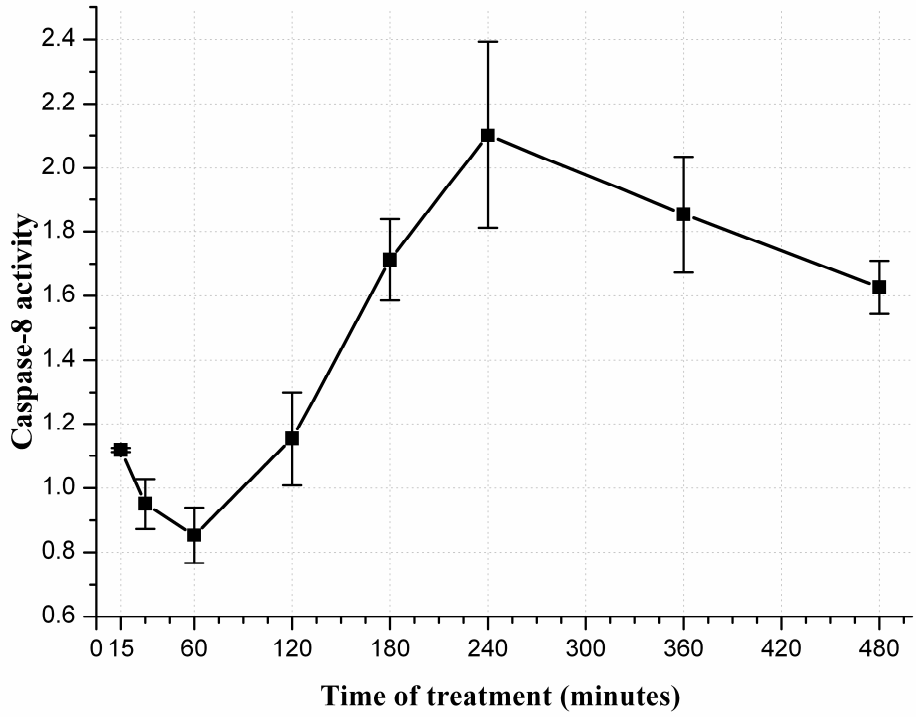

Figure 3.4 Time course of the pro-apoptotic effect of Apo2L/TRAIL in osteosarcoma cells 143B.TK$^-$. 3 x 10^5 cells were incubated for the shown time points with 1000ng/ml Apo2L/TRAIL. α_{C8}: *caspase-8 activity* was computed as the ratio between the measurements of caspase-3* concentration in stimulated cells and in non stimulated cells, at the end of the indicated time intervals of incubation. The values represent the average of three independent experiments. Bars: one standard deviation.

Figure 3.5 reports the comparison between the activities of caspase-3 and caspase-8 as a function of the time treatment with Apo2L/TRAIL. An important point must be highlighted: the time of activation of the two caspases (peaks) is different. Indeed, the activation of caspase-3 occurs nearly 60 minutes before the activation of caspase-8. From a qualitative point of view this behavior is similar to that of the model as can be seen by Figure 2.6. Also, we may note that the peak of α_{C3} is grater than the peak of α_{C8} (3.5 vs. 2.2).

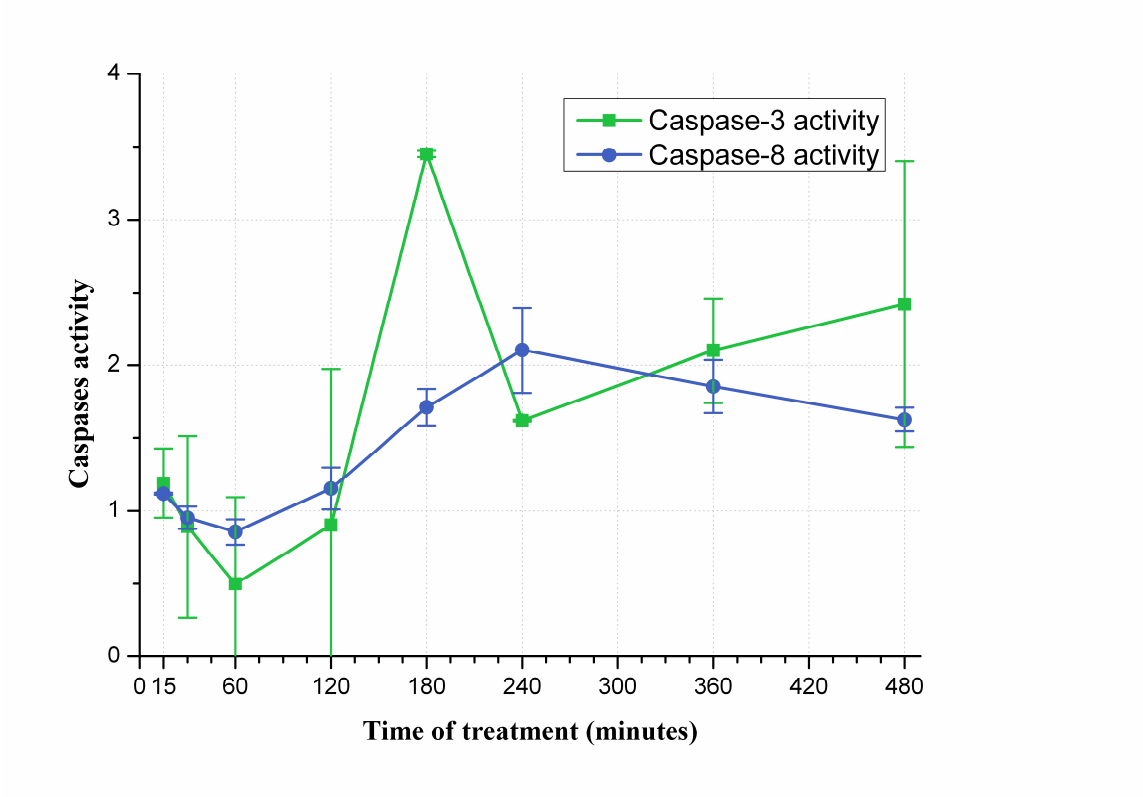

Figure 3.5 Comparison between the time courses of *caspase-8 and caspase-3 activities*. Symbols as in Figures 3.3, 3.4.

3.3.5 Phosphatidyl serine exposition

Although the final result of activation of caspases is cell death, it is important to follow caspases-dependent changes of the cell status that occur during and after their activation. One change is the translocation of phosphatidyl serine from the inner leaflet of the plasma membrane to its outer leaflet. We carried out a time course experiment in which cells were incubated in presence and absence of Apo2L/TRAIL for time intervals of different lengths. At the end of each interval translocation was detected: Figure 3.6 shows the fraction of cells positive to Annexin V test in treated and untreated cells, as a function of time treatment.

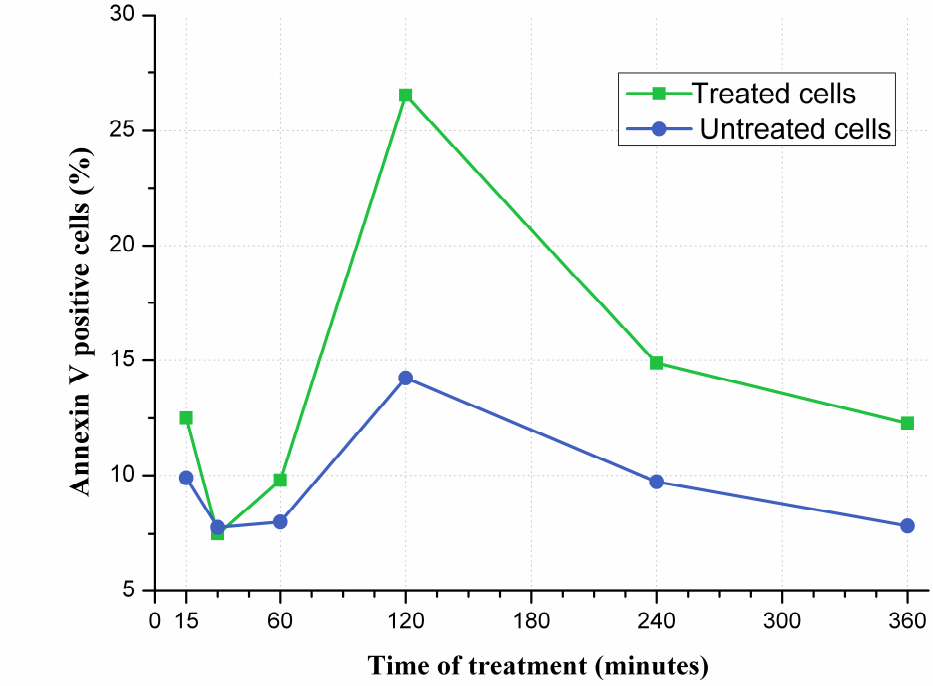

Figure 3.6 Binding of Annexin V. 2.5 x 10^5 cells were incubated with 1000ng/ml Apo2L/TRAIL for the indicated time points. Cells were collected and labeled with Annexin V and propidium iodide and then were analyzed by flow cytometry. The expositions of phosphatidyl serine is expressed as percentage of Annexin V positive cells.

The fraction of Annexin V positive cells is almost the same in both treated and untreated cells during the first 60 minutes; then it increases substantially in treated cells and reaches its maximum value (about 27%) after 120 minutes of treatment; finally it returns to its basal value after nearly 240 minutes. A small increase (about 15%) is observed also in non-stimulated cells: it may be due to the fact that all cells (treated and not treated), were subjected to the stress of synchronization which by itself may induce some level of apoptosis.

3.3.6 Determination of DNA fragmentation

Another important caspases-dependent change during the apoptotic process is the activation of endonucleases that cause the internucleosomal fragmentation of DNA. We carried out a DNA fragmentation test in which cells were incubated in presence and absence of Apo2L/TRAIL for times interval of different length (from 15 minutes to 6 hours). At each time point the cells were collected and the total DNA was extracted as

described in the Material and Methods and visualized by gel electrophoresis. Figure 3.7 shows the fragmentation pattern of untreated and treated cells at the specified times.

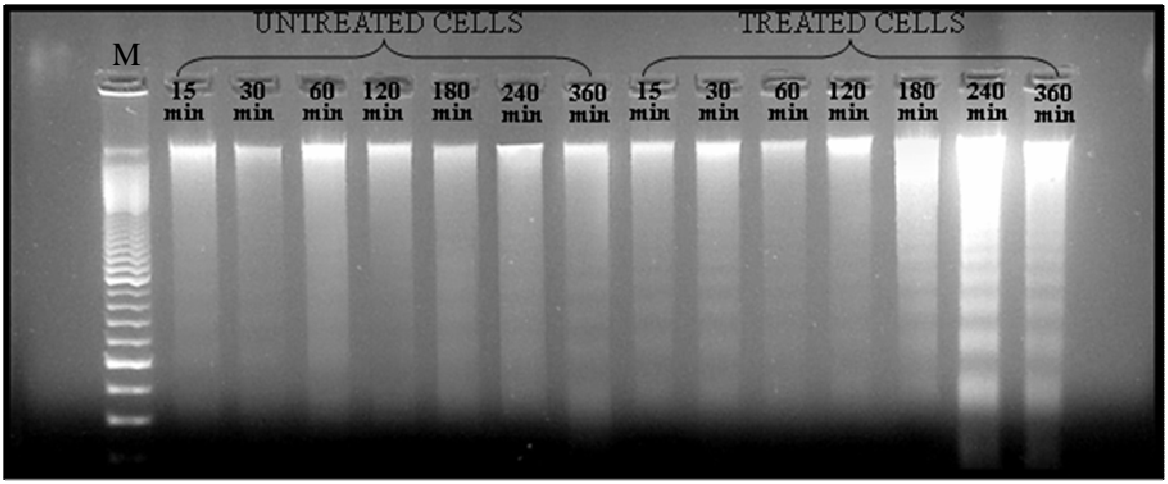

Figure 3.7 DNA fragmentation. For this analysis 3 x 10^5 cells were incubated for the shown times with 1000ng/ml Apo2L/TRAIL. At the end of each time the cells were collected and washed with PBS and the total DNA was extracted. DNA samples were loaded on a 1.5% agarose gel, electrophoresed in TAE (Tris/Acetate/EDTA) buffer and stained with ethidium bromide electrophoresis.

Only a qualitative statement can be given: it is apparent that the lanes of treated cells corresponding to 180, 240, 360 minutes show a considerable fragmentation, in comparison with the parallel lanes of untreated cells. A small level of fragmentation exists also in untreated cells, but may be regarded as "noise" background due to previous synchronization stress.

3.3.7 Cell mortality

The activation of caspase-3 and caspase-8, the exposition of phosphatidyl serine and the fragmentation of DNA are specific hallmark of cells that underwent apoptosis. To complete the picture of this process the effect of Apo2L/TRAIL on cell mortality is here analyzed. Figure 3.8 shows the fraction of dead cells at the end of different intervals of treatment, together with the fraction of dead cells in control populations. For time intervals up to 120 minutes the cell mortality is almost the same in both treated and untreated cells. Then treated cells show an increase up to a value of 60% within 720 minutes. On the contrary, the fraction of dead cell in the untreated population does not exceed 34% for all time intervals.

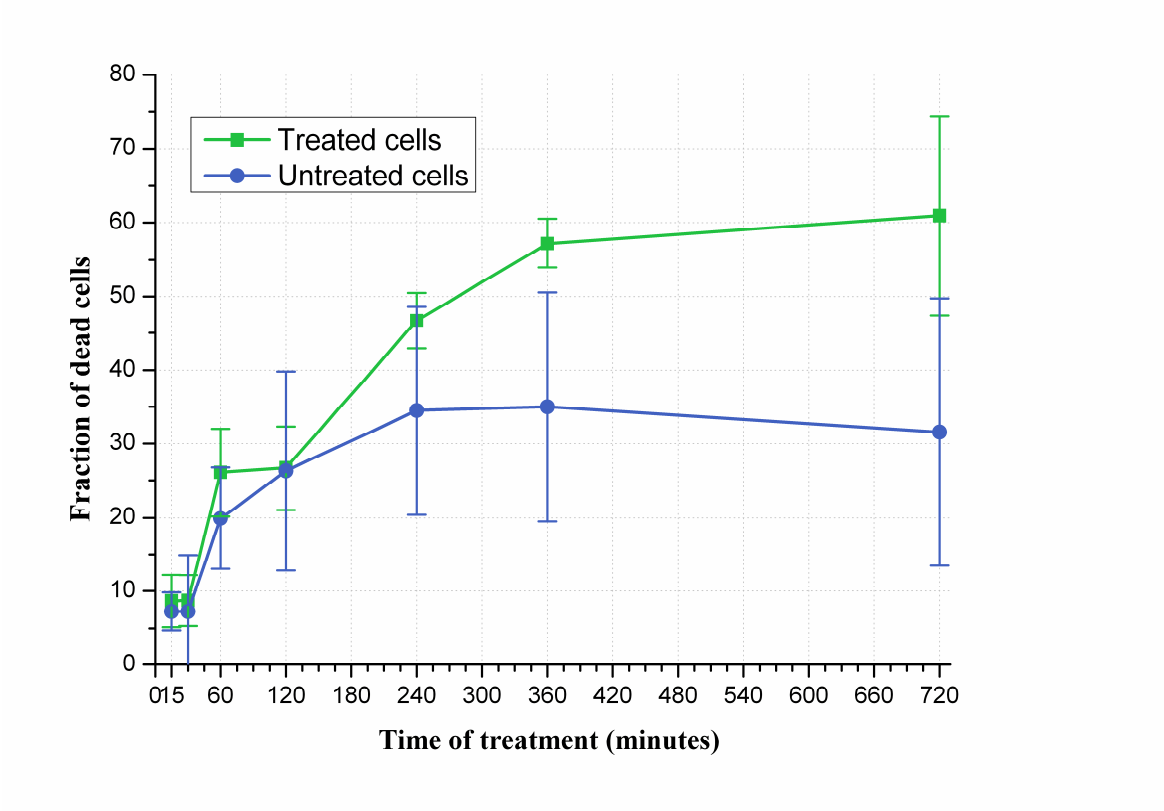

Figure 3.8 Fraction of dead cells after treatment with 1000ng/ml Apo2L/TRAIL. 3 x 10^5 cells were seeded in 6-well plates, allowed to adhere for 12 hours, washed in PBS and incubated in serum-free medium for 36 hours. After this period the cells were incubated in the absence (blue line) or presence of 1000ng/ml of Apo2L/TRAIL (green line) for the indicated time points. Cell death for each time point was assessed by counting living versus dead cells by trypan blue exclusion assay. The values represent the average of three independent experiments. Bars: one standard deviation.

3.3.8 Role of BAR on apoptosis: gene silencing

As pointed out in the *section 1.2.5*, BAR protein acts on the apoptotic process by reversibly binding caspase-8*: in this way the initiator caspase-8 is prevented from activating the effector caspase-3. In the model previously introduced the effect of changing the supply rate of BAR was investigated (*Section 2.5*): in particular it was noticed that low values of the production rate make the model response (in terms of [C3*]) much faster. To address the question whether the inhibition mechanism hypothesized for BAR and analyzed in the model works *in vivo*, we carried out several experiments on cells where the *BAR* gene was silenced.

We first tested the ability of siRNA to reduce the endogenous level of the *BAR*-mRNA in the osteosarcoma 143B.TK$^-$ cells. Cells were transfected *in vitro* with BAR-siRNA at a concentration of 5 nM. Thus, mRNA levels were determined by a semi-quantitative

RT-PCR by using as template total RNA isolated from transfected osteosarcoma cells. No reduction of *BAR* mRNA levels was observed at 24 and 48 hours after transfection (data not shown). On the contrary, we can see a significant reduction of around 80% of *BAR*-mRNA at 72 hours after the beginning of transfection (Figure 3.9).

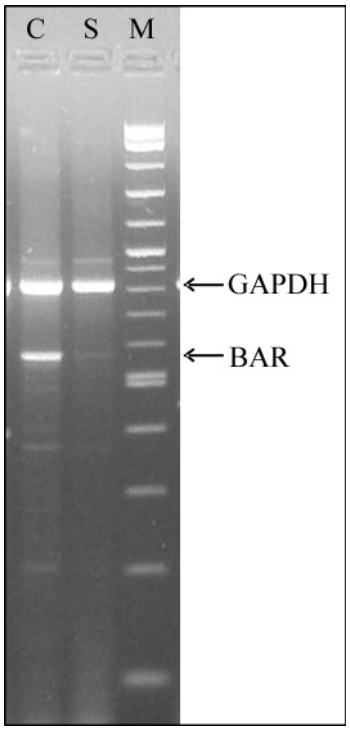

Figure 3.9 Effect of small interfering RNA (siRNA) transfection on *BAR* mRNA levels in osteosarcoma cells 143B.TK$^-$. 2 x10^5 cells were incubated with BAR-siRNA (Quiagen) for 72 hours. C: non-silenced cells (control cells); S: *BAR*-silenced cells; M: marker. The expression level of *BAR* was evaluated as described in *Materials and Methods*.

Before starting with caspase-3* analysis, we carried out preliminary experiments to evaluate a) the effect of Apo2L/TRAIL on *BAR*-mRNA levels in non silenced cells and b) the effect of Apo2L/TRAIL on *BAR*-mRNA levels in silenced cells.

As for point a), we treated osteosarcoma 143B.TK$^-$ with Apo2L/TRAIL for time intervals of different length. Then we evaluated *BAR*-mRNA levels by RT-PCR. Figure 3.10 shows a representative electrophoresis pattern of *BAR*-mRNA levels in non-silenced cells stimulated with Apo2L/TRAIL. Figure 3.11 shows the densitometer analysis of *BAR*-mRNA levels normalized with respect to *GAPDH*-mRNA levels. We observed a regular decrease of *BAR*-mRNA levels by increasing the treatment time up to 180 minutes; after 240 minutes of Apo2L/TRAIL treatment, the level of *BAR*-mRNA has become negligible. This result suggests a direct role of the inductor Apo2L/TRAIL

on the regulation of expression of *BAR* gene. Such phenomenon is not reported in the literature, and of course is not kept into account by the model: however it is known that Apo2L/TRAIL acts on other regulator proteins such as Bcl2 family members (Schaefer et al., 2007).

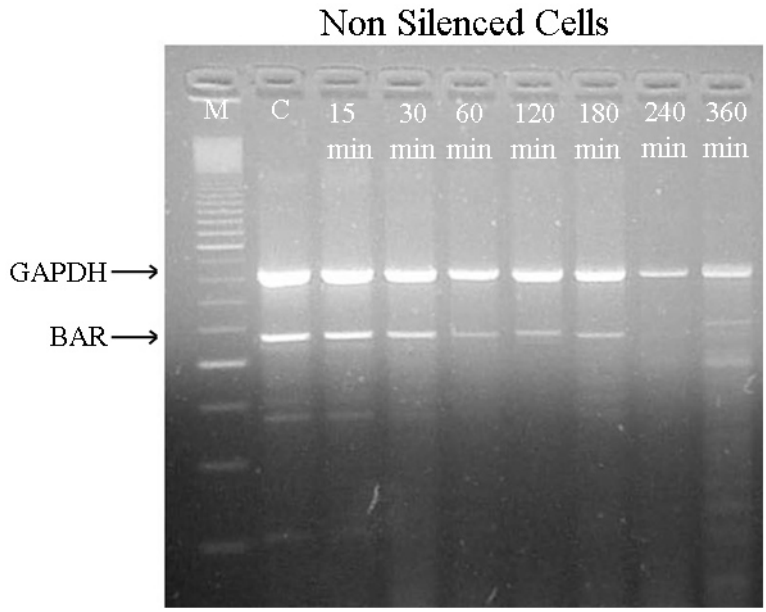

Figure 3.10 Effect of Apo2L/TRAIL on *BAR*-mRNA levels in non silenced osteosarcoma cells 143B.TK$^-$. For this analysis, for each sample, the cells were collected and the total RNA was extracted. Reverse Transcriptase reaction was performed to create cDNA. Then we carried out a semi-quantitative PCR experiments to evaluate *BAR*-mRNA levels at different times and conditions.

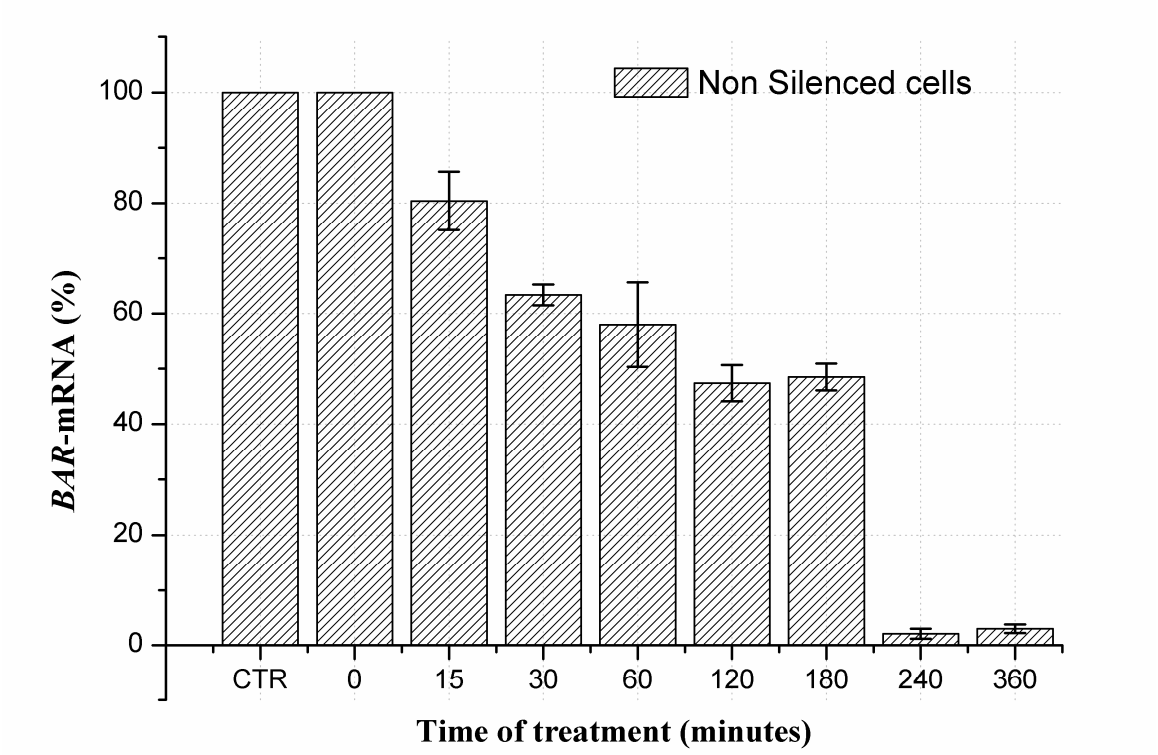

Figure 3.11 Effect of Apo2L/TRAIL on *BAR*-mRNA level. 2.5 x 10^5 were incubated for different times with 1000ng/ml Apo2L/TRAIL. For each time *BAR*-mRNA levels were analyzed as described in *Materials and Methods*. *BAR*-mRNA levels are reported as ratio between *BAR*-mRNA and *GAPDH*-mRNA levels for each time treatment with Apo2L/TRAIL. The values represent the average of three independent experiments. Bars: one standard deviation.

As for point b), 143B.TK$^-$ cells were silenced with BAR siRNA at 5nM for 72 hours and incubated with Apo2L/TRAIL for time intervals of different length. Then we evaluated *BAR*-mRNA levels by RT-PCR. Figure 3.12 shows a representative electrophoresis pattern of *BAR*-mRNA levels in silenced cells stimulated with Apo2L/TRAIL (Fig. 3.12). Figure 3.13 shows the densitometer analysis of *BAR*-mRNA levels normalized for control *GAPDH*-mRNA levels (Fig. 3.13). As expected, silencing produces a remarkable decrease (more than 60%) of the level of *BAR*-mRNA in untreated cells. This level remains constant for short treatments, and a further decrease is observed by increasing the stimulation time.

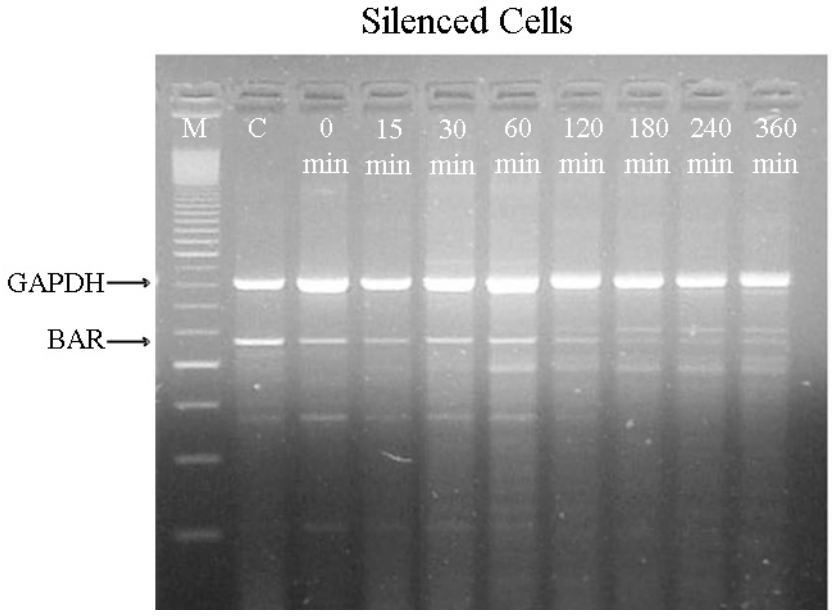

Figure 3.12 Effect of Apo2L/TRAIL on *BAR*-mRNA levels in silenced osteosarcoma cells 143B.TK$^-$. For this analysis, for each sample, the cells were collected and the total RNA was extracted. Reverse Transcriptase reaction was performed to create cDNA. Then we carried out a semi-quantitative PCR experiments to evaluate *BAR*-mRNA levels at different times and conditions.

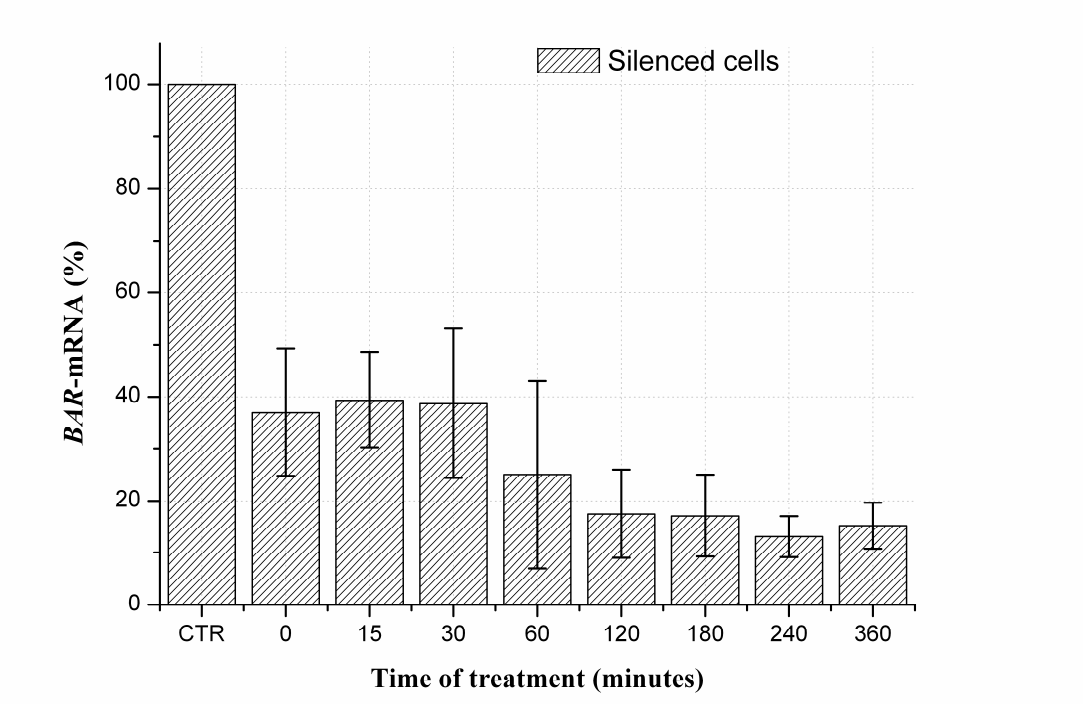

Figure 3.13 Effect of BAR-siRNA and Apo2L/TRAIL on *BAR*-mRNA level. 2.5 x 10^5 cells were incubated with BAR-siRNA for 72 hours. 1000ng/ml Apo2L7TRAIL were added 360, 240, 180, 120, 60, 30, 15 minutes before the end of 72th hours for each sample when the measurements were taken. Total RNA was extracted and levels of *BAR*-mRNA were analyzed as described in *Materials* and *Methods*. *BAR*-mRNA levels are reported as ratio between *BAR*-mRNA and *GAPDH*-mRNA levels for each time

treatment with Apo2L/TRAIL. The values represent the average of three independent experiments. Bars: one standard deviation.

The following step was the measurement of caspase-3* in *BAR*-silenced and non silenced cells stimulated with Apo2L/TRAIL. In this case, synchronized cells were divided into two distinct groups. The first group was incubated for 72 hours in absence of BAR-siRNA; in the second group *BAR* was silenced as described before. Note that during this time interval cells in both groups undergo cellular processes that can modify their response. Then the results of experiments on non-silenced cells are not quantitatively comparable with the results of the former set of experiments, where cells were not incubated for such a long time. In both groups of cells the stimulation with Apo2L/TRAIL began at defined time points before the end of the 72 hours of incubation, when measurements were taken.

Figure 3.14 shows the caspase-3* activity in silenced and non-silenced cells, expressed as the percentage of FITC-DEVD-FMK positive cells (see *Materials and Methods*), as a function of time treatment with Apo2L/TRAIL. Note that this definition is different from that used in the former series of experiments.

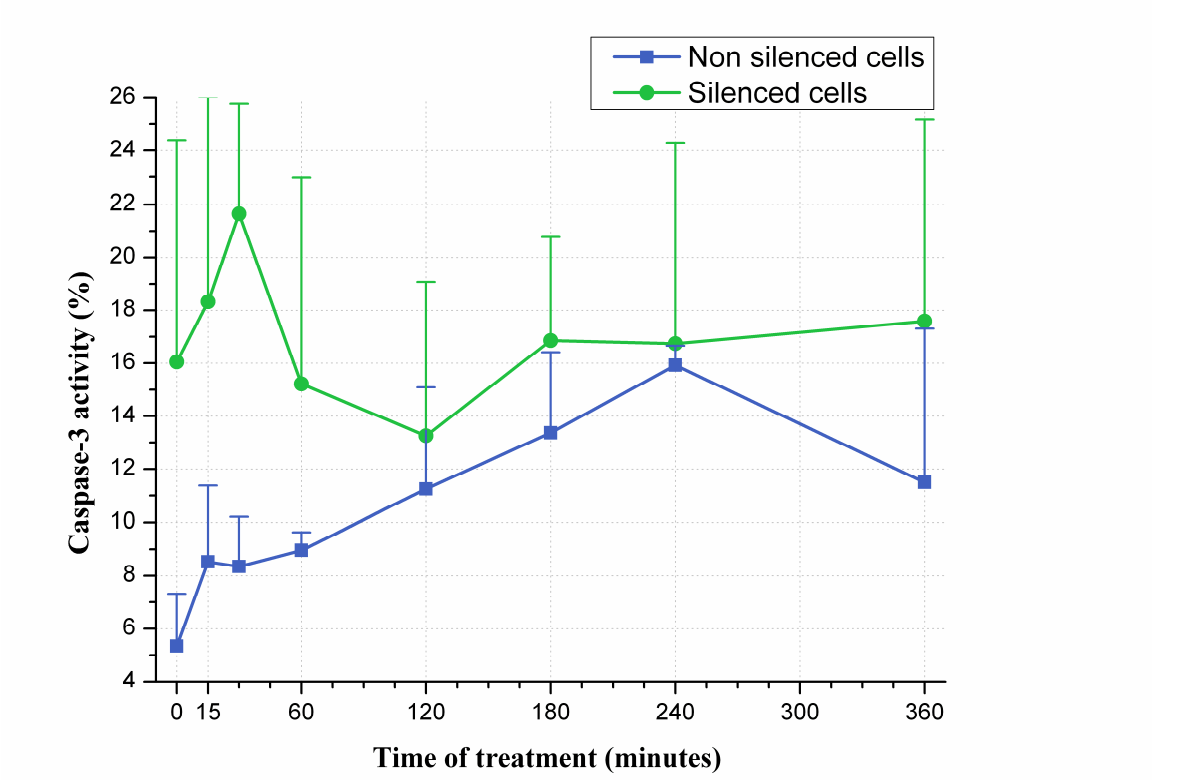

Figure 3.14 Effect of Apo2L/TRAIL in silenced and non silenced cells on caspase-3 activity. caspase-3 activity was measured in silenced and non silenced cells at different times of treatment with 1000ng/ml Apo2L/TRAIL as described in *Materials and*

Methods. caspase-3 activity is reported as percentage of positive cells to FITC-DEVD-FMK as a function of times treatment revealed by flow cytometry. The values represent the average of three independent experiments. Bars: one standard deviation.

This representation (different from the ratio used in Figure 3.3) makes clearer the comparison between silenced and non-silenced cells. For the sake of clarity, the points labeled as "0" give the caspase-3 activity measured after 72 hours of incubation on cells not subjected to treatment; the points at 15 minutes give the caspase-3 activity measured after 72 hours of incubation on cells which had been subjected to a 15-minutes treatment before the expiring of the incubation; the points at 30 minutes give the caspase-3 activity measured after 72 hours of incubation on cells which had been subjected to a 30-minutes treatment before the expiring of the incubation and so on.

In non-silenced cells we observe a significant peak of caspase-3* occurring after 240 minutes of treatment. Where silenced cells are concerned the standard deviation of measurements is high: however the caspase-3* level has a clear maximum at 15-30 minutes of treatment, much earlier than in non-silenced cells, after which the level is nearly constant at values higher than those of non-silenced cells. The activation of caspase-3 seems to demand a shorter interval of stimulation when *BAR* is silenced. This result is in line with the mathematical model prediction, and confirms that silenced cells are more responsive to TRAIL treatment than non-silenced ones.

As mentioned above, the late event of apoptosis is the internucleosomal DNA fragmentation. Thus, in order to analyze this event at the same time of caspase-3 activation, we performed a fragmentation assay in silenced and non-silenced cells.

Figure 3.15 shows the fragmentation pattern of non silenced and silenced cells treated with Apo2L/TRAIL at the specified times.

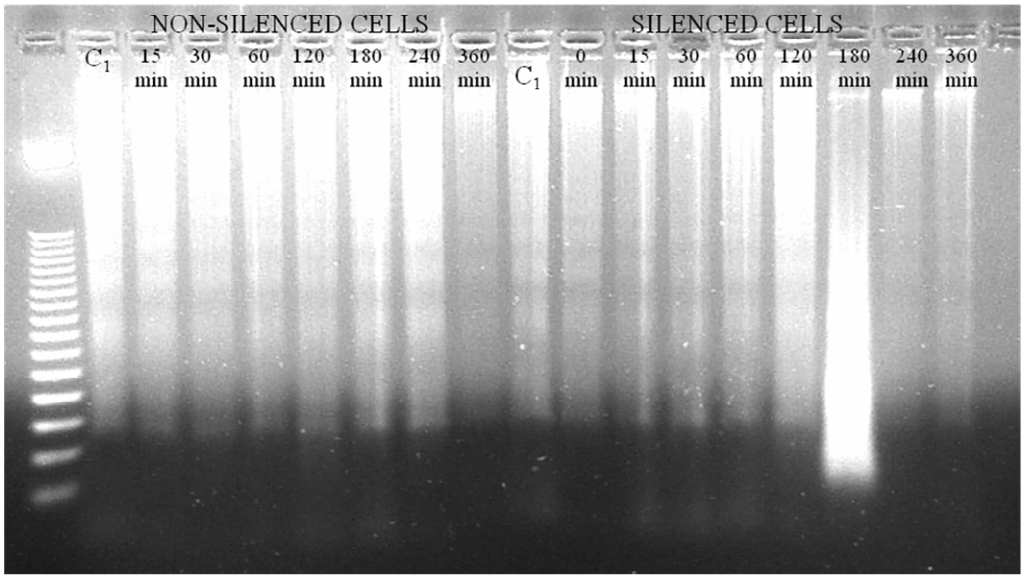

Figure 3.15 DNA fragmentation. The lanes "C" contain the DNA samples extracted from non stimulated and non silenced cells (control cells). The lane "0 min" contains the DNA extracted from silenced and non-stimulated cells. The other lanes contain the DNA extracted non-silenced and silenced cells treated for time interval of different length with Apo2L/TRAIL.

Internucleosomal fragmentation exists in both non silenced and silenced cells, demonstrating that the apoptosis process occurs in these cells. But the lanes of silenced cells corresponding to 180, 240, 360 minutes show a smear of DNA, representing pieces of genomic DNA that are degraded into a series of smaller fragments in random way and not in internucleosomal-specific way.

To complete this picture in which BAR seems to be an important key, we evaluated if there are differences in cell mortality between silenced and non-silenced cells exposed to Apo2L/TRAIL.

Figure 3.16 compares the fraction of dead cells in the silenced and non-silenced conditions as a function of time treatment with Apo2L/TRAIL.

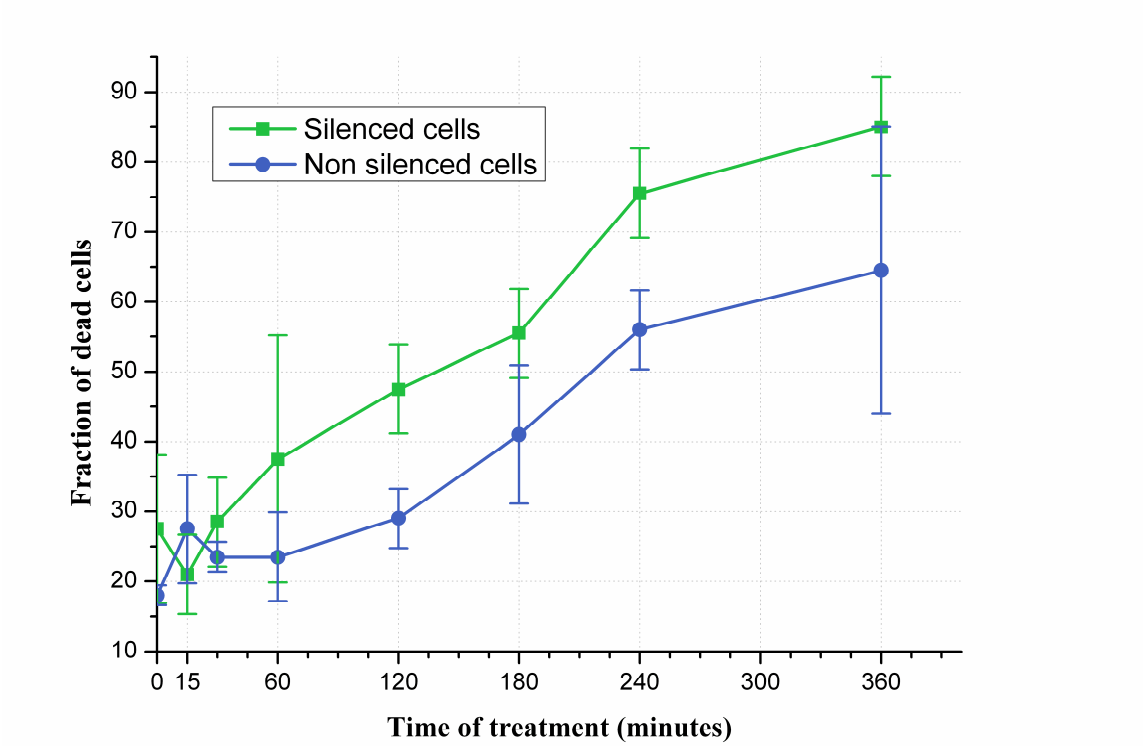

Figure 3.16 Fraction of dead cells in silenced and non-silenced cell groups, after Apo2L/TRAIL treatments of different time length. Cell death for each time point was assessed by counting living versus dead cells by trypan blue exclusion assay (see *Materials and Methods*). The values represent the average of three independent experiments. Bars: one standard deviation.

Both silenced and non-silenced cells show the same fraction of dead cells in the first 30 minutes; a relevant increase of this fraction (from 35% to 55%) is observed in silenced cells between 60 and 180 minutes of treatment, after which the percentage reaches 95% after 360 minutes. In non-silenced cells an increase from 25% to 40% occurs between 60-180 minutes of treatment, resulting nearly around 70% after 360 minutes.

The qualitative shape of the experimental fraction of dead cells is in agreement with the curves of Figure 2.13, obtained by model simulation.

4. Discussion

"A cell, an organ, or organism, understood as a "system", is a network of components whose relationships and properties are largely determined by their function in the whole. The functionality is observed as the "behaviour" of the system. The first and probably most important lesson of systems theory is that we can only understand the behaviour of a system if we systematically perturb it and record it response." This sentence from a recent paper entitled *Defining Systems Biology: an Engineering Perspective* (Wolkenauer, 2007) published in the July 2007 issue of the Journal *IET Systems Biology* well captures the approach behind the present work. Regarding the integrative study of biological systems and the way they respond to external perturbations as the essence of systems biology is not a new idea (Auffray et al., 2003). Such an approach leads to hypotheses formalized in mathematical models: on the one hand these models are built from the results of studies about functional genomics, protein-protein interactions, signalling and metabolic pathways. On the other hand, since a systems approach is characterized by input/output descriptions relating stimuli (inputs) to responses (outputs) "the most important role of the modeller in system biology is to support the design of stimulus/response experiments" (Wolkenauer, 2007).
In this work the paradigm outlined above has been applied to apoptosis, a very important physiological process normally occurring in cells, and whose malfunction has been related to severe pathologies such as cancer and neurodegenerative diseases. Apoptosis involves a very complex interplay between several pathways: aim of the work is to gain a better understanding of one of these pathways and to validate/falsify some hypotheses on the underlying molecular mechanisms. To attain the objective two routes have been followed: construction, analysis and simulation of a dynamic mathematical model (Chapter 2), and implementation of *in vitro* experiments, designed according to guidelines in part provided by the analysis of the model (Chapter 3).
In the cascade of events that characterizes the apoptotic process we focused the attention on the first fundamental step, the activation of caspases. The choice was motivated by the observation that this step was the best studied, from the phenomenological point of view, among those which form the cascade. Moreover several mathematical models describing different aspects of the process had been proposed and discussed by various research groups. Even if the attention is restricted to the activation of caspases, an extremely complex landscape still appears: then we

considered, at the level of mathematical modeling, only the extrinsic pathway which leads to the production of active caspase-3 starting from the binding of suitable ligands to receptors on the exterior of the cell membrane. We did not build up a new model: rather we considered the more complex of the two models proposed by Eissing and coworkers (Eissing et al., 2004). The reason of this choice is that this model, although simple enough to allow an analytical study and a large number of numerical simulations, incorporates three phenomena probably critical in the evolution of the process. These phenomenon are: *activation of procaspase-8 by the external stimulus→ activation of procaspase-3 by active caspase-8*; a positive feedback loop, by which active caspase-3 activates procaspase-8;

the concentration of active caspase-8 is controlled by the reversible formation of an inactive complex with the inhibitor protein BAR; the concentration of active capase-3 is controlled by the reversible formation of an inactive complex with the inhibitor protein IAP.

The model consists of a system of eight ordinary differential equations in the concentrations of the species taken into account (state variables): the solution of such equations provides the time evolution of the state of the system. Reaction rates, decay rates and production rates are assumed as simple as possible: this implies that the equations contain only constant, linear and bilinear terms. Another modeling assumption regards the external stimulus: from the binding of the ligand to the activation of initiator procaspase-8 a complex sequence of reactions occurs. In fact we summarize all the process either into a change of the initial state of the model, in which an amount of active caspase-8 appears, or into the continuous production of active caspase-8 (input to the model) for a given time interval: the first choice represents a transient stimulus, the second a persistent stimulus. In the literature (Eissing et al., 2004, 2005) only the transient stimulus, represented as a change of the initial state is considered: the analysis of the effect of a persistent stimulus is new.

Obviously many known interactions with other proteins are overlooked, more complex reaction kinetics are not considered, but a model is necessarily an abstract, partial and approximate representation of the reality: what we may expect by the comparison between model predictions and experimental results is a validation of the main assumptions on which the model is based.

As regards the formal properties of the model, although some suggestions may come from models of other biological processes or from the numerical simulations, the results

of the equilibrium and stability analysis are new. In the absence of persistent stimulus, the system may have one, two or three equilibrium states, depending on model parameters (reaction constants, decay coefficients, production rates). To evaluate the actual occurrence of the patterns, we generated 100000 parameter vectors (models) in a neighborhood of a set of parameters given in Eissing et al., 2004 (the *nominal* model) and numerically evaluated the respective equilibrium patterns: all the patterns were present in the "sample", with a prevalence of models with two equilibria (type 2 models), followed by models with three equilibria (type 3 models). One of the equilibria is characterized by the absence of active caspases, and has been called the *life* equilibrium. From the theoretical analysis we have that if the *life* equilibrium is the unique equilibrium state (type 1 models), it is asymptotically stable, i.e. the time evolutions of the state variables converge to it. If there exist two equilibria, the *life* one is unstable, i.e. any perturbation moves the state away from it. The other equilibrium state, which is characterized by non-zero concentrations of active caspases, can be either asymptotically stable or unstable: the first case is by far the most common in the set of randomly generated models, and suggests that the state trajectories that leave the *life* equilibrium converge to it. The few cases in which both equilibria are unstable are characterized by oscillating trajectories. If the model has three equilibria, the *life* one is again asymptotically stable; in most of the randomly generated models which show three equilibria also one of the remaining is asymptotically stable, and the other is unstable. This pattern is denoted by the term "*bistable*": much emphasis has been given in the literature to *bistability*, not only in the study of apoptosis (Eissing et al., 2004, 2005, Bagci et al., 2005), but as "an important recurrent theme in cell signaling" (Angeli et al, 2004). The reason is that the behavior of a bistable model seems to reproduce qualitatively the expected behavior of a normal living cell: assume that the model is in the *life* equilibrium, and that an increment is given at the initial time t=0 to the state variable representing active caspase-8. If the perturbation is below a certain threshold, the evolution of the variables returns, after a transient, to the *life* equilibrium; if the perturbation is above the threshold the trajectory "jumps" beyond the unstable equilibrium, falls irreversibly into the basin of attraction of the second stable equilibrium, and converges to it. Likewise we expect that a cell is not moved to apoptosis if the external stimulus is not able to induce a substantial amount of active caspase-8. On the contrary, if the stimulus is appropriate, we expect that the process goes on to the production of a sufficient amount of active caspase-3, which in turn

elicits the subsequent pathways. However the analogy is not complete because the "equilibrium" is a property of the model and not of the real system: a model remains indefinitely in the equilibrium state, whereas the cell cannot stay for a long time in a situation characterized by a high concentration of active caspase-3. As a bistable model may represent a normal cell, a model with only the asymptotically stable life equilibrium may be regarded as representative of a cell refractory to apoptosis, and possibly prone to cancer transformation: even a large perturbation ultimately vanishes. An obvious criticism to this analogy is that we cannot exclude that during the transient phase of the evolution the variable representative of the active caspase-3 concentration reaches a sufficiently high value, for a sufficiently long time interval. At last a model with unstable *life* equilibrium and asymptotically stable *non-life* equilibrium may be taken as representative of a hypersensitive cell, which undergoes apoptosis even in the presence of very small stimuli. However, as in the case of bistable models, the assumption that the *non-life* asymptotically stable equilibrium represents the "apoptotic status" may be inappropriate if the level of activation of caspase-3 is not sufficiently high.

In the presence of a constant persistent stimulus, an equilibrium characterized by the absence of active caspases (*life*) does not exist, and the equilibrium pattern depends on the level of the stimulus. In most models of type 1 the equilibrium remains unique, with a low value of active caspase-3. In models of type 2 the unstable *life* equilibrium disappears and the other equilibrium remains at almost the same value. Bistable models maintain this property only for low values of the stimulus; when the stimulus increases, only one asymptotically stable equilibrium remains.

Several points of the above discussion emphasize that the static description of the equilibrium points and of their stability properties is not sufficient to characterize the model behavior and its biological plausibility: the dynamics of the process cannot be overlooked, both for the model and for the biological system.

The dynamic behavior of the model was analyzed by numerically solving equations (1)-(8) for the nominal and the 100000 randomly generated models, both as response to the transient stimulus, and as response to constant persistent stimuli of variable length and intensity. A wealth of qualitative and quantitative differences have been observed in the response of models with different parameters. However some features of the model responses are common to all cases: apart from the few cases of oscillatory behavior, we observe a "decision phase", during which the variables representing active caspases

concentrations are at very low levels. For a given parameter set, the duration of this phase depends on the intensity (and possibly duration of the stimulus). At the end of this phase an increase of the concentration of active caspases occurs: this increase may lead within a few minutes (activation phase) to a peak of concentrations up to values of thousands of molecules/cell, or the increase is negligible and the trajectory settles to very low (or vanishing) values of the concentration of active caspases. When the response shows a significant peak of active caspases the maximum concentration value and the duration of the activation phase are almost independent of the level of the stimulus. Typical shapes of the active caspase-3 response are in figures 2.5a, 2.7. Apart from these general qualitative features, the quantitative results of the simulations of the randomly generated models show a wealth of possible behaviors, even if each parameter may vary at most by a factor of twenty. Indeed in the region of parameter space under examination the peak value during the response to the stimulus may vary of five orders of magnitude, as well as the steady state value of [C3*] at the asymptotically stable *non-life* equilibrium. Also the duration of the decision phase for a given initial perturbation may vary from dozens of minutes to days.

The wide variability of relevant features of the model response, also within a class of models which exhibit the same equilibrium and stability pattern, suggests to critically evaluate the role of the obvious classification: *bistable* models, *monostable* models with stable or unstable *life* equilibrium, and the associated biological interpretation. If we assume that a level of some thousands molecules per cell of C3* attained for a time interval of few minutes is necessary and sufficient to irreversibly start up the cleavage of downstream proteins and DNA fragmentation, then some important remarks arise from the results of the simulations of *Section 2.4*:

- instability of the *life* equilibrium of a model does not imply that a cell corresponding to that model is appointed to apoptosis, because the concentration of active caspase-3 may not reach the threshold: out of 50263 type 2 models with asymptotically stable *non-life* equilibrium, 11230 models (22.3%) have responses to an initial transient perturbation $[C8^*]_{IN}$=1000 *mol/cell* with peak values $[C3^*]_{Max}$<8000 *mol/cell*;
- a model with the sole, asymptotically stable *life* equilibrium may represent a cell in which the caspase-activation cascade takes place over meaningful time intervals, provided that the external stimulus is sufficiently high: 800 models of type 1 (5.5% of the model of this type in the sample) have responses with peak values

$[C3^*]_{Max}$>8000 *mol/cell*, for an initial transient perturbation $[C8^*]_{IN}$=10000 *mol/cell*;

- in the sub-sample consisting of the bistable models only 48% of the responses to the initial perturbation $[C8^*]_{IN}$=10000 *mol/cell* attain the activation phase within 36000 min from the application of the stimulus, and 10% of these responses show peak values lower than 8000 *mol/cell*.

The qualitative and quantitative variability highlighted by the numerical experiments may be interpreted as the variability that we observe in single cells of a population: how can we characterize the collective behavior? Two numerical experiments have been performed, one trying to reproduce the time progression of the fraction of dead cells in a rather homogeneous population, the other which evaluates the mean value of [C3*] in a number of randomly chosen groups of models, subject to persistent stimuli of the same intensity, and different duration (15-360 minutes). The results show that the variability is smoothed out and salient features can be found both in the mortality curves and in the mean values of [C3*]. This remark is important because the *in-vitro* experiments reveal only collective properties of the cell culture and average values of the measured quantities.

In conclusion, we believe that the static behavior (pattern of equilibrium states and respective stability properties) is not sufficient to qualify a model as suited to represent the extrinsic caspase activation pathway: the dynamical response cannot be overlooked, and its relevant features (peak value of active caspase-3 concentration, delay between the application of the stimulus onset of the activation, attainment of the peak) must be kept into account when evaluating a model.

The sensitivity of static and dynamic properties of the model to parameter changes indicates that the reactions involving the inhibitors BAR and IAP play a fundamental role in determining the equilibrium patterns and the features of the response. Indeed a comparison between models with “high” and “low” peak values of the active caspase-3 response shows that “high” values are associated to high values of k_{-3}, k_{-11} (dissociation rates of the complexes), k_4 (cleavage of IAP), and low values of k_3, k_{11} (formation of complexes), k_7, k_{13} (decay of complexes), k_{-8}, k_8 (production and decay of IAP). This remark suggested to investigate more closely the role of inhibitor proteins: in particular we analyzed static and dynamic properties of the nominal model where only the production rate of BAR (IAP, respectively) is changed, because in a living cell such rate is genetically controlled, and can be experimentally modified by the silencing RNA

method. The main result is that, with an appropriate stimulus, the variation of BAR production essentially affects the delay of the activation phase: lower rates produce faster responses. As regards IAP, it affects not only the delay, but also the level of the peak concentration, in an almost linear fashion. Such effects on the timing of the process had been pointed out experimentally for IAP by Rhem et al., 2006, whilst the result for BAR is new.

Consistently with the relevance of the dynamical behaviour highlighted by the study of the model, the *in-vitro* experiments described in Chapter 3 were designed to study the time evolution of active caspases in suitably chosen cell populations. A preliminary remark is here necessary: only a qualitative comparison can be made between the results of the theoretical and numerical analyses of the model and the results of *in vitro* experiments. Indeed the experimental procedures impose severe limitations which make an *in vitro* experiment very different from a conceptually identical experiment performed *in silico*: *a*) the cells are subjected to continuous changes due to the normal cell cycle; *b*) the cells are continuously subjected to random external perturbations, that the experimenter cannot control; *c*) in all the experiments (time courses of caspases activity, phosphatidyl serine exposition, DNA fragmentation, cell mortality) the measurements that correspond to treatments of different time length are carried out on different subgroups of cells, although derived from the same initial population. On the other hand the model takes into account only the reactions which are regarded as the most relevant in the pathway; it does not consider all the other processes that occur in the cells, and that are "disturbances" from the model point of view.

The experimental setup was chosen in such a way that the above sources of uncertainty and lack of homogeneity be reduced, but it is impossible to eliminate them. For instance, in order to obtain an experimental system as homogeneous as possible, we synchronized osteosarcoma cells in G0/G1 phase. However, the test revealed that about 20% of the cell population was out of phase. Moreover, the synchronization treatment, which consists of serum deprivation for 36 hours, induces by itself apoptosis in a fraction of cells. However, the vital state of the population as a whole is not seriously impaired because the fraction of dead cells remains around 30% for the first 12 hours after the synchronization treatment. Note that the model does not consider in any way the cell cycle or the events that lead to the death of a cell after caspases activation; moreover it assumes that in *normal conditions* (the *life* equilibrium) no cell in the population undergoes apoptosis.

Apoptosis was elicited by treating the synchronized cell populations with an appropriate concentration of Apo2L/TRAIL. We chose this inductor because it acts on cancer cells (such as osteosarcoma cells).

As regards the time course of events in the pathway, as resulting from the measurements taken on cell subpopulations after treatments with Apo2L/TRAIL for different time intervals we observe:

- for the first 60 minutes no difference exists between treated and untreated cells;
- after this time interval there is an increase of phosphatidyl serine exposition, followed by a subsequent increase of caspase-3 activity and caspase-8 activity: these three apoptotic indicators reach the maximum value at 120, 180, 240 minutes respectively. The fact that phosphatidylserine exposition forestalls full activation of caspases is in line with the known mechanisms of the whole apoptotic process. As to the relationship between caspase-3 and caspase-8 activation, the model response predicts that the peak of [C3*] occurs earlier than the peak of [C8*] (Figure 2.14), as a consequence of the positive feedback of active caspase-3 on procaspase-8; DNA fragmentation experiments suggest that a substantial fragmentation is reached after 240 minutes of treatment.
- for the first 120 minutes the fraction of dead cells (as revealed by the Trypan-Blue exclusion assays) in treated samples is not different from the fraction of dead cells in controls; only after 120 minutes the mortality in treated samples systematically exceeds that in non treated cells. This behaviour qualitatively agrees with the trend of "mortality" that the model predicts in a population of *virtual cells* (Figure 2.13): the fraction of *virtual cells* which undergoes the transition to *virtual apoptosis* is very low for an initial time interval, then increases to reach a value which remains constant for the subsequent time.

From these observations the following course of events appears: an external perturbation is imposed on an extremely variable biological system; the perturbation induces the activation of a process which produces a response that can be recorded *in vitro*, with a specific timing of the various phases. The response of the cells can be compared with the simulation results: although *in vitro* and *in silico* experiments are deeply different, we have verified a good qualitative agreement between the dynamical simulation of caspase-3* and caspase-8* and their real temporal changes in stimulus response experiments. On the basis of this agreement we can assert that the processes underlying the model assumptions (positive feedback, action of inhibitors) are the most

important in shaping the time course of the pathway. In any case the discovery that a treatment with Apo2L/TRAIL causes the death of 60% of the osteosarcoma cell culture within about 6 hours (compare with Figure 3.1 for untreated cells) is new with respect to literature data.

The dynamical simulations in which the production rate of BAR is modified show that the time evolution of [C3*] is influenced by this parameter. We demonstrated this phenomenon *in vitro by* modulating the expression level of *BAR* in synchronized osteosarcoma cells. We first reduced the expression level of *BAR* by silencing RNA (Figure 3.9). The level of silencing that we obtained was satisfactory: since it is plausible that a low level of *BAR*-mRNA corresponds to a low concentration of the BAR protein in the cell, the experiments on silenced cells are the *in vitro* analogous of the numerical experiments with reduced k_{-12}. Before carrying out the measurements of caspase activity and of the other indicators, we compared the expression levels of *BAR* in non-silenced and silenced cells at different time intervals of treatment with Apo2L/TRAIL. It is noteworthy that the treatment with Apo2L/TRAIL causes by itself a progressive reduction of the expression level of *BAR* (Figures 3.10 and 3.11). This finding has not been reported in the literature, and is not kept into account by the model: it suggests an even major role of the BAR protein in the extrinsic apoptotic pathway triggered by Apo2L/TRAIL. Of course the expression pattern of *BAR* in silenced cells is very low, as expected, already before the Apo2L/TRAIL treatment (Figures 3.12 and 3.13).

As regards the time evolution of caspase-3* in non-silenced and silenced cells treated with Apo2L/TRAIL, the main effect of silencing is on the time of activation (Figure 3.14): we observed a faster response in silenced cells than in non-silenced cells. This phenomenon is simply explained because the level of *BAR*-mRNA, and then of BAR protein, is low just at the beginning of the treatment. Therefore the onset of the pathway occurs earlier than in non-silenced cells. Also the experimental determination of the fraction of dead cells confirms the pro-apoptotic role by *BAR* silencing: both the increase of dead cells is anticipated and the level after 6 hours of treatment is higher (85% vs. 60%).

In conclusion, the second set of experiments gave a complete picture of the effects produced by a change of the BAR inhibitor level: most of the effects were anticipated by the analysis of the model, but also a new interaction (the direct effect of Apo2L/TRAIL on *BAR* expression) has been discovered.

5. References

Abrams JM. An emerging blueprint for apoptosis in Drosophila. Trends Cell Biol. 1999 Nov;9(11):435-40.

Angeli D, Ferrell JE Jr, Sontag ED. Detection of multistability, bifurcations, and hysteresis in a large classo f biological positive-feedback systems. Procl Natl Acad Sci U S A. 2004 Feb 17;101(7):1822-7.

Aloya R, Shirvan A, Grimberg H, Reshef A, Levin G, Kidron D, Cohen A, Ziv I. Molecular imaging of cell death in vivo by a novel small molecule probe. Apoptosis. 2006 Dec;11(12):2089-101.

Ashkenazi A, Dixit VM. Apoptosis control by death and decoy receptors. Curr Opin Cell Biol. 1999 Apr;11(2):255-60.

Ashkenazi A, Dixit VM. Death receptors: signaling and modulation. Science. 1998 Aug 28;281(5381):1305-8.

Auffray C, Imbeaud S, Roux-Rouquié M, Hood L. From functional genomics to system biology: concepts and practices. C R Biol. 2003 Oct-Nov;326(10-11):879-92.

Bagci EZ, Vodovotz Y, Billiar TR, Ermentrout GB, Bahar I. Bistability in apoptosis: roles of bax, bcl-2, and mitochondrial permeability transition pores. Biophys J. 2006 Mar 1;90(5):1546-59. Epub 2005 Dec 9.

Bentele M, Lavrik I, Ulrich M, Stosser S, Heermann DW, Kalthoff H, Krammer PH, Eils R. Mathematical modeling reveals threshold mechanism in CD95-induced apoptosis. J Cell Biol. 2004 Sep 13;166(6):839-51.

Bodmer JL, Burns K, Schneider P, Hofmann K, Steiner V, Thome M, Bornand T, Hahne M, Schröter M, Becker K, Wilson A, French LE, Browning JL, MacDonald HR,

Tschopp J. TRAMP, a novel apoptosis-mediating receptor with sequence homology to tumor necrosis factor receptor 1 and Fas(Apo-1/CD95). Immunity. 1997 Jan;6(1):79-88.

Borden KL. RING domains: master builders of molecular scaffolds? J Mol Biol. 2000 Feb 4;295(5):1103-12.

Carotenuto L, Pace V, Bellizzi D, De Benedictis G. Dynamical Analysis of the Programmed Cell Death Pathway. Proceedings of the European Control Conference 2007 Kos, Greece, July 2-5, 2007a.

Carotenuto L, Pace V, Bellizzi D, De Benedictis G. Equilibrium, Stability, and Dynamical Response in a Model of the Extrinsic Apoptosis Pathway. Journal of Biological Systems, vol. 15, pp. 261-285, September 2007b.

Chai J, Shiozaki E, Srinivasula SM, Wu Q, Datta P, Alnemri ES, Shi Y. Structural basis of caspase-7 inhibition by XIAP. Cell. 2001 Mar 9;104(5):769-80.

Cox JS, Shamu CE, Walter P. Transcriptional induction of genes encoding endoplasmic reticulum resident proteins requires a transmembrane protein kinase. Cell. 1993 Jun 18;73(6):1197-206.

Cox JS, Walter P. A novel mechanism for regulating activity of a transcription factor that controls the unfolded protein response. Cell. 1996 Nov 1;87(3):391-404.

Denault JB, Salvesen GS. Caspases: keys in the ignition of cell death. Chem Rev. 2002 Dec;102(12):4489-500.

Dhein J, Walczak H, Bäumler C, Debatin KM, Krammer PH. Autocrine T-cell suicide mediated by APO-1/(Fas/CD95). Nature. 1995 Feb 2;373(6513):438-41.

Di Ventura B, Lemerle C, Michalodimitrakis K, Serrano L. From in vivo to in silico biology and back. Nature. 2006 Oct 5;443(7111):527-33.

Eissing T, Allgöwer F, Bullinger E. Robustness properties of apoptosis models with respect to parameter variations and intrinsic noise. IEE Proc Syst Biol. 2005 Dec;152(4):221-8.

Eissing T, Conzelmann H, Gilles ED, Allgöwer F, Bullinger E, Scheurich P. Bistability analyses of a caspase activation model for receptor-induced apoptosis. J Biol Chem. 2004 Aug 27;279(35):36892-7. Epub 2004 Jun 18.

Feldman DE, Chauhan V, Koong AC. The unfolded protein response: a novel component of the hypoxic stress response in tumors. Mol Cancer Res. 2005 Nov;3(11):597-605.

Fussenegger M, Bailey JE, Varner J. A mathematical model of caspase function in apoptosis. Nat Biotechnol. 2000 Jul;18(7):768-74.

Graf D, Bode JG, Haussinger D. Caspases and receptor cleavage.Arch Biochem Biophys. 2007 Jun 15;462(2):162-70. Epub 2007 Apr 10.

Green D, Kroemer G. The central executioners of apoptosis: caspases or mitochondria? Trends Cell Biol. 1998 Jul;8(7):267-71.

Green DR, Reed JC. Mitochondria and apoptosis. Science. 1998 Aug 28;281(5381):1309-12.

Ho PK, Hawkins CJ. Mammalian initiator apoptotic caspases. FEBS J. 2005 Nov;272(21):5436-53.

Hsu SL, Yu CT, Yin SC, Tang MJ, Tien AC, Wu YM, Huang CY. Caspase 3, periodically expressed and activated at G2/M transition, is required for nocodazole-induced mitotic checkpoint. Apoptosis. 2006 May;11(5):765-71.

Hunter AM, Lacasse EC, Korneluk RG. The inhibitors of apoptosis (IAPs) as cancer targets. Apoptosis. 2007 Sep;12(9):1543-1568.

Irmler M, Thome M, Hahne M, Schneider P, Hofmann K, Steiner V, Bodmer JL, Schröter M, Burns K, Mattmann C, Rimoldi D, French LE, Tschopp J. Inhibition of death receptor signals by cellular FLIP. Nature. 1997 Jul 10;388(6638):190-5.

Kerr JF, Wyllie AH, Currie AR. Apoptosis: a basic biological phenomenon with wide-ranging implications in tissue kinetics. Br J Cancer. 1972 Aug;26(4):239-57.

Kitson J, Raven T, Jiang YP, Goeddel DV, Giles KM, Pun KT, Grinham CJ, Brown R, Farrow SN. A death-domain-containing receptor that mediates apoptosis. Nature. 1996 Nov 28;384(6607):372-5.

Kroemer G, Dallaporta B, Resche-Rigon M. The mitochondrial death/life regulator in apoptosis and necrosis. Annu Rev Physiol. 1998;60:619-42.

Kurakin A, Bredesen DE. An unconventional IAP-binding motif revealed by target-assisted iterative screening (TAIS) of the BIR3-cIAP1 domain. J Mol Recognit. 2007 Jan-Feb;20(1):39-50.

Lockshin RA and Williams CM. Programmed cell death. II. Endocrine potentiation of the breakdown of the intersegmental muscles of silkmoths. J. Insect Physiol. 1964 Aug;10(4): 643–9.

Ma Y, Hendershot LM. The role of the unfolded protein response in tumour development: friend or foe? Nat Rev Cancer. 2004 Dec;4(12):966-77.

MacFarlane M, Ahmad M, Srinivasula SM, Fernandes-Alnemri T, Cohen GM, Alnemri ES. Identification and molecular cloning of two novel receptors for the cytotoxic ligand TRAIL. J Biol Chem. 1997 Oct 10;272(41):25417-20.

Marsters SA, Sheridan JP, Pitti RM, Brush J, Goddard A, Ashkenazi A. Identification of a ligand for the death-domain-containing receptor Apo3. Curr Biol. 1998 Apr 23;8(9):525-8.

Martinon F, Tschopp J. Inflammatory caspases and inflammasomes: master switches of inflammation. Cell Death Differ. 2007 Jan;14(1):10-22. Epub 2006 Sep 15.

Medema JP, Scaffidi C, Kischkel FC, Shevchenko A, Mann M, Krammer PH, Peter ME. FLICE is activated by association with the CD95 death-inducing signaling complex (DISC). EMBO J. 1997 May 15;16(10):2794-804.

Meier P, Finch A, Evan G. Apoptosis in development. Nature. 2000 Oct 12;407(6805):796-801.

Melino G, Knight RA, Green DR. Publications in cell death: the golden age. Cell Death Differ. 2001 Jan;8(1):1-3.

Metzstein MM, Stanfield GM, Horvitz HR. Genetics of programmed cell death in C. elegans: past, present and future. Trends Genet. 1998 Oct;14(10):410-6.

Meyn RE, Stephens LC, Milas L. Programmed cell death and radioresistance. Cancer Metastasis Rev. 1996 Mar;15(1):119-31.

Mori K, Kawahara T, Yoshida H, Yanagi H, Yura T. Signalling from endoplasmic reticulum to nucleus: transcription factor with a basic-leucine zipper motif is required for the unfolded protein-response pathway. Genes Cells. 1996 Sep;1(9):803-17.

Mori K, Ma W, Gething MJ, Sambrook J. A transmembrane protein with a cdc2+/CDC28-related kinase activity is required for signaling from the ER to the nucleus. 1: Cell. 1993 Aug 27;74(4):743-56.

Muzio M, Salvesen GS, Dixit VM. FLICE induced apoptosis in a cell-free system. Cleavage of caspase zymogens. J Biol Chem. 1997 Jan 31;272(5):2952-6.

Pan G, O'Rourke K, Chinnaiyan AM, Gentz R, Ebner R, Ni J, Dixit VM. The receptor for the cytotoxic ligand TRAIL. Science. 1997 Apr 4;276(5309):111-3.

Rehm M, Huber HJ, Dussmann H, Prehn JH. Systems analysis of effector caspase activation and its control by X-linked inhibitor of apoptosis protein. EMBO J. 2006 Sep 20;25(18):4338-49. Epub 2006 Aug 24.

Riedl SJ, Salvesen GS. The apoptosome: signalling platform of cell death. Nat Rev Mol Cell Biol. 2007 May;8(5):405-13. Epub 2007 Mar 21.

Roth W, Kermer P, Krajewska M, Welsh K, Davis S, Krajewski S, Reed JC. Bifunctional apoptosis inhibitor (BAR) protects neurons from diverse cell death pathways. Cell Death Differ. 2003 Oct;10(10):1178-87.

Roy N, Deveraux QL, Takahashi R, Salvesen GS, Reed JC. The c-IAP-1 and c-IAP-2 proteins are direct inhibitors of specific caspases. EMBO J. 1997 Dec 1;16(23):6914-25.

Salvesen GS, Dixit VM. Caspase activation: the induced-proximity model. Proc Natl Acad Sci U S A. 1999 Sep 28;96(20):10964-7.

Schaefer U, Voloshanenko O, Willen D, Walczak H. TRAIL: a multifunctional cytokine. Front Biosci. 2007 May 1;12:3813-24.

Schlegel RA, Williamson P. Phosphatidylserine, a death knell. Cell Death Differ. 2001 Jun;8(6):551-63. Comment in: Cell Death Differ. 2001 Jun;8(6):545-8.

Scorrano L, Oakes SA, Opferman JT, Cheng EH, Sorcinelli MD, Pozzan T, Korsmeyer SJ. BAX and BAK regulation of endoplasmic reticulum Ca2+: a control point for apoptosis. Science. 2003 Apr 4;300(5616):135-9. Epub 2003 Mar 6.

Sharpe JC, Arnoult D, Youle RJ. Control of mitochondrial permeability by Bcl-2 family members. Biochim Biophys Acta. 2004 Mar 1;1644(2-3):107-13.

Soler F, Lax A, Fernández-Belda F. Cellular death linked to irreversible stress in the sarcoplasmic reticulum: The effect of inhibiting Ca(2+)-ATPase or protein glycosylation in the myocardiac cell model H9c2.Arch Biochem Biophys. 2007 Jun 29; [Epub ahead of print].

Srinivasula SM, Ahmad M, Fernandes-Alnemri T, Litwack G, Alnemri ES. Molecular ordering of the Fas-apoptotic pathway: the Fas/APO-1 protease Mch5 is a CrmA-inhibitable protease that activates multiple Ced-3/ICE-like cysteine proteases. Proc Natl Acad Sci U S A. 1996 Dec 10;93(25):14486-91.

Steller H. Mechanisms and genes of cellular suicide. Science. 1995 Mar 10;267(5203):1445-9.

Stucki JW, Simon HU. Mathematical modeling of the regulation of caspase-3 activation and degradation. J Theor Biol. 2005 May 7;234(1):123-31. Epub 2005 Jan 22.

Tartaglia LA, Rothe M, Hu YF, Goeddel DV. Tumor necrosis factor's cytotoxic activity is signaled by the p55 TNF receptor. Cell. 1993 Apr 23;73(2):213-6.

Walczak H, Degli-Esposti MA, Johnson RS, Smolak PJ, Waugh JY, Boiani N, Timour MS, Gerhart MJ, Schooley KA, Smith CA, Goodwin RG, Rauch CT. TRAIL-R2: a novel apoptosis-mediating receptor for TRAIL. EMBO J. 1997 Sep 1;16(17):5386-97.

Williams GT. Role of apoptosis in the immune system. 1: Biochem Cell Biol. 1994 Nov-Dec;72(11-12):447-50.

Wolkenhauer O. Defining Systems Biology: An Engineering Perspective. IETD Syst. Biol. 2007;1(4):204-206.

Wu J, Kaufman RJ. From acute ER stress to physiological roles of the Unfolded Protein Response. Cell Death Differ. 2006 Mar;13(3):374-84.

Wyllie AH, Kerr JF, Currie AR. Cell death: the significance of apoptosis. Int Rev Cytol. 1980;68:251-306.

Yang YL, Li XM. The IAP family: endogenous caspase inhibitors with multiple biological activities. Cell Res. 2000 Sep;10(3):169-77.

Yuan J, Yankner BA. Apoptosis in the nervous system. Nature. 2000 Oct 12;407(6805):802-9.

Zamzami N, Marchetti P, Castedo M, Zanin C, Vayssiére JL, Petit PX, Kroemer G. Reduction in mitochondrial potential constitutes an early irreversible step of programmed lymphocyte death in vivo. J Exp Med. 1995 May 1;181(5):1661-72.

Zamzami N, Susin SA, Marchetti P, Hirsch T, Gómez-Monterrey I, Castedo M, Kroemer G. Mitochondrial control of nuclear apoptosis. J Exp Med. 1996 Apr 1;183(4):1533-44.

Zhang JH, Zhang Y, Herman B. Caspases, apoptosis and aging. Ageing Res Rev. 2003 Oct;2(4):357-66.

Zong WX, Li C, Hatzivassiliou G, Lindsten T, Yu QC, Yuan J, Thompson CB. Bax and Bak can localize to the endoplasmic reticulum to initiate apoptosis. J Cell Biol. 2003 Jul 7;162(1):59-69.

Zou H, Li Y, Liu X, Wang X. An APAF-1.cytochrome c multimeric complex is a functional apoptosome that activates procaspase-9. J Biol Chem. 1999 Apr 23;274(17):11549-56.

End section

Dynamical Analysis of the Programmed Cell Death Pathway

Luciano Carotenuto, Vincenza Pace, Dina Bellizzi, Giovanna De Benedictis

Abstract—**The biochemical processes that lead to the programmed death of the cell (apoptosis) have been studied since a long time. Recently several mathematical models have been proposed, that try to describe the essential features of the pathway. In this paper we consider one of such models and compare two possible scenarios of activation of the apoptotic process: an instantaneous perturbation or a persistent stress, represented respectively by an appropriate initial state or a constant input to the system. The new results here reported are i) the proof that the system with constant input has at least one equilibrium state; ii) the characterization of equilibrium and stability patterns in the presence of the constant input; iii) the analysis of the sensitivity of the dynamic time response both to the intensity of an initial perturbation, and to the level and duration of a persistent stress. Finally, the effect of modulating the level of expression of genes involved in the pathway is analyzed, with the aim of exploring the control mechanism of this crucial process.**

I. INTRODUCTION

Apoptosis, or programmed cell death, is the mechanism by which multicellular organisms regulate cell number in tissues, and eliminate damaged or unneeded cells [1]. Embryonic development, aging of tissues, immune response, are examples of processes where apoptosis plays a critical role. Furthermore, defects in the normal functioning of the process which cause either too low or too high death rates may be related to neoplastic or to neurodegenerative diseases, respectively. The executioners of apoptosis are proteins denoted as caspases [2]. Caspases normally exist in cells in inactive forms (pro-caspases): at the onset of apoptosis they undergo a cascade of catalytic activations. The cascade (Fig. 1) involves *initiator* pro-caspases (such as C8, C9, C10), which activate *effector* pro-caspases (such as C3, C6, C7) [3]. The activated *effector* caspases cleave the downstream substrates leading to DNA damaging and cell death. In the *extrinsic* apoptosis pathway the cascade is triggered by external molecules such as FasL and TNF that lead to C8 activation by binding cell surface receptors. In the *intrinsic* pathway the mitochondria activate pro-caspase

Manuscript received October 11, 2006. This work was supported in part by Fondo Sociale Europeo – FSE (PhD course in Molecular Biopathology, University of Calabria, Italy).

L. C. Author is with the Department of Electronics, Computer Science & System Science University of Calabria, 87036 Rende, Italy (phone and fax +39-0984-494723; e-mail carotenuto@unical.it).

V. P., D. B., G. d. B. Authors are with Department of Cell Biology, University of Calabria, 87036 Rende, Italy (e-mail g.debenedictis@unical.it)

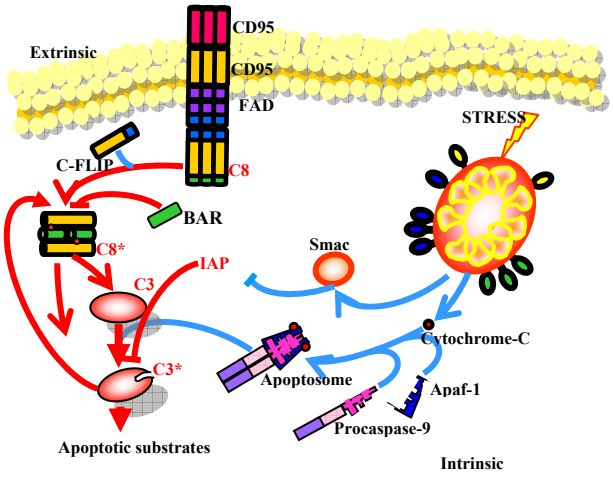

Fig. 1. Extrinsic and intrinsic pathways of apoptosis. The red arrows show the reactions considered in the model.

C9 in response to stress (thermal, radiogenic, oxidative). Several regulating factors intervene in the process: in the extrinsic pathway a key role has been recognized to the Inhibitor Apoptosis Proteins (IAP) [4] and the BAR protein [5]. Several mathematical models (see e.g. [6-9]) have been proposed to describe various aspects of the apoptotic process. In this paper a mathematical model of the extrinsic pathway is considered: it modifies a model originally proposed by Eissing and coworkers [9], and thoroughly analyzed in [10]. The model considers the dynamical interactions between pro-caspases C8 and C3, active caspase C8* and C3*, and inhibitor proteins BAR and IAP. It describes the production and decay of pro-caspases C8 and C3, and of inhibitors IAP and BAR; the activation of C8 by C3* and of C3 by C8* in a positive feedback loop; the regulation of concentration of C8* (C3*) by reversible binding of BAR and C8* (IAP and C3*) into the complex C8*÷BAR (C3*÷IAP).

Let x_i, i=1,2,..8 denote the concentrations of the proteins taken into account by the model:

x_1=[C8], x_2=[C8*], x_3=[C8*÷BAR], x_4=[BAR],
x_5=[C3], x_6=[C3*], x_7=[C3*÷IAP], x_8=[IAP].

As units we use *molecules per cell* (*mol/cell*) for the concentrations, *minutes* (*min*) for the time. Note that the notation is slightly changed with respect to [9] and [10]. By applying the mass-action law, and assuming first order kinetics for the decays (details on the biochemical assumptions are in [9]), a set of ODEs is obtained

ISBN: 978-960-89028-5-5

$$\dot{x}_1(t) = -k_2 x_1(t) x_6(t) - k_9 x_1(t) + k_{-9} - q(t) \quad (1)$$

$$\dot{x}_2(t) = k_2 x_1(t) x_6(t) - k_5 x_2(t) - k_{11} x_2(t) x_4(t) + k_{-11} x_3(t) + q(t) \quad (2)$$

$$\dot{x}_3(t) = k_{11} x_2(t) x_4(t) - k_{-11} x_3(t) - k_{13} x_3(t) \quad (3)$$

$$\dot{x}_4(t) = -k_{11} x_2(t) x_4(t) + k_{-11} x_3(t) - k_{12} x_4(t) + k_{-12} \quad (4)$$

$$\dot{x}_5(t) = -k_1 x_2(t) x_5(t) - k_{10} x_5(t) + k_{-10} \quad (5)$$

$$\dot{x}_6(t) = k_1 x_2(t) x_5(t) - k_3 x_6(t) x_8(t) + k_{-3} x_7(t) - k_6 x_6(t) \quad (6)$$

$$\dot{x}_7(t) = k_3 x_6(t) x_8(t) - k_{-3} x_7(t) - k_7 x_7(t) \quad (7)$$

$$\dot{x}_8(t) = (-k_4 - k_3) x_6(t) x_8(t) + k_{-3} x_7(t) - k_8 x_8(t) + k_{-8} \quad (8)$$

The dynamical system (1)-(8) is characterized by nineteen parameters. The numerical values shown in Table I are from [9]: these values will be denoted as k_i^{nom}, i=1,...,13,−3,−8,...,−12, and the corresponding model will be said *nominal*.

The effect of an external stimulus temporarily applied through the cell membrane is modeled by imposing the conversion, at time t=0, of a number of C8 molecules into C8*, after which the model evolves without "external" forcing. The effect of a stress acting continuously on the receptors is modeled by transforming $q(t)>0$ *mol/cell/min* of C8 into an equal number of C8* molecules (Eqs.(1,2)) on a given time interval.

II. Analysis of the Model

We begin this section by proving a general result about equilibrium of system (1)-(8). Performing straightforward substitutions into Eqs. (1)-(8) with $\dot{x}(t) = 0$ we obtain

$$x_1 = \frac{k_{-9} - q}{k_9 + k_2 x_6},\ x_3 = \frac{k_{11} k_{-12} x_2}{k_{12} k_{-11} + k_{12} k_{13} + k_{11} k_{-12} x_2},$$

$$x_4 = \frac{k_{-11} k_{-12} + k_{13} k_{-12}}{k_{12} k_{-11} + k_{12} k_{13} + k_{11} k_{-12} x_2},\ x_5 = \frac{k_{-10}}{k_{10} + k_1 x_2},$$

$$x_7 = \frac{k_3 k_{-8} x_6}{(k_7 + k_{-3}) k_8 + [(k_7 + k_{-3}) k_4 + k_7 k_3] x_6},$$

$$x_8 = \frac{(k_7 + k_{-3}) k_{-8}}{(k_7 + k_{-3}) k_8 + [(k_7 + k_{-3}) k_4 + k_7 k_3] x_6}$$

$$\frac{k_2 x_6 (k_{-9} - q)}{k_9 + k_2 x_6} = k_5 x_2 - q + \frac{k_{-12} k_{11} k_{13} x_2}{k_{12} k_{13} + k_{12} k_{-11} + k_{11} k_{13} x_2}$$

$$\frac{k_1 k_{-10} x_2}{k_{10} + k_1 x_2} = k_6 x_6 + \frac{k_{-8} k_3 k_7 x_6}{(k_7 + k_{-3}) k_8 + [(k_7 + k_{-3}) k_4 + k_3 k_7] x_6}$$

The variables at equilibrium are constrained by: $x_i \geq 0, i = 1, \cdots, 8$, $k_9 x_1 + k_5 x_2 + k_{13} x_3 = k_{-9}$, $k_{10} x_5 + k_6 x_6 + k_7 x_7 = k_{-10}$. The constant input is constrained by $q_c \leq q_{cMAX} = k_{-9}$.

TABLE I
Nominal Model Parameters

Parameter	Dimension[a]	Value[b]	Reaction where the parameter appears
k_1	$[C]^{-1}[t]^{-1}$	5.80×10^{-5}	C3+C8* → C3*
k_2	$[C]^{-1}[t]^{-1}$	1.00×10^{-5}	C8+C3* → C8*
k_3	$[C]^{-1}[t]^{-1}$	5.00×10^{-4}	C3*+IAP → C3* ÷ IAP
k_{-3}	$[t]^{-1}$	2.10×10^{-1}	C3* ÷ IAP → C3*+IAP
k_{11}	$[C]^{-1}[t]^{-1}$	5.00×10^{-4}	C8*+BAR → C8* ÷ BAR
k_{-11}	$[t]^{-1}$	2.10×10^{-1}	C8* ÷ BAR → C8*+BAR
k_{-8}	$[C][t]^{-1}$	$4.64 \times 10^{+2}$	production of IAP
k_{-9}	$[C][t]^{-1}$	$5.07 \times 10^{+2}$	production of C8
k_{-10}	$[C][t]^{-1}$	$8.19 \times 10^{+1}$	production of C3
k_{-12}	$[C][t]^{-1}$	$4.00 \times 10^{+1}$	production of BAR
k_8	$[t]^{-1}$	1.16×10^{-2}	decay of IAP
k_9	$[t]^{-1}$	3.90×10^{-3}	decay of C8
k_{10}	$[t]^{-1}$	3.90×10^{-3}	decay of C3
k_{12}	$[t]^{-1}$	1.00×10^{-3}	decay of BAR
k_5	$[t]^{-1}$	5.80×10^{-3}	decay of C8*
k_6	$[t]^{-1}$	5.80×10^{-3}	decay of C3*
k_7	$[t]^{-1}$	1.73×10^{-2}	decay of C3* ÷ IAP
k_{13}	$[t]^{-1}$	1.16×10^{-2}	decay of C8* ÷ BAR
k_4	$[C]^{-1}[t]^{-1}$	3.00×10^{-4}	cleavage of IAP

The numerical values in the third column are from [9].
[a] [C]: concentration; [t]: time; [b] concentration is measured in *molecules/cell*; time is measured in *minutes*.

In order to simplify the analysis it is convenient to define the dimensionless variables and parameters:

$$\xi_2 = \frac{k_5 x_2}{k_{-9}},\ \xi_6 = \frac{k_6 x_6}{k_{-10}},\ u = \frac{q}{k_{-9}},\ \alpha_1 = \frac{k_2 k_{-10}}{k_9 k_6},\ \alpha_2 = \frac{k_1 k_{-9}}{k_5 k_{10}},$$

$$\alpha_3 = \frac{k_3 k_{-10}}{k_6 k_8},\ \alpha_4 = \frac{k_4 k_{-10}}{k_6 k_8},\ \alpha_5 = \frac{k_{11} k_{-9}}{k_5 k_{12}},\ \varepsilon = \frac{k_{-11}}{k_{13}},$$

$$\theta = \frac{k_{-12}}{k_{-9}},\ \gamma = \frac{k_{-3}}{k_7},\ \delta = \frac{k_{-8}}{k_{-10}}.$$

With these new variables the equations which relate x_2 and x_6 become:

$$\frac{\alpha_1 \xi_6 (1-u)}{1 + \alpha_1 \xi_6} = \xi_2 + \frac{\alpha_5 \theta \xi_2}{1 + \varepsilon + \alpha_5 \xi_2} - u \quad (9)$$

$$\frac{\alpha_2 \xi_2}{1 + \alpha_2 \xi_2} = \xi_6 + \frac{\delta \alpha_3 \xi_6}{1 + \gamma + [(1+\gamma)\alpha_4 + \alpha_3] \xi_6} \quad (10)$$

The problem of finding the equilibrium states of the system is then reduced to solving Eqs. (9)-(10) and selecting the solutions that satisfy the constraints $0 \leq \xi_2 < 1$, $0 \leq \xi_6 < 1$. The direct approach is to deduce ξ_2 from (10) and to substitute it into (9). In this way a 5-th degree algebraic equation is obtained (say $p(\xi_6) = 0$) whose coefficients are explicit functions of the parameters and of the input u. The equilibrium values of ξ_6 are obtained as the real roots of the equation $p(\xi_6) = 0$ belonging to the interval $0 < \xi_6 < 1$, and such that ξ_2 belongs to the interval $0 < \xi_2 < 1$. The other components are finally computed by their explicit expressions. This approach was used for a very

efficient and accurate numerical evaluation of the equilibrium states. However the formulas giving the coefficients of the equation $p(\xi_6)=0$ are extremely intricate and cannot be used to deduce qualitative properties of the roots. Therefore we adopted a different approach to prove that

Proposition 1. *The dynamical system* (1)-(8) *has at least one equilibrium state*.

Proof. We notice that by simple manipulations Eqs. (9)-(10) can be written into the form

$$\xi_2 = f(\xi_6) = a_1 \frac{a_2\xi_6 + a_3\xi_6^2}{a_4 + (a_3 - a_2)\xi_6 - a_3\xi_6^2}$$

$$\xi_6 = g(\xi_2) = a_{10} \frac{-a_8 u + (a_6 - a_7 u)\xi_2 + a_7\xi_2^2}{a_8 + (a_7 - a_6)\xi_2 - a_7\xi_2^2}$$

with obvious definitions of the new symbols. Therefore the equilibrium pairs (ξ_{2E}, ξ_{6E}) can be obtained by solving the equation $\xi_6 - g(f(\xi_6)) = 0$ and selecting among the solutions those which satisfy the constraints $0 < \xi_6 < 1, 0 < f(\xi_6) < 1$.

The relevant properties of the functions *f* and *g* are:

- the poles of f and g are real and of opposite sign;
- let p_f^+, p_g^+ the positive poles of *f*, *g*: then $p_f^+ < 1$, $p_g^+ < 1$;
- f is continuous and strictly increasing for $\xi_6 \in [0, p_f^+)$;
- $f(0) = 0$, $f(\xi_6) \to +\infty$ for $\xi_6 \to p_f^+$;
- g is continuous and strictly increasing for $\xi_2 \in [0, p_g^+)$;
- $g(0) = -a_{10}u$, $g(\xi_2) \to +\infty$ for $\xi_2 \to p_g^+$

Immediate consequences of these properties are

- the equation $f(\xi_6) = p_g^+$ has a unique solution $p_1 < p_f^+$
- the composite function $h(\xi_6) = g(f(\xi_6))$ is continuous and strictly increasing for $\xi_6 \in [0, p_1)$.

Therefore when ξ_6 spans the interval $[0, p_1)$, the function $\xi_6 - g(f(\xi_6))$ takes all values in the interval $[a_{10}u, -\infty)$, and in particular there exists at least one value ξ_{6E} for which $\xi_{6E} - g(f(\xi_{6E})) = 0$. From the construction it is clear that ξ_{6E} and the corresponding ξ_{2E} satisfy the constraints. □

A. Equilibrium states and stability analysis of the unforced model ($q(t) = 0\ \forall t$).

If $q(t) = 0\ \forall t$ a solution of Eqs. (9),(10) is clearly (ξ_{2E}, ξ_{6E})=(0,0): then the vector

$$\underline{x}_{EL} = \left[\frac{k_{-9}}{k_9}\ 0\ 0\ \frac{k_{-12}}{k_{12}}\ \frac{k_{-10}}{k_{10}}\ 0\ 0\ \frac{k_{-8}}{k_8}\right]^T = \quad (11)$$
$$[x_{L1}\ 0\ 0\ x_{L4}\ x_{L5}\ 0\ 0\ x_{L8}]^T$$

is an equilibrium state, characterized by the absence of active caspases: it is denoted as the *life* equilibrium and may represent the cell in its "unperturbed" condition. In a previous paper we exploited the simplification that results in Eqs. (9),(10) when u=0 to prove [10]:

Proposition 2. *The dynamical system* (1)-(8) *may have one, two or three equilibrium states, one of which – the "life" equilibrium – is given by* (11).

Moreover the special structure of the Jacobian matrix evaluated at the *life* equilibrium $\underline{x}_{EL}$ enabled to prove

Proposition 3. *Let*

$$S = \frac{(k_{-11}k_5 + k_{13}k_5 + k_{13}k_{11}x_{L7})(k_{-3}k_6 + k_7k_6 + k_7k_3x_{L5})}{x_{L1}x_{L3}(k_{-11} + k_{13})(k_{-3} + k_7)}$$

if $k_1k_2 < S$, *then the life equilibrium state is asymptotically stable; if* $k_1k_2 > S$, *then the "life" equilibrium state is unstable because of one real positive eigenvalue of the Jacobian matrix of system* (1)-(8) *evaluated at the "life" equilibrium*.

Finally there is a connection between stability of the *life* equilibrium and number of equilibria:

Proposition 4. *If the "life" equilibrium is unstable, then there exists a unique "non-life" equilibrium; if the "life" equilibrium is asymptotically stable, then we have, generically, either no "non-life" equilibrium, or two "non-life" equilibria.*

Proof of Propositions 2 and 3 are in [10], where linearization [11] and root locus techniques [12] are used.

TABLE II
EQUILIBRIUM STATES OF THE NOMINAL MODEL

Variables	E_L (*life*) asym. stable	E_{NL1} unstable	E_{NL2} (*apoptosis*) asym. stable
	(*mol/cell*)	(*mol/cell*)	(*mol/cell*)
[C8]	130000	129870	9132
[C8*]	0	0	74380
[C8* ÷ BAR]	0	44	3447
[BAR]	40000	39492	21
[C3]	21000	20848	19
[C3*]	0	0	5162
[C3* ÷ IAP]	0	34	3000
[IAP]	40000	39546	264

The *nominal* model has three equilibrium states, denoted by E_L (the *life* one), E_{NL1}, E_{NL2}, whose numerical values are shown in Table II. The *life* equilibrium is asymptotically stable, equilibrium E_{NL1} is unstable, and equilibrium E_{NL2} is asymptotically stable. The components of E_{NL2} are very different from those of the *life* equilibrium: the concentrations of pro-caspases C8, C3, and inhibitors BAR and IAP are very low, wherease active caspases C8*, C3* and complexes C8* ÷ BAR, C3* ÷ IAP have concentrations ranging from 36.6% of the maximum value ([C3*]) to 99.9% ([C8* ÷ BAR]). We assume that the value [C3*]= 5162 *mol/cell* (Table II) is sufficiently high to define the

E_{NL2} equilibrium state as the *apoptosis* equilibrium.

The effect of parameter variations on the pattern of equilibrium states and on their stability has been analyzed numerically in [10]. In summary, equilibrium states and eigenvalues of the corresponding Jacobian matrices were computed for a set Σ of 100000 models, whose parameter vectors belong to a rectangular neighborhood of the nominal parameter vector. For each model the parameters k_i, i=1,...,13,−3,−11, are pseudorandom numbers uniformly distributed on the intervals I_i=[0.1 k_i^{nom}, 1.9 k_i^{nom}], whereas k_{-8}, k_{-9}, k_{-10}, k_{-12} are computed from k_8, k_9, k_{10}, k_{12} in such a way that the *life* equilibrium (11) is the same as the *life* equilibrium of the nominal model. The sample generation simulates the production of a population of different cells characterized by parameters whose average values are the nominal ones. The constraints on k_{-8}, k_{-9}, k_{-10}, k_{-12} impose that all the cells, in normal conditions, have the same concentrations of C8, C3, IAP, BAR.

The set of models thus generated can be partitioned into three subsets: Σ_1, Σ_2, Σ_3. Σ_1 consists of the models with the sole *life* equilibrium, which is asymptotically stable. Σ_2 consists of the models with two equilibria: the *life* one, which is unstable, and the *non-life* equilibrium, which in most cases is asymptotically stable; when it is unstable, the numerical experiments show that the model exhibits periodic time evolution. Σ_3 consists of the models with three equilibria: most models in Σ_3 are bistable like the nominal model; the few ones with unstable *non-life* equilibria are shown to have time evolutions similar to those of models in Σ_1. The pattern of two asymptotically stable equilibria separated by one unstable point suggests that a threshold may exist which separates initial states whose trajectories settle back to the *life* equilibrium and initial states whose trajectories converge to the other asymptotically stable equilibrium.

To characterize the static properties of a model with one asymptotically stable *non-life* equilibrium also the corresponding value of C3* (say $[C3^*]_A$) is relevant because it is conceivable that a sufficiently high concentration of C3* is necessary to trigger the subsequent steps leading to cell death. The relative frequency distributions of the values of $[C3^*]_A$ span several orders of magnitude. Indeed minimum, median, maximum of ($[C3^*]_A$ for models with two equilibria are 0.02 *mol/cell*, 7255 *mol/cell*, 248930 *mol/cell*, respectively, for bistable models with three equilibria 2.22 *mol/cell*, 6080 *mol/cell*, 223110 *mol/cell*, respectively.

As to the biological interpretation of these results, models showing the bistable pattern with high values of $[C3^*]_A$ are regarded as representative of a normal cell [9],[10]: the reactions that activate pro-caspase C3 to a relevant concentration are triggered if the level of the external stimulus exceeds a threshold. On the contrary, a parameter vector which produces the single asymptotically stable *life* equilibrium may represent a cell refractory to apoptosis, and then prone to cancer onset. Finally a model showing an unstable *life* equilibrium and an asymptotically stable *non-life* equilibrium with high value of $[C3^*]_A$ may be regarded as representative of a hypersensitive cell: however slight the stimulus may be, the caspase activation process is started and that cell undergoes apoptosis. The biological meaning of a *non-life* asymptotically stable equilibrium with low value of $[C3^*]_A$ is not clear, as well as the plausibility of oscillating trajectories, observed in the cases with two unstable equilibria. However we cannot exclude that further experiments will explain also such behaviors.

B. Equilibrium states and stability analysis of the model with persistent input: $q(t) = q_c > 0 \; \forall t$.

Since $x_6 = 0$ is not an equilibrium value for [C3*] when $q_c > 0$, $\underline{x}_{EL}$ as given by [11] is not an equilibrium state and the notion of *life* equilibrium loses its significance. The Jacobian matrix of Eqs.(1)-(8) evaluated at the new equilibria does not show any special structure: then no stability criterion can be given and the analysis can be performed only numerically.

The *nominal* model loses its bistability for $q_c = 5 \times 10^{-6} k_{-9}$: above this value it has a unique asymptotically stable equilibrium, with $[C3^*] \cong 5162$ *mol/cell*, almost independently of q_c.

In the numerical experiments we computed equilibrium states and eigenvalues of the corresponding Jacobian matrices of the 100000 models with random parameter vectors belonging to the set Σ defined in section II.A. Two levels of the persistent perturbation have been considered: $q_c = 0.01 k_{-9}$ (low-level) and $q_c = 0.8 k_{-9}$ (high-level). In this way two equilibrium and stability patterns have been obtained, which can be compared with the patterns for q_c=0. The results are shown in Table III, where models are again classified according to the number of equilibria when q_c=0, as belonging to the sets Σ_1, Σ_2, Σ_3.

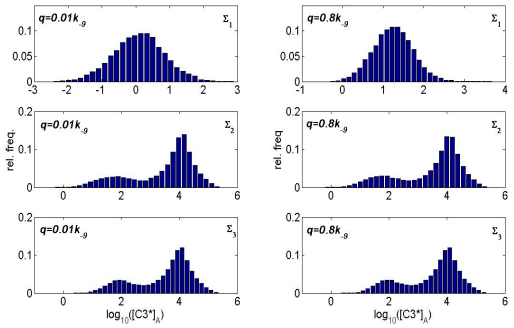

Fig. 2. Distributions of the relative frequencies of the values of $[C3^*]_A$ in models belonging to Σ_1, Σ_2, Σ_3, subjected to low-level (q=0.01k_{-9}) and high-level (q=0.8k_{-9}) persistent stress.

The other relevant feature of the static behavior of the models is the value of [C3*] at an asymptotically stable equilibrium, selecting the largest value in case of bistability.

It is again denoted by $[C3^*]_A$, and its frequency distributions in the sets Σ_1, Σ_2, Σ_3 are shown in Fig. 2.

From Table III we note that a wide variety of patterns is present: some patterns are rare, but their existence is evidence of the complexity of possible model behaviors. As for the case where q_c=0, we have verified by numerical simulation that models with only unstable equilibria have periodic time evolutions. The main features of the equilibrium patterns and of the distributions of $[C3^*]_A$ are:

- when q_c >0 models with two equilibria do not exist: this is a striking difference from the case q_c=0;
- for models in Σ_2 the unstable *life* equilibrium disappears when a persistent input is applied; the value of [C3*] at the unique asymptotically stable equilibrium is nearly independent of q_c: then the static behavior is essentially determined by model parameters;

TABLE III
EQUILIBRIUM AND STABILITY PATTERNS OF RANDOMLY GENERATED MODELS (SET Σ OF SECT. IIA)

q_c	Σ_1 (14678)	Σ_2 (50566)	Σ_3 (34756)
0	one equilibrium a.s. 14678*	one equilibrium -	one equilibrium -
	two equilibria -	two equilibria a.s.-u. 50263 u.-u. 303	two equilibria -
	three equilibria -	three equilibria -	three equilibria a.s-u-a.s 34659 a.s-u-u 97
$0.01k_{-9}$	one equilibrium a.s. 14072 u. 22	one equilibrium a.s. 50440 u. 126	one equilibrium a.s. 18878 u. 7
	three equilibria a.s-u.-a.s 542 a.s-u-u 41 u.u.u. 1	three equilibria -	three equilibria a.s-u.-a.s 15827 a.s-u-u 44
$0.8k_{-9}$	one equilibrium a.s. 14671 u. 5	one equilibrium a.s. 50566	one equilibrium a.s. 34756
	three equilibria a.s-u.-a.s 1 a.s-u-u 1	three equilibria -	three equilibria -

* n° of models that exhibit the specific pattern;
a. s. : asymptotically stable equilibrium; u. : unstable equilibrium;
Σ_K: set of models having k equilibrium states when q = 0.

- a relevant fraction of models in Σ_2 has a low level of $[C3^*]_A$ (f.i. $[C3^*]_A$ < 1000 *mol/cell* in about 27% of cases with q_c=0.8 q_{cMAX}): in view of this result it is simplistic to associate the models of Σ_2 with proneness to apoptosis;
- most of the models belonging to Σ_1 have a unique asymptotically stable equilibrium also when exposed to persistent stress; the exceptions occur with the low-level input: few models (4.0%) have three equilibria and very few have a single unstable equilibrium. Concentrations of C3* at equilibrium are small: with q_c=0.8 q_{cMAX} only 26 (0.18%) of the models have $[C3^*]_A$>1000 *mol/cell*;
- models belonging to Σ_3 partly retain the bistable pattern with the low-level stress; on the contrary the high-level stress "destroys" any track of the *life* equilibrium and of its unstable partner;
- for models in Σ_3 the distribution of the values of $[C3^*]_A$ is almost the same for q_c=0, q_c=0.01 q_{cMAX}, q_c=0.8 q_{cMAX}. Also in this case the steady-state concentrations are determined essentially by model parameters.

III. DYNAMICAL RESPONSE ANALYSIS

In this section we report and discuss the results of a large number of simulations of model (1)-(8). The simulations aim at revealing the characteristic features of the time evolution of protein concentrations in response to an extrinsic action on the cell. The instantaneous perturbation is modeled by imposing the initial state $\underline{x}_p = \underline{x}_{EL} + [-c\ c\ 0\ 0\ 0\ 0\ 0]^T$, where $\underline{x}_{EL}$ is the *life* equilibrium, and c>0 (*mol/cell*) is the number of C8 molecules suddenly activated to C8* at t=0. For t>0 the model evolves without external forcing ($q(t)$=0). To represent a continuous stress we take the *life* equilibrium as initial state: $\underline{x}(0) = \underline{x}_{EL}$, and assume that a number of C8 molecules is "continuously" transformed into C8* at a constant rate $q(t)$=q > 0 (*mol/cell/min*), for an interval of T minutes.

A. Response of the Nominal Model

Although already discussed in [9],[10], we summarize for the sake of completeness the results on instantaneous perturbations. In [9] it is reported that there exists a threshold perturbation (estimated as $c \approx 75$ *mol/cell*) below which the evolution returns to the *life* equilibrium; perturbations larger than the threshold cause the trajectory to convergence to the *apoptosis* equilibrium. Our simulations fully confirm this behavior, and add further insights on the process.

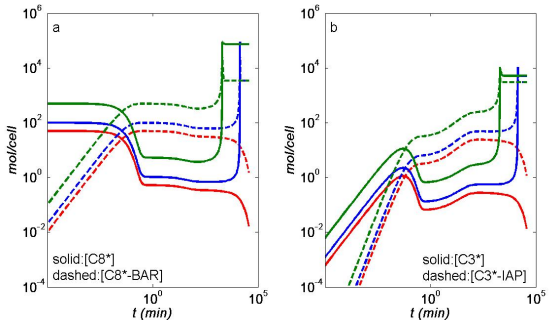

Fig. 3. Time evolutions, in logarithmic scales, of [C8*], [C8* ÷ BAR] (a) and of [C3*], [C3* ÷ IAP] (b) for the nominal model; initial perturbations: c=50 *mol/cell* (red), c=100 *mol/cell* (blue), c=500 *mol/cell* (green).

The time evolutions of [C8*], [C8*÷BAR] are shown in Fig. 3a, the evolutions of [C3*], [C3*÷IAP] in Fig. 3b for initial perturbations of different intensities, both below and above the threshold.

The distinctive features of the time responses are:

- a very short initial transient, lasting less than one minute, during which the initial molecules of C8* are captured by the inhibitor BAR to form the complex C8*÷BAR. Negligible amounts of free C3* and of the complex C3*÷IAP are produced in this phase;
- a very long intermediate phase characterized by very low values of [C8*] and [C3*], slow increase of [C3*÷IAP] and slow decrease of [IAP];
- a final phase, where either [C3*] and [C8*] reach very high values in a few minutes, then converge to the *apoptosis* equilibrium, or [C3*] and [C8*] decrease and the system returns to the *life* equilibrium. The transition corresponding to c=100 *mol/cell* is shown in Fig. 4.

Remark 1. The time evolution of the state variables of the model suggests that the fate of the cell is mainly determined by the interactions between inhibitors (IAP, BAR) and active caspases (C3*, C8*, respectively): the transition that leads to apoptosis seems to start when IAP is no more sufficient to bind new C3*, which causes a very fast increase of [C3*], followed by the increase of [C8*].

The response is quantitatively characterized by: the *delay time* t_D, measured as the time, during the transition, at which the derivative of [C3*] attains its maximum; the *peak value* of [C3*]: $M_6=max[x_6(t)]$; the *rise time* t_R, that is the time required for [C3*] to change from 10% to 90% of the peak value. In Table IV we report these parameters evaluated by simulations in which the initial perturbation is increased from c=100 to c=10000 *mol/cell*. The conclusion is that once the perturbation exceeds the threshold, only the time interval needed to reach the transition is sensibly affected by the intensity of the perturbation: t_D is almost inversely proportional to c, as already noted in [9]. The least squares fitting is $t_D = 1.661\times10^6 \times c^{-1.071}$.

Let us now consider the effect of a continuous stress. In the first experiment, the response to an initial perturbation of intensity c=1000 *mol/cell* is compared with the response to stresses characterized by values of the level q and of the duration T such that qT = 1000 *mol/cell*. Note that in this case the maximum *permanent* rate compatible with the reach of an equilibrium is q_{cMAX} = 507 *mol/cell/min*.

The time responses of [C3*] are shown in Fig. 6 and their parameters in Table V: the shape of the time response does not change: only the delay t_D is sensibly affected by level and duration of the perturbation, with a saturation for high levels and short durations of the action.

In the second numerical experiment the continuous stress is applied until the *life-apoptosis* transition takes places and the new equilibrium is reached. Several levels of stress are tested: again the responses show the same qualitative features; the relation between level q and delay time t_D is an inverse power law, as for the case of instantaneous perturbation, obviously with different parameters: the least square fitting is $t_D = 1.511\times10^3 \times q^{-0.517}$.

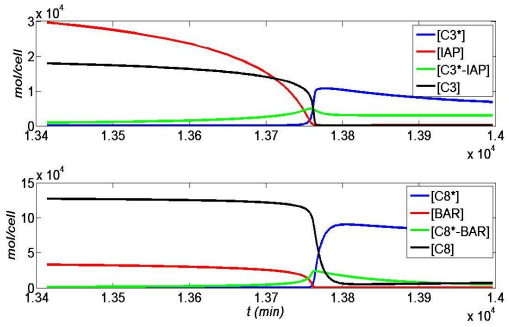

Fig. 4. Time evolution of the state variables of the nominal model restricted to the time interval [13400, 14000] minutes; initial perturbation: c =100 *mol/cell*.

TABLE IV
RELEVANT PARAMETERS OF THE TIME RESPONSE OF [C3*] TO INITIAL PERTURBATIONS OF VARIOUS INTENSITY

c (*mol/cell*)	t_D (*min*)	M_6 (*mol/cell*)	t_R (*min*)
100	13787.9	10716	9.0
250	4036.2	10716	9.2
500	1983.6	10706	9.0
1000	988.7	10682	9.1
2000	479.8	10898	9.3
3000	311.2	11271	9.5
4000	229.1	11611	9.2
5000	181.0	11879	9.2
6000	149.5	12082	9.1
7000	127.3	12232	9.2
8000	110.8	12343	9.1
9000	98.0	12426	9.3
10000	87.7	12489	9.3

Remark 2. In this experiment no threshold level has been found for the level of the continuous input. It seems that if the perturbation is applied for a sufficiently long time, the transition finally occurs.

TABLE V
RELEVANT PARAMETERS OF THE TIME RESPONSES OF [C3*] TO AN INITIAL PERTURBATION AND TO CONTINUOUS STRESS

q (*mol/cell/min*)	T (*min*)	t_D (*min*)	M_6 (*mol/cell*)	t_R (*min*)
0.1	10000	4931.4	10719	9.1
1	1000	1593.2	10694	9.3
10	100	1044.8	10683	9.2
100	10	994.1	10683	9.3
1000	1	989.2	10683	9.1
q=0, c=1000		988.7	10682	9.1

B. *Responses of the Randomly Generated Models*

With reference to models belonging to the set Σ, their time responses to perturbations of the initial state were analyzed in [10]. Here we consider again the models in

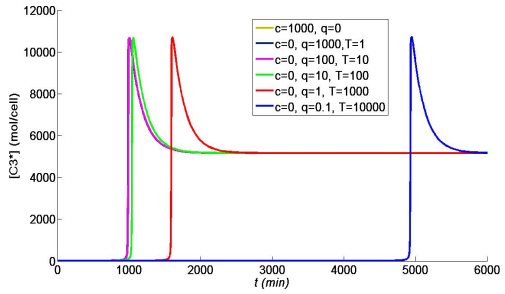

Fig. 5. Time evolutions of [C3*] corresponding to different types of stimulus/stress. c: intensity of the initial perturbation; q,T: level and duration of the continuous action. The curves for c=1000, q=1000, q=100 are indistinguishable

Σ: for each model we computed the time response due to a constant input, both at low-level ($q(t)$=0.01k_{-9}) and high-level ($q(t)$=0.8k_{-9}), with the *life* equilibrium as initial state (c=0). The simulation interval is [0, 36000] minutes (25 days): this interval may seem extremely long with respect to the timescales of laboratory experiments on cell cultures (typically from minutes to hours). However cells in living tissues may behave very differently from those in cultures.

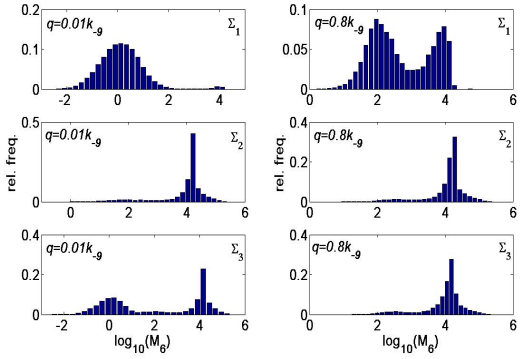

Fig. 6. Distributions of the relative frequencies of the peak values of [C3*] responses in models belonging to Σ_1, Σ_2, Σ_3, subjected to low-level (q=0.01k_{-9}) and high-level (q=0.8k_{-9}) persistent stress.

Fig. 6 and Table VI summarize the results of this numerical experiment, with the exception of the models showing periodic behavior. The evolution of [C3*] shows either a monotone increase to the equilibrium value or a sharp maximum followed by a decrease to equilibrium; the monotone increase is found in about 50% of the cases with low-level input, 21% with high-level input. For models in Σ_2 both shape and peak value of the responses are almost independent of the input level, which affects only the delay. For the bistable models of Σ_3 the effect of increasing the input level is to increase the number of models which undergo the transition: indeed [C3*] is still increasing at

TABLE VI
RELEVANT PARAMETERS OF THE TIME RESPONSES OF [C3*] TO CONTINUOUS STRESSES FOR RANDOMLY GENERATED MODELS

Models and input [a]	t_D (*min*)[b]	M_4 (*mol/cell*)[b]	t_R (*min*)[b]
Σ_1 (*l-l*)	0.07-52.8-35510	0.004-1.30-17128	5.10-428-35230
Σ_1 (*h-l*)	0.18-8.28-2894	1.57-297-66102	3.20-38.1-2863
Σ_2 (*l-l*)	14.4-277-18293	0.93-15917-248930	3.03-16.5-12100
Σ_2 (*h-l*)	0.25-50.2-1013	8.48-15947-248930	3.07-16.5-3799
Σ_3 (*l-l*)	0.07-447-35977	0.003-118-223110	2.78-404-35674
Σ_3 (*h-l*)	0.31-86.0-1660	17.7-13284-223110	2.98-22.0-3824

[a] Σ_1, Σ_2, Σ_3 : sets of models defined in section II.A; (*l-l*) low-level input, (*h-l*) high-level input.
[b] minimum-median-maximum of the delay times, peak values, rise times.

the end of the simulation interval for many models in Σ_3 with q=0.01k_{-9}; models in Σ_1 are the most sensitive to the input level: when q=0.01k_{-9} only 172 (1.2%) peak values exceed 5000 *mol/cell*, versus 3378 (27.1%) when q=0.8k_{-9}.

Remark 3. The numerical experiment mimics the application of a persistent stress to a population of cells. It is clear from the results that the dynamical behavior cannot be overlooked: the application of a constant input may produce a response with high overshoot with respect to the steady state value, depending on the model parameters. Laboratory experiments should clarify if the death of the cell can be triggered by a short intense pulse of [C3*], or else a high constant level of [C3*] must be maintained.

IV. PROCESS REGULATION

Production and decay of regulator proteins BAR, IAP, represented by the terms $v_4 = -k_{12}x_4(t) + k_{-12}$ (BAR) in Eq. (5) and $v_8 = -k_8 x_8(t) + k_{-8}$ (IAP) in Eq.(8), are under genetic control. Since genetic engineering technologies enable researchers to silence/enhance the activity of genes involved in protein synthesis, experimental regulation of apoptosis might be exerted in this way. We simulate this action by changing the values of the source terms k_{-8} for IAP and k_{-12} for BAR, with respect to the nominal values $k_{-12}^{nom} = 40$ *mol/cell/min* (BAR), and $k_{-8}^{nom} = 464$ *mol/cell/min* (IAP). From now on the units of k_{-8} and k_{-12} will be omitted for the sake of brevity.

We analyzed equilibrium, stability, dynamical responses to initial perturbations for $4 \le k_{-12} \le 80$ (the other parameters at nominal values), and for $46.4 \le k_{-8} \le 928$ (the other parameters at nominal values).

The results can be summarized as follows:

- for $k_{-12} < 39.371$ we have two equilibrium states: the *life* equilibrium is unstable, the *non-life* equilibrium is asymptotically stable; for $k_{-12} \ge 39.371$ the model shows the

bistable pattern. The dependence of equilibria on k_{-8} is exactly the same: for $k_{-8} < 456.71$ the *life* equilibrium is unstable, for $k_{-8} \geq 456.71$ the bistable pattern arises. Note that the nominal values are very close to the bifurcation.

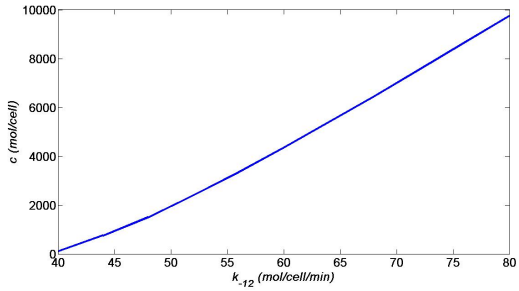

Fig. 7. Dependence of the threshold perturbation on the BAR source k_{-12} .

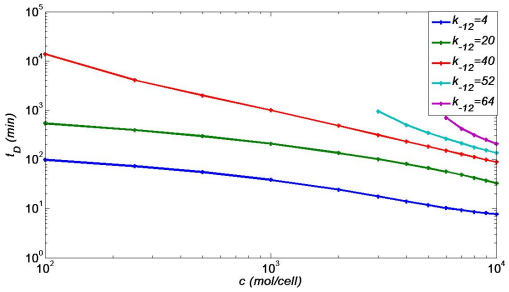

Fig. 8. Dependence of the delay time t_D on the perturbation intensity c and on the BAR source k_{-12}.

- The concentration of C3* at the *non-life* asymptotically stable equilibrium is almost independent of k_{-12}: $5160 \leq [C3^*]_A \leq 5163$; on the contrary $[C3^*]_A$ strongly depends on k_{-8}: it decreases almost linearly from 13210 *mol/cell* for k_{-8} = 46.4 to 117 *mol/cell* for k_{-8} = 928. Indeed if k_{-8} is increased to k_{-8} = 1310 the *non-life* equilibrium states disappear and the unique equilibrium is the *life* one.
- Within the range $40 \leq k_{-12} \leq 80$ characterized by the bistable behavior the increase of k_{-12} causes an almost linear increase (Fig. 7) of the threshold perturbation above which the transition to apoptotic state occurs. The same qualitative behavior is observed when k_{-8} varies in the interval $464 \leq k_{-8} \leq 835$; when $k_{-8} > 835$ the threshold perturbation exceeds 10000 *mol/cell*: in this case the and has not been evaluated.
- The time delay t_D of the transition depends on the intensity of the perturbation approximately according to a power law $t_D = \alpha c^{-\beta}$ (Fig. 8) ; both α and β increase with k_{-12}, that is low values of k_{-12} produce much faster responses. The dependence on k_{-8} is quite similar, and is not shown for the sake of brevity. Consistently with the insensitivity of $[C3^*]_A$ to changes of k_{-12}, the peak value M_6 is slightly affected by k_{-12}. On the contrary, M_6 decreases considerably when k_{-8} increases, in the same way as the *non-life* equilibrium value $[C3^*]_A$. For example when c=10000 *mol/cell* we have:

k_{-8}	46.4	278.4	464	510.4	742.4	881.6
$[C3^*]_{NL}$	13210	8726	5162	4280	544	149
M_6	19685	15713	12889	11618	6251	855

V. Conclusions

The study here reported highlights several features of the model of the apoptotic pathway in the presence of a perturbation, either instantaneous or persistent. The variety of patterns of equilibrium and stability, and of types of dynamical response shows the ability of the model structure to represent several different situations, The results of the huge number of simulations show that the dynamic behavior cannot be overlooked, because both the timing of transitions and the concentration levels in the transitions vary of orders of magnitude. The key role of regulator proteins BAR and IAP has been confirmed, and the effects of decreasing/increasing their production rate have been quantitatively evaluated. For every result a plausible biological interpretation has been given. The analysis of the model and the numerical simulations have provided, as first consequence, the guidelines for designing *in vitro* experiments which are now in progress, with encouraging results.

References

[1] M.O. Hengartner, "The biochemistry of apoptosis," *Nature*, vol. 407, pp. 770-776, 2000.

[2] S.J. . Riedl and Y. Shi, "Molecular mechanisms of caspase regulation during apoptosis," *Nat. Rev. Mol. Cell Biol.,* vol. 5, pp. 897-907, 2004.

[3] J. M. Adams, "Ways of dying: multiple pathways to apoptosis," *Genes & Dev.*, vol. 17, pp. 2481-2495, 2003.

[4] G.S. Salvesen and C.S. Duckett, "IAP proteins: blocking the road to death's door," *Nat. Rev. Mol. Cell Biol.,* vol. 3, pp. 401-410, 2002.

[5] H. Zhang, Q. Xu, S. Krajewski, M. Krajewska, Z. Xie, S. Fuess, S. Kitada, K. Pawlowski, A. Godzik, and J.C. Reed, "BAR: an apoptosis regulator at the intersection of caspases and Bcl-2 family proteins," *Proc. Nat. Acad. Sci.,*vol. 97, pp. 2597-2602, 2000.

[6] M. Fussenegger, J.E. Bailey, and J. Varner, "A mathematical model of caspase function in apoptosis," *Nat. Biotechnol*., vol. 18, pp. 768-774, 2000.

[7] M. Bentele, I. Lavrik, M. Ulrich, S. Stosser, D.W. Heermann, H. Kalthoff, P.H. Krammer, and R. Eils, "Mathematical modeling reveals threshold mechanism in CD95-induced apoptosis," *J. Cell Biol*., vol. 166, pp. 839-851, 2004.

[8] J.W. Stucki and H.U. Simon, "Mathematical modeling of the regulation of caspase-3 activation and degradation," *J. Theor. Biol.,* vol. 234, pp. 123-131,2005.

[9] T. Eissing, H. Colzemann, E.D. Gilles, F. Allgower, E. Bullinger, and P. Scheurich, "Bistability Analyses of a Caspase Activation Model for Receptor-induced Apoptosis," *J. Biol. Chem.,* pp. 279, pp. 36892-36897, 2004.

[10] L. Carotenuto, V. Pace, D.Bellizzi, G. De Benedictis, "Equilibrium, stability and dynamical response in a model of the extrinsic apoptosis pathway," *J. Biol. Syst.,* to be published.

[11] J.L. Willems, *Stability analysis of dynamical systems* , New York, NY, Nelson, 1970.

[12] K. Ogata, *Modern Control Engineering,* 4th ed. Upper Saddle River, NJ, Prentice Hall, 2002.

Journal of Biological Systems, Vol. 15, No. 3 (2007) 261–285

World Scientific
www.worldscientific.com

EQUILIBRIUM, STABILITY AND DYNAMICAL RESPONSE IN A MODEL OF THE EXTRINSIC APOPTOSIS PATHWAY

LUCIANO CAROTENUTO*, VINCENZA PACE†, DINA BELLIZZI†
and GIOVANNA DE BENEDICTIS†

*Department of Electronics, Computer Science and System Science
†Department of Cell Biology University of Calabria, 87036 Rende, Italy
*carotenuto@unical.it

Received 8 September 2006
Revised 6 February 2007

In the past few years several mathematical models have been proposed to formally represent the biochemical processes that lead to the programmed death of the cell (apoptosis) starting from an intrinsic or extrinsic stimulus. In this paper we consider the model proposed by Eissing and colleagues in 2004 and, compared to the previously published results, provide several original contributions. We prove formally that the model can have one, two or three equilibrium states; one of these (the *life* equilibrium) represents the normal state of the cell: we state a stability criterion for this equilibrium and prove that its stability/instability is related to the number of equilibrium states. A large sample of models with randomly generated parameter vectors (representative of a population of cells) is numerically analyzed as regards both the equilibria and respective stability properties, and the dynamical behavior. Many patterns of stable/unstable equilibrium states, and different types of bifurcations are discovered. Correlations between model parameters, equilibrium patterns and equilibrium concentration of a critical protein are also carried out. The analysis of the dynamical time responses shows that the richness of behaviors accounted by the model is much larger than that implied by the classification into *life-monostable*, *bistable*, *death-monostable* models.

Keywords: Apoptosis; Dynamical Models; Stability; Parametric Sensitivity.

1. Introduction

Apoptosis, or programmed cell death, is a cellular process essential for development and survival, that involves one of the most complex signaling pathways.[1–3] It enables multicellular organisms to regulate cell number in tissues, and to eliminate damaged or unneeded cells. Accordingly, programmed cell death plays a critical role in a wide variety of physiological processes, from embryonic development to tissue aging. Furthermore, several lines of evidence indicate that defects in the apoptosis mechanisms may impair normal cell turnover, thus promoting either cell accumulation and tumor progression, or abnormal death rates, as in neurodegenerative diseases.[4] The executioners of apoptosis are caspases, a family of conserved cystine proteases that cleave target proteins at specific aspartate residues.[2] Caspases exist

as inactive zymogens (pro-caspases) in cells and undergo a cascade of catalytic reactions that transform them into active caspases at the onset of apoptosis. The mechanism of caspases activation has been studied in depth and the existence of several homologous members of the family has been recognized. Caspases are classified[5] as *initiator*, such as C8, C9, C10, and *effector* caspases, such as C3, C6, C7: the latter are activated by the active form of *initiator* pro-caspases, and start up substrate cleavage and subsequent processes involving genomic DNA fragmentation and leading to cell death. In mammalian cells two apoptosis pathways are known: extrinsic or intrinsic. In the extrinsic pathway[6] cell surface receptors (DR4, DR5, CD95, etc.) are activated by external stimuli such as Apo2L/TRAIL, FasL, TNF. On stimulation of the receptor, pro-caspase-8 is recruited and activated; in turn this active form activates the downstream *effector* pro-caspases. Cells characterized by this process are known as *type I* cells. In the intrinsic pathway the mitochondrion releases cytochrome c[7] which causes the activation of pro-caspase-9, which in turn activates *effector* pro-caspases. This pathway is stimulated by several types of stress (radiative, thermal, chemical, etc.). A connection between the receptor- and mitochondrion-mediated pathways is established by Bid protein which, if cleaved by caspase-8, may cause the release of cytochrome c. Cells where this pathway is followed in response to an external stimulus are known as *type II* cells.

The complexity of the apoptotic pathways arises from the existence of multiple levels of regulation, through activation or inhibition of key proteins. A most relevant role in the regulatory mechanisms has been recognized for proteins from the IAPs family[8–10] as inhibitors of caspase-3, and for the protein BAR[11] as inhibitor of caspase-8. The overall pattern of caspases activation is made even more intricate by the presence of several other molecules that interfere with the process (Bcl-2 family, Smac/Diablo, for example), by the observation that IAPs and BAR may have other functions besides inhibition, and by the presence of feedback mechanisms of active *effector* caspases on *initiator* pro-caspases.

In recent literature, mathematical modeling has been recognized as a powerful tool (1) to understand various aspects of apoptotic processes, (2) to lay down guidelines to design new experiments, and (3) to evaluate the effects of therapeutic actions designed to enhance or restrain apoptotic cell death. The models proposed up to now mainly describe the caspases activation process, which is in fact only the first step of the pathway. These models consist of systems of ordinary differential equations (ODEs) whose solution describes the time evolution of concentrations of chemical species regarded as relevant in the process. Fussenegger *et al.*[12] built up a model of 13 ODEs and carried out simulations mainly with the aim of testing inhibitory strategies. Simulative analysis of caspase-3 regulation is reported also in Ref. 13. Eissing *et al.*[14] proposed a six- and an eight-order model (reduced and extended models, respectively) of the extrinsic pathway: they carried out both analytical and numerical investigations of system equilibria, stability, and parameter sensitivity. Special attention was devoted to the model property of

bistability,[14] i.e. the existence of two attractive equilibrium states, between which the model can commute, on the assumption that this property is "an essential condition" for a model to describe appropriately the caspase activation. In a further paper,[15] Eissing *et al.* consider the robustness of the bistable behavior with respect to parameter variations as a selection criterion between the reduced and extended models. Bistability is also addressed in Ref. 16, where the mitochondrial pathway is described by 31 ODEs. Finally, two papers[17,18] present the results both of model analysis/simulation, and of *in vitro* experiments specifically designed to calibrate and validate the model. In particular, Bentele *et al.*[17] perform sensitivity analysis, model reduction and least-square parameter estimation for a very complex model of the complete receptor-mediated pathway, showing the existence of a threshold in the intensity of the external stimulus. Rhem *et al.*[18] analyze the regulation of caspase-3 in the intrinsic pathway, and compare model predictions to single cell behavior detected by specific imaging techniques.

In this paper we consider the eight-order model of the extrinsic pathway proposed by Eissing *et al.*[14] The model incorporates:

- production and decay of pro-caspase-8 (C8) and of pro-caspase-3 (C3), and of inhibitors IAP and BAR;
- mutual feedback activation of C8 by active caspase-3 ($C3^*$) and of C3 by active caspase-8 ($C8^*$);
- inactivation of $C8^*$ by BAR through reversible formation of the complex $C8^* \div$ BAR;
- inactivation of $C3^*$ by IAP through reversible formation of the complex $C3^* \div$ IAP.

Further details on the biochemical processes, modeling assumptions, numerical estimates of model parameters can be found in Ref. 14.

In the present paper, several issues not covered by the previous works are considered: (1) formal proofs of some results about existence and stability of equilibrium states, and (2) complete analysis of the equilibrium states, of the respective stability properties, of the time responses to perturbations which simulate the application of an external stimulus for a large sample of models whose parameters are randomly generated in a neighborhood of a reference parameter vector taken from the literature. The analysis will provide a clear picture of the richness of behaviors predicted by the model, as well as a better understanding of the role played by individual parameters and by the reactions in which they appear. The information on the collective response of a population of cells gained by simulating the responses of a huge number of models characterized by different parameter values may provide guidelines to design laboratory experiments of apoptosis involving cell cultures, and may be used, in comparison with the results of these experiments, for the calibration and validation of the model.

2. Analysis of the Model

Let $x_i, i = 1, 2, \ldots, 8$ denote the concentration of the relevant chemical species: $x_1 = [\mathrm{C8}], x_2 = [\mathrm{C8}^*], x_3 = [\mathrm{C3}], x_4 = [\mathrm{C3}^*], x_5 = [\mathrm{IAP}], x_6 = [\mathrm{C3}^* \div \mathrm{IAP}], x_7 = [\mathrm{BAR}], x_8 = [\mathrm{C8}^* \div \mathrm{BAR}]$. The units *molecules per cell* (*mol/cell*) for the concentrations, *minutes* (*min*) for the time will be used. The time evolution of the concentrations satisfies the set of ordinary differential equations[14]

$$\dot{x}_1(t) = -k_2 x_1(t) x_4(t) - k_9 x_1(t) + k_{-9} \tag{2.1}$$

$$\dot{x}_2(t) = k_2 x_1(t) x_4(t) - k_5 x_2(t) - k_{11} x_2(t) x_7(t) + k_{-11} x_8(t) \tag{2.2}$$

$$\dot{x}_3(t) = -k_1 x_2(t) x_3(t) - k_{10} x_3(t) + k_{-10} \tag{2.3}$$

$$\dot{x}_4(t) = k_1 x_2(t) x_3(t) - k_3 x_4(t) x_5(t) + k_{-3} x_6(t) - k_6 x_4(t) \tag{2.4}$$

$$\dot{x}_5(t) = (-k_4 - k_3) x_4(t) x_5(t) + k_{-3} x_6(t) - k_8 x_5(t) + k_{-8} \tag{2.5}$$

$$\dot{x}_6(t) = k_3 x_4(t) x_5(t) - k_{-3} x_6(t) - k_7 x_6(t) \tag{2.6}$$

$$\dot{x}_7(t) = -k_{11} x_2(t) x_7(t) + k_{-11} x_8(t) - k_{12} x_7(t) + k_{-12} \tag{2.7}$$

$$\dot{x}_8(t) = k_{11} x_2(t) x_7(t) - k_{-11} x_8(t) - k_{13} x_8(t). \tag{2.8}$$

The model is characterized by 19 parameters that we collect in the vector $\underline{k} = [k_1 \ldots k_{13} k_{-3} k_{-8} \ldots k_{-12}]$. The numerical values given by Eissing *et al.*[14] will be used as *nominal parameters* (Table 1), and denoted by $k_i^{nom}, i = 1, \ldots, 13, -3, \ldots, -12$. The corresponding model will be said *nominal*.

Table 1. Model parameters. The numerical values in the third column are from Eissing *et al.*[14]

Parameter	Physical dimension [C]: concentration [*t*]: time	Nominal value [C]: *mol/cell*, [t]: *min*	Reaction where the parameter appears
k_1	$[\mathrm{C}]^{-1}[t]^{-1}$	5.80×10^{-5}	$\mathrm{C3} + \mathrm{C8}^* \rightarrow \mathrm{C3}^* + \mathrm{C8}^*$
k_2	$[\mathrm{C}]^{-1}[t]^{-1}$	1.00×10^{-5}	$\mathrm{C8} + \mathrm{C3}^* \rightarrow \mathrm{C8}^* + \mathrm{C3}^*$
k_3	$[\mathrm{C}]^{-1}[t]^{-1}$	5.00×10^{-4}	$\mathrm{C3}^* + \mathrm{IAP} \rightarrow \mathrm{C3}^* \div \mathrm{IAP}$
k_4	$[\mathrm{C}]^{-1}[t]^{-1}$	3.00×10^{-4}	Cleavage of IAP
k_5	$[t]^{-1}$	5.80×10^{-3}	Decay of $\mathrm{C8}^*$
k_6	$[t]^{-1}$	5.80×10^{-3}	Decay of $\mathrm{C3}^*$
k_7	$[t]^{-1}$	1.73×10^{-2}	Decay of $\mathrm{C3}^* \div \mathrm{IAP}$
k_8	$[t]^{-1}$	1.16×10^{-2}	Decay of IAP
k_9	$[t]^{-1}$	3.90×10^{-3}	Decay of C8
k_{10}	$[t]^{-1}$	3.90×10^{-3}	Decay of C3
k_{11}	$[\mathrm{C}]^{-1}[t]^{-1}$	5.00×10^{-4}	$\mathrm{C8}^* + \mathrm{BAR} \rightarrow \mathrm{C8}^* \div \mathrm{BAR}$
k_{12}	$[t]^{-1}$	1.00×10^{-3}	Decay of BAR
k_{13}	$[t]^{-1}$	1.16×10^{-2}	Decay of $\mathrm{C8}^* \div \mathrm{BAR}$
k_{-3}	$[t]^{-1}$	2.10×10^{-1}	$\mathrm{C3}^* \div \mathrm{IAP} \rightarrow \mathrm{C3}^* + \mathrm{IAP}$
k_{-8}	$[\mathrm{C}][t]^{-1}$	$4.64 \times 10^{+2}$	Production of IAP
k_{-9}	$[\mathrm{C}][t]^{-1}$	$5.07 \times 10^{+2}$	Production of C8
k_{-10}	$[\mathrm{C}][t]^{-1}$	$8.19 \times 10^{+1}$	Production of C3
k_{-11}	$[t]^{-1}$	2.10×10^{-1}	$\mathrm{C8}^* \div \mathrm{BAR} \rightarrow \mathrm{C8}^* + \mathrm{BAR}$
k_{-12}	$[\mathrm{C}][t]^{-1}$	$4.00 \times 10^{+1}$	Production of BAR

2.1. *Equilibrium states*

By inspection of Eqs. (2.1)–(2.8), it is apparent that the vector

$$\underline{x}_{EL} = [x_{L1}0x_{L3}0x_{L5}0x_{L7}0]^T = \left[\frac{k_{-9}}{k_9}0\frac{k_{-10}}{k_{10}}0\frac{k_{-8}}{k_8}0\frac{k_{-12}}{k_{12}}0\right]^T \tag{2.9}$$

is an equilibrium state, characterized by the absence of active caspases, either free or bound to BAR, IAP: this equilibrium will be denoted as the *life* one, and will be taken as the "standard" state of the cell.

The other equilibrium states (called *non-life*) are the non-negative real solutions of the algebraic equations resulting from Eqs. (2.1)–(2.8) when the derivatives are set to zero ($\dot{x}_i(t) = 0$).

Some continuity relations among concentrations at equilibrium are immediately obtained:

$$k_9x_1 + k_5x_2 + k_{13}x_8 = k_{-9} \tag{2.10}$$

$$k_{12}x_7 + k_{13}x_8 = k_{-12} \tag{2.11}$$

$$k_{10}x_3 + k_6x_4 + k_7x_6 = k_{-10} \tag{2.12}$$

$$(k_4x_4 + k_8)x_5 + k_7x_6 = k_{-8}. \tag{2.13}$$

Equations (2.10)–(2.13) and the physical constraint $x_i \geq 0, i = 1, \ldots, 8$ provide upper bounds to the concentrations at equilibrium. Furthermore, Eqs. (2.10)–(2.13) suggest to define the dimensionless state variables and parameters

$$\xi_1 = \frac{x_1}{x_{L1}}, \quad \xi_2 = \frac{k_5x_2}{k_{-9}}, \quad \xi_3 = \frac{x_3}{x_{L3}}, \quad \xi_4 = \frac{k_6x_4}{k_{-10}},$$

$$\xi_5 = \frac{x_5}{x_{L5}}, \quad \xi_6 = \frac{k_7x_6}{k_{-10}}, \quad \xi_7 = \frac{x_7}{x_{L7}}, \quad \xi_8 = \frac{k_{13}x_8}{k_{-12}},$$

$$\alpha_1 = \frac{k_2k_{-10}}{k_6k_9}, \quad \alpha_2 = \frac{k_1k_{-9}}{k_5k_{10}}, \quad \alpha_3 = \frac{k_3k_{-8}}{k_6k_8}, \quad \alpha_4 = \frac{k_4k_{-10}}{k_6k_8},$$

$$\alpha_5 = \frac{k_{11}k_{-9}}{k_5k_{12}}, \gamma = \frac{k_{-3}}{k_7}, \quad \delta = \frac{k_{-10}}{k_{-8}}, \quad \varepsilon = \frac{k_{-11}}{k_{13}}, \quad \theta = \frac{k_{-12}}{k_{-9}}.$$

With such choices the corresponding equilibrium equations are:

$$-\alpha_1\xi_1\xi_4 - \xi_1 + 1 = 0 \tag{2.14}$$

$$\alpha_1\xi_1\xi_4 - \xi_2 - \theta\alpha_5\xi_2\xi_7 + \varepsilon\theta\xi_8 = 0 \tag{2.15}$$

$$-\alpha_2\xi_2\xi_3 - \xi_3 + 1 = 0 \tag{2.16}$$

$$\alpha_2\xi_2\xi_3 - \xi_4 - \alpha_3\xi_4\xi_5 + \gamma\xi_6 = 0 \tag{2.17}$$

$$-(\alpha_3\delta + \alpha_4)\xi_4\xi_5 - \xi_5 + \gamma\delta\xi_6 + 1 = 0 \tag{2.18}$$

$$\alpha_3\xi_4\xi_5 - (\gamma + 1)\xi_6 = 0 \tag{2.19}$$

$$-\alpha_5\xi_2\xi_7 - \xi_7 + \varepsilon\xi_8 + 1 = 0 \tag{2.20}$$

$$\alpha_5\xi_2\xi_7 - (\varepsilon + 1)\xi_8 = 0. \tag{2.21}$$

Equations (2.14)–(2.21) are easier to manipulate than the equilibrium version of (2.1)–(2.8). The dimensionless state variables at equilibrium take values in the interval [0,1], and the *life* equilibrium is $\xi_{EL} = [1\,0\,1\,0\,1\,0\,1\,0]^T$.

A direct approach to the analysis of equilibrium states would be to perform successive substitutions into Eqs. (2.14)–(2.21), until a single algebraic equation is obtained. By such a procedure a fifth degree algebraic equation in the variable ξ_4 is obtained. One solution is $\xi_4 = 0$, which gives the *life* equilibrium; the other equilibrium states are obtained as the real positive roots of a fourth degree equation. This equation has been used for a very efficient and accurate numerical evaluation of the equilibrium states. However the explicit expressions of the coefficients of the equation are extremely intricate, and are of no use to decide if, or how many, positive roots exist. We then adopted a different approach to prove that.

Proposition 2.1. *Equations* (2.1)–(2.8) *may have one, two or three equilibrium states, one of which — the "life" equilibrium — is given by* (2.9).

The result of Proposition 2.1 is cited without proof in Eissing *et al.*,[14] so that it is not clear whether it is guessed from numerical experiments. Therefore we report a proof in Appendix A (Supplementary Material).

Models with one, two and three equilibrium states will be called types 1, 2 and 3 models, respectively.

2.2. *Stability of equilibrium states*

Stability of the equilibrium states is analyzed here by linearization.[19] Since the general expression of the Jacobian matrix of Eqs. (2.1)–(2.8) is very complex, the stability of the *non-life* equilibrium states can be checked only by numerical computation of the eigenvalues of the appropriate Jacobian matrix. On the contrary, the Jacobian matrix at the *life* equilibrium, $J(\underline{x}_{EL})$, has a special structure which enables us to prove that:

Proposition 2.2. *Let*

$$f(\underline{k}) = k_1k_2x_{L1}x_{L3} - \left(k_5 + \frac{k_{11}}{1 + k_{-11}/k_{13}}x_{L7}\right)\left(k_6 + \frac{k_3}{1 + k_{-3}/k_7}x_{L5}\right); \tag{2.22}$$

if $f(\underline{k}) < 0$ *then the life equilibrium state is asymptotically stable*; *if* $f(\underline{k}) > 0$ *then the life equilibrium state is unstable because of one real positive eigenvalue of* $J(\underline{x}_{EL})$.

Proposition 2.2 is proved in Appendix B (Supplementary Material), using the explicit expression of the characteristic polynomial of $J(\underline{x}_{EL})$, and applying the techniques of "root locus" analysis[20]: in this way it is shown that if $f(\underline{k}) < 0$, then

the eigenvalues of $J(\underline{x}_{EL})$ are real and negative, if $f(\underline{k}) > 0$ then one eigenvalue of $J(\underline{x}_{EL})$ is positive. Equation $f(\underline{k}) = 0$ defines a separation surface S_B in the parameter space.

Remark 2.1. From Eq. (2.22) we observe that

- parameter k_4, (rate of cleavage of IAP by C3*) has no effect on stability;
- parameter pairs (k_{-8},k_8), (k_{-9}, k_9), (k_{-10},k_{10}), (k_{-12}, k_{12}) affect stability through their ratios, i.e. the *life* equilibrium concentrations of IAP, C8, C3, BAR;
- also the parameter pairs (k_{-11},k_{13}), (k_{-3}, k_7) affect stability through their ratios; note that k_{-11} (k_{-3}) is the rate of dissociation of the complex C8$^* \div$ BAR (C3$^* \div$ IAP) into C8* and BAR (C3* and IAP), k_{13} (k_7) is the rate of degradation of C8$^* \div$ BAR (C3$^* \div$ IAP).

From a qualitative point of view we may assert as general properties of the model that

(1) an *increase* (*decrease*) of k_1, k_2, x_{L1}, x_{L3}, k_{-11}/k_{13}, k_{-3}/k_7 destabilizes (stabilizes) the *life* equilibrium;
(2) an *increase* (*decrease*) of k_5, k_6, x_{L5}, x_{L7}, k_{11}, k_3 stabilizes (destabilizes) the *life* equilibrium.

Quantitative examples of bifurcations across S_B will be given in the numerical experiments.

A relevant question in the analysis of the model is the existence of a connection between the stability of the *life* equilibrium and the number of equilibrium states. For the reduced model[14] it is shown that if that model has only one *non-life* equilibrium, then the *non-life* equilibrium is unstable. For the model considered here we are able to characterize completely the connection between the stability of the *life* equilibrium and the existence and number of *non-life* equilibria. Indeed, on the non-restrictive assumption that the Jacobian matrix at the *life* equilibrium is non-singular, the following result holds.

Proposition 2.3. *If the life equilibrium is unstable, then there exists a unique non-life equilibrium; if the life equilibrium is asymptotically stable, then we have, generically, either no non-life equilibrium, or two non-life equilibria.*

The proof of Proposition 2.3 is reported in Appendix C (Supplementary Material), together with a graphical illustration of the ideas below the technicalities.

Remark 2.2. The results of Propositions 2.1–2.3 remind us of similar properties of the model of enzyme activity regulation[21] (EAR) in the inducible case. However, substantial differences are: for the EAR model two equilibria arise only at the transition "surfaces" between one-equilibrium and three-equilibria patterns, whereas in our model the two-equilibria pattern may fill a large portion of the parameter space; when EAR has three equilibria, two of them are asymptotically stable, whereas in

our model the stability of the *non-life* equilibrium states is not constrained. We shall see in the numerical experiments that almost all possible patterns actually occur in a neighborhood of the nominal parameter vector.

Remark 2.3. If active caspases are initially absent, the model predicts that they are not produced, whilst the concentrations of C8, C3, IAP, BAR converge exponentially from any initial condition to the respective values of the *life* equilibrium, even if the *life* equilibrium is unstable. Conversely, if the *life* equilibrium is unstable, and at least one of the initial concentrations $x_2(0) = [\mathrm{C8}^*]_{\mathrm{IN}}$, $x_4(0) = [\mathrm{C3}^*]_{\mathrm{IN}}$, $x_6(0) = [\mathrm{C3}^* \div \mathrm{IAP}]_{\mathrm{IN}}$, $x_8(0) = [\mathrm{C8}^* \div \mathrm{BAR}]_{\mathrm{IN}}$ is positive, then the state trajectory moves away definitively from the *life* equilibrium (Appendix D in Supplementary Material).

2.3. *Equilibrium and stability of the nominal model*

Numerical solution of the algebraic equation obtained by manipulation of Eqs. (2.14)–(2.21) shows that the *nominal* model has three equilibrium states: the *life* equilibrium, denoted by $\mathrm{E_L}$ and two *non-life* equilibria, denoted by $\mathrm{E_{NL1}}$, $\mathrm{E_{NL2}}$. The respective values of the state variables are shown in Table 2. Equilibrium $\mathrm{E_{NL1}}$ is very close to the *life* one, whereas equilibrium $\mathrm{E_{NL2}}$ is characterized by very low concentrations of C8, C3, BAR and IAP with respect to those at *life* equilibrium, and high concentrations of active caspases $\mathrm{C8}^*$, $\mathrm{C3}^*$ and complexes $\mathrm{C8}^* \div \mathrm{BAR}$, $\mathrm{C3}^* \div \mathrm{IAP}$.

As regards stability, equilibrium $\mathrm{E_L}$ is asymptotically stable, $\mathrm{E_{NL1}}$ is unstable, $\mathrm{E_{NL2}}$ is asymptotically stable, thus revealing the *bistable* pattern.[14] However, the nominal model is very close to the separation surface S_B. Indeed $f(\underline{k}^{nom}) = -0.0252$, and easy calculations show that the relative increment of the parameters (or ratios of parameters) which make $f(\underline{k}) = 0$ are:

$$\delta k_1 = \delta k_2 = \delta x_{L1} = \delta x_{L3} = 1.59\%; \quad \delta k_3 = \delta k_{11} = \delta x_{L5} = \delta x_{L7} = -1.57\%;$$
$$\delta(k_{-11}/k_{13}) = 1.69\%; \quad \delta(k_{-3}/k_7) = 1.73\%.$$

Table 2. Numerical values of the equilibrium states $\mathrm{E_L}$ (*life*), $\mathrm{E_{NL1}}$, $\mathrm{E_{NL2}}$ of the nominal model.

	$\mathrm{E_L}$ (*Life*)	$\mathrm{E_{NL1}}$	$\mathrm{E_{NL2}}$ (*Apoptosis*)		$\mathrm{E_L}$ (*Life*)	$\mathrm{E_{NL1}}$	$\mathrm{E_{NL2}}$ (*Apoptosis*)
	Dimensionless variables				(*mol/cell*)	(*mol/cell*)	(*mol/cell*)
ξ_1	1	9.990×10^{-1}	7.025×10^{-2}	[C8]	130000	129870	9132
ξ_2	0	5.626×10^{-6}	8.509×10^{-1}	[C8*]	0	0	74380
ξ_3	1	9.927×10^{-1}	9.032×10^{-4}	[C3]	21000	20848	19
ξ_4	0	2.787×10^{-6}	3.655×10^{-1}	[C3*]	0	0	5162
ξ_5	1	9.887×10^{-1}	6.604×10^{-3}	[IAP]	40000	39546	264
ξ_6	0	7.233×10^{-3}	6.336×10^{-1}	[C3* ÷ IAP]	0	34	3000
ξ_7	1	9.873×10^{-1}	5.134×10^{-4}	[BAR]	40000	39492	21
ξ_8	0	1.271×10^{-2}	9.995×10^{-1}	[C8*÷BAR]	0	44	3447

If we assume that the value $[C3^*] = 5162\, mol/cell$ (Table 2) is sufficiently high to trigger the subsequent steps of apoptosis, we might define the equilibrium state E_{NL2} as the *apoptosis* equilibrium: however such term is not strictly appropriate because this state cannot be maintained by the cell. Indeed, full activation of caspase-3 is followed within minutes[18] by substrate cleavage, proteolytic cascades, inactivation of repair, DNA cleavage.

2.4. *Numerical experiments*

The dependence of the equilibrium states and of their stability on the model parameters was analyzed by numerical experiments, designed to enlighten different aspects of the dependence.

2.4.1. *Experiment 1*

Let us introduce the intervals $I(a, k_i^{nom}) = [k_i^{nom}(1-a), k_i^{nom}(1+a)]$, $i = 1, \ldots, 13, -3, \ldots, -12$, and let $R(a, \underline{k}^{nom})$ be a rectangular neighborhood of the nominal parameter vector defined by: $R(a, \underline{k}^{nom}) = \{\underline{k} \mid k_i \in I(a, k_i^{nom})\}$ with $a \in (0, 1)$. The parameter a is an index of its size. We considered 50 values of a, logarithmically scaled in the interval [0.01, 0.9]; for each a we generated a sample consisting of 10,000 parameter vectors belonging to $R(a, \underline{k}^{nom})$, and computed the corresponding equilibrium states and eigenvalues of the associated Jacobian matrix. The vectors were generated according to the rule that the ith components are pseudorandom numbers uniformly distributed on the interval $I(a, k_i^{nom})$, for $i = 1, \ldots, 13, -3, -11$. The parameters k_{-8}, k_{-9}, k_{-10}, k_{-12} were computed from k_8, k_9, k_{10}, k_{12} so that the *life* equilibrium state was the same as the *life* equilibrium of the nominal model:

$$\underline{x}_{EL} = \left[\frac{k_{-9}}{k_9} 0 \frac{k_{-10}}{k_{10}} 0 \frac{k_{-8}}{k_8} 0 \frac{k_{-12}}{k_{12}} 0\right]^T = \left[\frac{k_{-9}^{nom}}{k_9^{nom}} 0 \frac{k_{-10}^{nom}}{k_{10}^{nom}} 0 \frac{k_{-8}^{nom}}{k_8^{nom}} 0 \frac{k_{-12}^{nom}}{k_{12}^{nom}} 0\right]^T.$$

This procedure simulates the production of populations of cells characterized by parameters whose average values are the nominal ones; the value of a determines how much the cells are similar to each other. The constraints on k_{-8}, k_{-9}, k_{-10}, k_{-12} impose that all the cells of the population, in normal conditions, have the same concentrations of pro-caspase-8, pro-caspase-3, and of inhibitors IAP, BAR.

Figure 1a shows the relative frequencies of types 1, 2 and 3 models in the samples, as a function of the size parameter a. Clearly, if the neighborhood is very small, almost all the tested models behave as the nominal one. When a is increased, the fraction of models with two equilibrium states increases, and for even larger neighborhoods also models with the sole *life* equilibrium are present. In a wide range of a values, the fraction of models with two equilibrium states is almost constant at the value 0.5, and the increase of the fraction of models with one equilibrium state corresponds to a decrease of the fraction of models with three equilibrium states. This property is explained by the fact that the nominal model

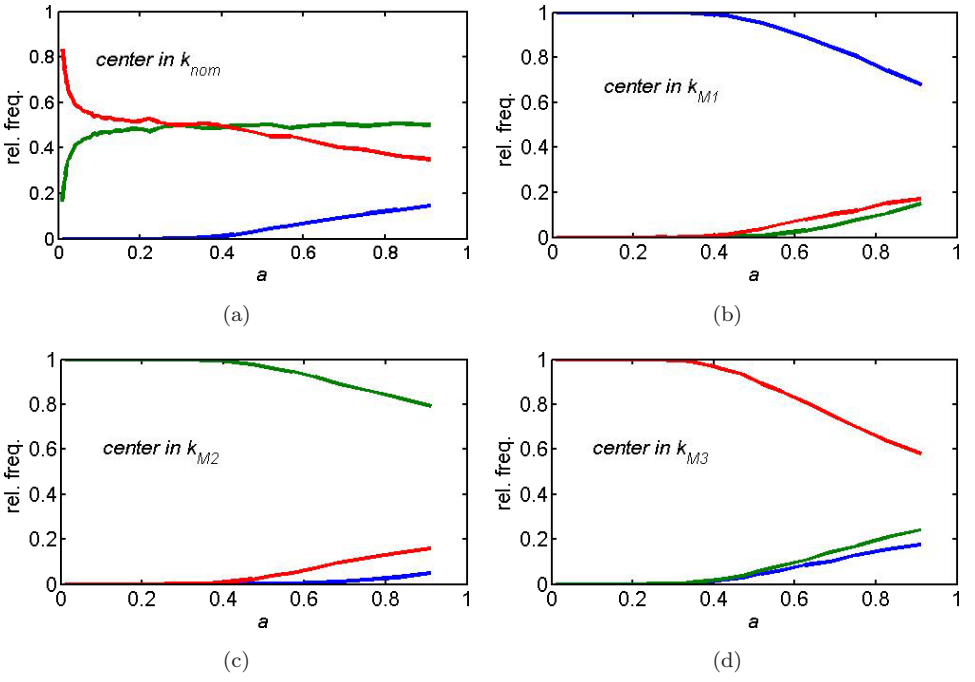

Fig. 1. Relative frequencies of types 1 (blue), 2 (green) and 3 (red) models in samples belonging to regions $R(a, \underline{k}^{nom})$ (panel a), $R(a, \underline{k}_{\mathrm{M1}})$ (panel b), $R(a, \underline{k}_{\mathrm{M2}})$ (panel c) and $R(a, \underline{k}_{\mathrm{M3}})$ (panel d) as a function of the size parameter a. For each centre $\underline{k}_c (\underline{k}_c = \underline{k}^{nom}, \underline{k}_{\mathrm{M1}}, \underline{k}_{\mathrm{M2}}, \underline{k}_{\mathrm{M3}})$ and for each a (50 logarithmically scaled values in [0.01, 0.9]) a sample consisting of 10000 parameter vectors was generated, with the components $k_i, i = 1, \ldots, 13, -3, -11$ pseudorandom numbers uniformly distributed on the intervals $I(a, k_{\mathrm{ci}}) = [k_{\mathrm{ci}}(1-a), k_{\mathrm{ci}}(1+a)]$. The parameters $k_{-8}, k_{-9}, k_{-10}, k_{-12}$ were computed from k_8, k_9, k_{10}, k_{12} in such a way that the *life* equilibrium state was the same as the *life* equilibrium of the nominal model.

is very close to the separation surface S_B: then for $a \geq 0.3$ (Fig. 1a) the volume in which models are sampled is split into almost equal parts by S_B. When the volume is increased, the region where the *life* equilibrium is stable contains more and more models with only one equilibrium.

2.4.2. *Experiment 2*

In this experiment we analyze equilibrium and stability patterns in a sample of 100,000 models, with parameter vectors randomly generated in the region $R(0.9, \underline{k}^{nom})$ according to the rules described in Sec. 2.4.1. The sample is denoted by $\mathcal{S}_{nom}$. Several different patterns have been observed:

- 14,678 models with one, asymptotically stable equilibrium (type 1 models, subsample $\mathcal{S}_1$);

- 50,566 models with two equilibria (type 2 models, sub-sample $\mathcal{S}_2$): the *life* equilibrium (unstable) and one *non-life* equilibrium which is asymptotically stable in most cases (50,263 models) and unstable in a few cases (303 models);
- 34,756 models with three equilibria (type 3 models, sub-sample $\mathcal{S}_3$): the *life* equilibrium (asymptotically stable), one "low" *non-life* equilibrium $\mathrm{E_{NL1}}$, one "high" *non-life* equilibrium $\mathrm{E_{NL2}}$ (the terms "low" and "high" refer to the values of $[\mathrm{C3^*}]$ at the respective equilibria: $0 < [\mathrm{C3^*}]_{\mathrm{NL1}} < [\mathrm{C3^*}]_{\mathrm{NL2}}$). The "low" equilibrium is unstable in all models, the "high" equilibrium is asymptotically stable in most cases (34,659 models), but there exist a few models (97) in which it is unstable.

Table 3 shows the vectors $\underline{k}_{\mathrm{M1}}$, $\underline{k}_{\mathrm{M2}}$, $\underline{k}_{\mathrm{M3}}$ of the median values of the parameters in sub-samples $\mathcal{S}_1$, $\mathcal{S}_2$, $\mathcal{S}_3$, respectively. We consider the median because the distributions are often skew. The problem of defining a maximal (in a suitable sense) region of the parameter space containing only bistable models is initially considered by Eissing *et al.*,[14] and is widely investigated to establish the robustness of the bistability property.[15] Using the procedure of *Experiment 1* (Figs. 1b to 1d) we can build rectangular neighborhoods of the median vectors $\underline{k}_{\mathrm{M1}}$, $\underline{k}_{\mathrm{M2}}$, $\underline{k}_{\mathrm{M3}}$ which contain only types 1, 2 or 3 models: the sizes of these neighborhoods are $a_1 = 0.27$, $a_2 = 0.24$, $a_3 = 0.22$, respectively. We can also make quantitative statements, based on the Chernov bound.[22] Let $P_i (i = 1, 2, 3)$ be the measure of the set $\mathcal{N}_i = \{\underline{k} \mid (1 - a_i)\underline{k}_{\mathrm{Mi}} \leq \underline{k} \leq (1 + a_i)\underline{k}_{\mathrm{Mi}}\}$, P_i^* the measure of the subset of $\mathcal{N}_i$ consisting of parameter vectors associated to type i models: then, with probability not less than 95%, we can assert that $0.99\ P_i < P_i^* \leq P_i$.

Table 3. Median values of parameters belonging to sets $\mathcal{S}_1$, $\mathcal{S}_2$, $\mathcal{S}_3$. $\mathcal{S}_i$: subset of $\mathcal{S}_{nom}$ comprising the parameter vectors for which the model has i equilibrium state(s).

Parameter	Median on $\mathcal{S}_1$ ($\underline{k}_{\mathrm{M1}}$)	Median on $\mathcal{S}_2$($\underline{k}_{\mathrm{M2}}$)	Median on $\mathcal{S}_3$($\underline{k}_{\mathrm{M3}}$)
k_1	4.92×10^{-5}	6.88×10^{-5}	4.34×10^{-5}
k_2	6.70×10^{-6}	1.19×10^{-5}	8.32×10^{-6}
k_3	6.87×10^{-4}	3.90×10^{-4}	5.52×10^{-4}
k_4	2.37×10^{-4}	3.01×10^{-4}	3.27×10^{-4}
k_5	5.92×10^{-3}	5.78×10^{-3}	5.69×10^{-3}
k_6	5.78×10^{-3}	5.79×10^{-3}	5.80×10^{-3}
k_7	2.31×10^{-2}	1.39×10^{-2}	1.89×10^{-2}
k_8	1.45×10^{-2}	1.16×10^{-2}	1.01×10^{-2}
k_9	3.74×10^{-3}	3.93×10^{-3}	3.94×10^{-3}
k_{10}	2.07×10^{-3}	3.90×10^{-3}	4.62×10^{-3}
k_{11}	5.60×10^{-4}	3.91×10^{-4}	6.10×10^{-4}
k_{12}	1.18×10^{-3}	1.00×10^{-3}	9.10×10^{-4}
k_{13}	1.28×10^{-2}	9.21×10^{-3}	1.40×10^{-2}
k_{-3}	1.08×10^{-1}	2.46×10^{-1}	1.97×10^{-1}
k_{-8}	$5.81 \times 10^{+2}$	$4.62 \times 10^{+2}$	$4.04 \times 10^{+2}$
k_{-9}	$4.87 \times 10^{+2}$	$5.10 \times 10^{+2}$	$5.12 \times 10^{+2}$
k_{-10}	$4.35 \times 10^{+1}$	$8.19 \times 10^{+1}$	$9.71 \times 10^{+1}$
k_{-11}	1.88×10^{-1}	2.48×10^{-1}	1.59×10^{-1}
k_{-12}	$4.72 \times 10^{+1}$	$4.00 \times 10^{+1}$	$3.64 \times 10^{+1}$

Larger sets of this kind can be built with an iterative procedure: for example we may generate 100,000 models in the region $R(0.9, \underline{k}_{\mathrm{M3}})$, take the median of the parameter vectors of type 3 in this region and find a new rectangular neighborhood which contains only type 3 models, and so on.

Although it seems impossible to disentangle the complex interactions between parameters that determine a specific equilibrium and stability pattern, the median values of Table 3 give some information. For example, compared to types 1 and 3 models, type 2 models are characterized by higher values of k_1, k_2, that affect the feedback loop between C8* and C3*, lower values of k_3, k_{11} (rates of formation of the complexes C3* ÷ IAP, C8*÷BAR), and higher values of k_{-3}, k_{-11} (rates of dissociation of the complexes C3* ÷ IAP, C8* ÷ BAR). It is also interesting to note that the median of k_4 taken on the union of $\mathcal{S}_1$ and $\mathcal{S}_3$ (models with stable *life* equilibrium) is 3.01×10^{-4} : k_4 does not affect stability (Proposition 2) but discriminates between types 1 and 3 models. Note that all differences between means (except for parameter k_6) were highly significant by a one-way ANOVA test[23] (data not shown).

Another relevant feature of both types 2 and 3 models is the concentration of C3* at the asymptotically stable *non-life* equilibrium (denoted by $[\mathrm{C3^*}]_{\mathrm{NLA}}$): as already pointed out, the value of $[\mathrm{C3^*}]_{\mathrm{NLA}}$ is important to qualify such equilibrium as representative of a pro-apoptotic condition of the cell. Figure 2 shows the relative frequency distributions of $\log_{10}([\mathrm{C3^*}]_{\mathrm{NLA}})$ in types 2 and 3 models.

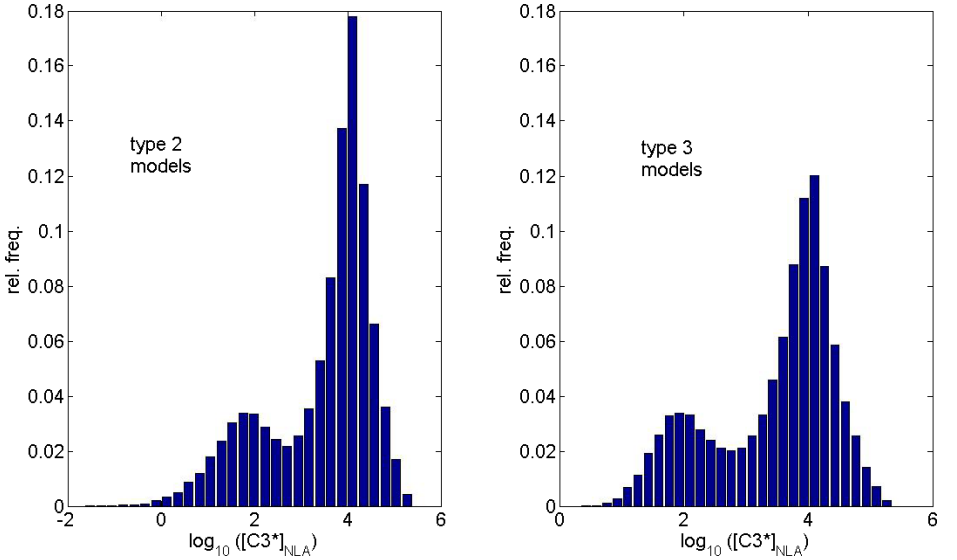

Fig. 2. Relative frequency distributions of the concentration of C3* at the asymptotically stable *non-life* equilibrium ($[\mathrm{C3^*}]_{\mathrm{NLA}}$) in the sub-samples of $\mathcal{S}_{nom}$ characterized by two or three equilibrium states. $\mathcal{S}_{nom}$ is a sample of 100,000 models whose parameters are generated as in Fig. 1, with $a = 0.9$.

Table 4. Correlation coefficients between $\log_{10}([C3^*]_{NLA})$ and parameters.

	Correlation coefficients	
Parameter	Type 2 models	Type 3 models
k_1	−0.0703	−0.0599
k_2	−0.0736	−0.2454
k_3	−0.2712	−0.1440
k_4	0.2682	0.2878
k_5	−0.0131	0.0254
k_6	−0.1913	−0.2184
k_7	−0.2493	−0.1350
k_8,k_{-8}	−0.2705	−0.3565
k_9,k_{-9}	−0.0038*	−0.0172
k_{10},k_{-10}	0.5683	0.3902
k_{11}	0.0936	0.0192
k_{12}, k_{-12}	−0.0055*	0.2031
k_{13}	0.0996	0.0081*
k_{-3}	0.2102	0.1586
k_{-11}	−0.0686	−0.0276

*Values non-significant at $\alpha = 0.05$ (t-test).

The distributions are very skew: 28% of the bistable models and 26.6% of type 2 models have $[C3^*]_{NLA} < 1000\,mol/cell$, and the median of the distributions are $6117\,mol/cell$ and $7330\ mol/cell$ respectively (for comparison, the nominal model has $[C3^*]_{NLA} = 5612\,mol/cell$).

The correlation coefficients between $\log_{10}([C3^*]_{NLA})$ and the parameters are reported in Table 4: most values are significantly different from zero both for types 2 and 3 models. We note the strong negative correlation of $[C3^*]_{NLA}$ with k_3, k_6, k_7, (k_8, k_{-8}), and the strong positive correlation with k_{-3}, k_4, (k_{10}, k_{-10}).

2.4.3. *Experiment 3*

In this experiment equilibrium and stability analysis is performed for two sets of models, in order to show two different kinds of transition from asymptotic stability to instability of the *life* equilibrium.

The analysis of Eissing *et al.*[14] and the proof of Proposition 3 suggest that bistable models are to some extent intermediate between type 1 models with the unique, asymptotically stable *life* equilibrium (representative of refractory cells) and type 2 models, characterized by unstable *life* equilibrium (hypersensitive cells). Firstly, we consider the bistable model with parameters $\underline{k}_{M3}$ (the median of $\mathcal{S}_3$), and change k_{-8} (logarithmically) in the interval [40.45, 4045] *mol/cell/min*. The effect of varying the parameter k_{-8} is interesting in itself, because in this way we may simulate the silencing/enhancing of the genes that regulate the synthesis of inhibitor proteins IAP. Figure 3a shows the bifurcation diagram of $[C3^*]$ at the equilibrium states, enlarged in Fig. 3b. Small values of k_{-8} correspond to type 2 models; for $k_{-8} = 102.2\,mol/cell/min$ the first transition occurs, and the bistable pattern appears. At the second transition, which occurs for $k_{-8} = 1122\,mol/cell/min$ the

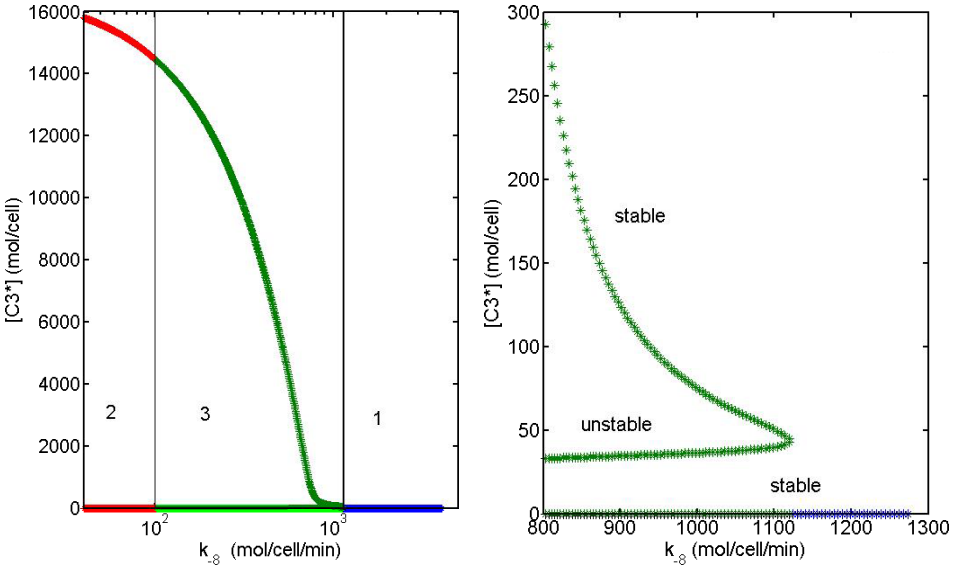

(a) (b)

Fig. 3. Bifurcation diagram of [C3*] at the equilibrium states of the models whose parameters are the components of the vector $\underline{k}_{\mathrm{M3}}$ (Table 3) except for k_{-8} which varies in the interval [40.45, 4045] *mol/cell/min*. Type 1 models are blue, type 3 models are green and type 2 models are red. (a) Natural axes and (b) bistable $\rightarrow$ monostable transition enlarged.

non-life equilibria disappear, leaving the *life* equilibrium alone. In this case we find the standard pattern: stability of the *apoptosis* equilibrium $\rightarrow$ bistability $\rightarrow$ stability of the *life* equilibrium.

As a second example, let us perform equilibrium and stability analysis along the segment $\Sigma(k_1)$ in the parameter space defined in the legend of Fig. 4. The parameter k_1 varies in the interval $8.46 \times 10^{-6} \leq k_1 \leq 1.69 \times 10^{-4}$: here and in the following we omit, for the sake of brevity, the units of k_1 $(mol/cell \times min)^{-1}$.

Figure 4a shows the bifurcation diagram of [C3*] at the equilibrium states. For low values of k_1 only the *life* equilibrium exists; by increasing k_1 (see Propositions 2 and 3) we have a transition from models of type 1 to models of type 2, without passing through bistable models. The transition occurs for $k_1 = k_1^* \cong 7.63212 \times 10^{-5}$ where the *non-life* equilibrium $\underline{x}_{ENL}$ appears and the *life* equilibrium becomes unstable. The stability of $\underline{x}_{ENL}$ changes with k_1 according to a rather complex pattern (see Figs. 4b and 4c):

- for $k_1^* < k_1 < 7.64166 \times 10^{-5}$ $\underline{x}_{ENL}$ is asymptotically stable;
- for $7.64168 \times 10^{-5} < k_1 < 10.8876 \times 10^{-5}$ $\underline{x}_{ENL}$ is unstable;
- for $k_1 > 10.8878 \times 10^{-5}$ $\underline{x}_{ENL}$ is asymptotically stable.

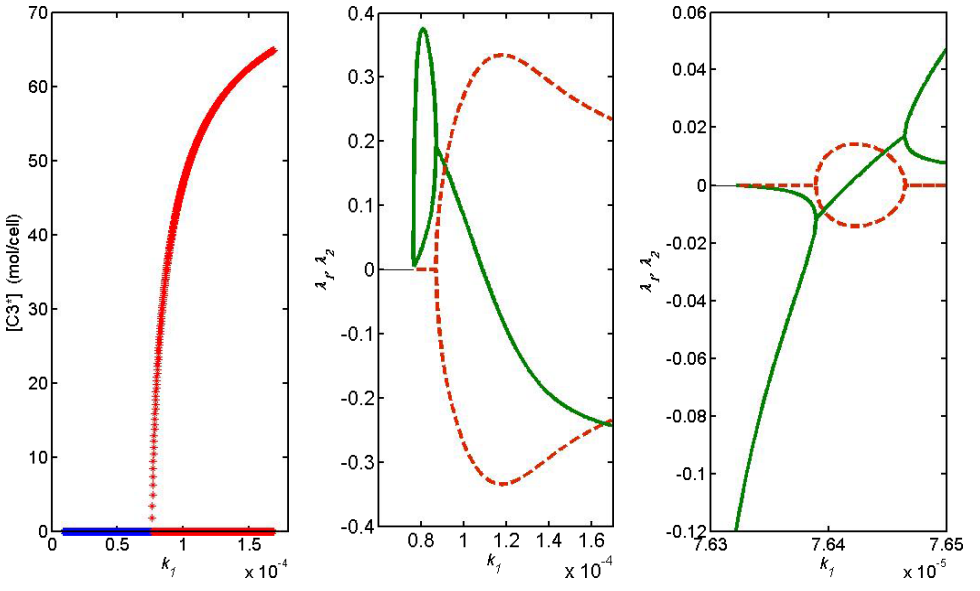

(a) (b) (c)

Fig. 4. Bifurcation diagram along the segment $\Sigma(k_1) = [k_1, 5.09\times10^{-6}, 5.44\times10^{-4}, 1.60\times10^{-4}, 2.98\times10^{-3}, 7.42\times10^{-3}, 2.12\times10^{-2}, 1.93\times10^{-3}, 6.53\times10^{-3}, 7.81\times10^{-4}, 1.19\times10^{-4}, 1.77\times10^{-3}, 1.79\times10^{-2}, 2.22\times10^{-1}, 7.74\times10^{+1}, 8.49\times10^{+2}, 1.64\times10^{+1}, 1.36\times10^{-1}, 7.08\times10^{+1}]$, with $8.46\times10^{-6} \leq k_1 \leq 1.69\times10^{-4}$. The units of k_1 $(mol/cell \times min)^{-1}$ are omitted for the sake of brevity. (a) Diagram of [C3*] at the equilibrium states; type 1 models are blue, type 2 models are red; (b) and (c) real (solid green) and imaginary parts (dashed red) of the pair of eigenvalues (λ_1, λ_2) with largest real part of the Jacobian matrix evaluated at the *non-life* equilibrium; in (c) the interval $7.63\times10^{-5} < k_1 < 7.65\times10^{-5}$ is enlarged. Note the sequence of patterns of (λ_1, λ_2) for increasing k_1: real negative → complex with negative real part → complex with positive real part → real positive → complex with positive real part → complex with negative real part; two Hopf bifurcations occur when $Re[\lambda_1] = Re[\lambda_2] = 0$: the first for $k_1 = k_1^a \in (7.64166, 7.64168)\times10^{-5}$, the second for $k_1 = k_1^b \in (10.8876, 10.8878)\times10^{-5}$.

The intervals above do not overlap because equilibria and eigenvalues are evaluated at discrete values of k_1. From Figs. 4b and 4c we note that two Hopf bifurcations[21] occur: this suggests (and numerical simulations confirm) the existence of a set of models with periodic trajectories.

3. Dynamical Response Analysis

The time evolution of the concentrations of chemicals relevant in the extrinsic pathway in response to an external stimulus has been simulated by solving Eqs. (2.1)–(2.8). The MATLAB function *ode15s* has been used, with enhanced precision set by the function *odeset*. The effect of the external stimulus applied through the cell membrane was simulated by imposing the initial state $\underline{x}(0) = [x_{L1}\, x_{02}\, x_{L3}\, 0 x_{L5}\, 0 x_{L7}\, 0]^T$ in which, besides C8, C3, BAR and IAP at the *life*

equilibrium concentrations, a number of C8* molecules are present: $[C8^*]_{IN} = x_2(0) = x_{02} > 0$. From this initial condition the model evolves for $t > 0$ without external forcing.

The response of the nominal bistable model to perturbations $[C8^*]_{IN}$ in the range 10–15,013 *mol/cell* is analyzed in depth in Ref. 15, both by solving Eqs. (2.1)–(2.8) and by running a stochastic version of the model to follow situations where very few (1–10) molecules of some species are present. We replicated the deterministic simulations: since the results are fully consistent with those of Ref. 15, we only report the distinctive features of the time evolutions:

- a very short initial transient, lasting less than one minute, during which the initial molecules of C8* are captured by the inhibitor BAR to form the complex C8* ÷ BAR. Negligible amounts of free C3* and of the complex C3* ÷ IAP are produced in this phase;
- a very long intermediate phase (decision phase[15]) characterized by very low values of [C8*] and [C3*], slow increase of [C3* ÷ IAP] and slow decrease of [IAP];
- a final phase, where either active caspases concentrations [C3*], [C8*] vanish and the system returns to the *life* equilibrium, or [C3*] abruptly increases. The latter case occurs if the initial perturbation exceeds a threshold (about 75 *mol/cell*[14]): the transition (activation phase[15]) lasts few minutes and leads to very high values of [C3*] and [C8*], after which the *apoptosis* equilibrium is reached;
- the model evolution is determined by a subtle balance between dissociation and formation of the complexes C8*÷BAR, C3*÷IAP: only when the level of inhibitor IAP is no longer sufficient, the positive feedback loop between C8* and C3* can become active and produce the fast increase of the concentration of C3* (in about nine minutes for the nominal model) characterizing the onset of apoptosis;
- the duration of the decision phase (t_D) is almost inversely proportional to the level of the initial perturbation $[C8^*]_{IN}$, and is very long for $[C8^*]_{IN}$ close to the threshold (e.g. if $[C8^*]_{IN} = 100$, $t_D = 13800\,min$, that is 9 days and 14 hours).

3.1. *Randomly generated models*

With an approach complementary to that of Refs. 14 and 15, we analyzed the dynamic behavior of the models in the sample $\mathcal{S}_{nom}$ defined in Sec. 2.4.2, that we completely characterized as regards equilibrium states and stability properties. We considered large initial perturbations, for which the deterministic simulation is adequate,[15] and focused the attention on the time evolution of [C3*]. As parameters that quantitatively characterize the features of the time responses we have chosen:

- the *delay time* t_D, measured as the time at which the derivative of [C3*] attains its maximum;
- the *peak value* of [C3*]: $[C3^*]_M = max[x_4(t)]$ and the time at which this value is attained: $t_P = argmax[x_4(t)]$.

Responses were simulated on a time interval of 36,000 minutes, that is 25 days: such a time span is about two orders of magnitude larger than the characteristic times of the caspase-3 response in laboratory experiments involving either HeLa cells,[18] or human B-limphoblastoid cell line SKW,[17] or osteosarcoma cells (experiments running in our laboratory; manuscript in preparation). However, we believe it is worth analyzing the model response also on such long intervals because of the extreme variety of cells which may undergo apoptosis in living human tissues. On the other hand, the structure of model (2.1)–(2.8) allows to change arbitrarily the time scale of the response by multiplying all parameters by the same constant.

Type 1 models. The 14,678 models (with the unique, asymptotically stable *life* equilibrium) were simulated with an initial perturbation $[\mathrm{C8}^*]_{\mathrm{IN}} = 10,000\, mol/cell$. On the basis of the values of t_D and t_P, Figure 5a shows that the population consists of three subgroups:

- 13,133 models (type 1a) characterized by very small delay and peak times ($< 2^*10^{-1}\, min$); in these models $[\mathrm{C3}^*]_{\mathrm{M}}$ ranges from 13 to 1372 *mol/cell*;

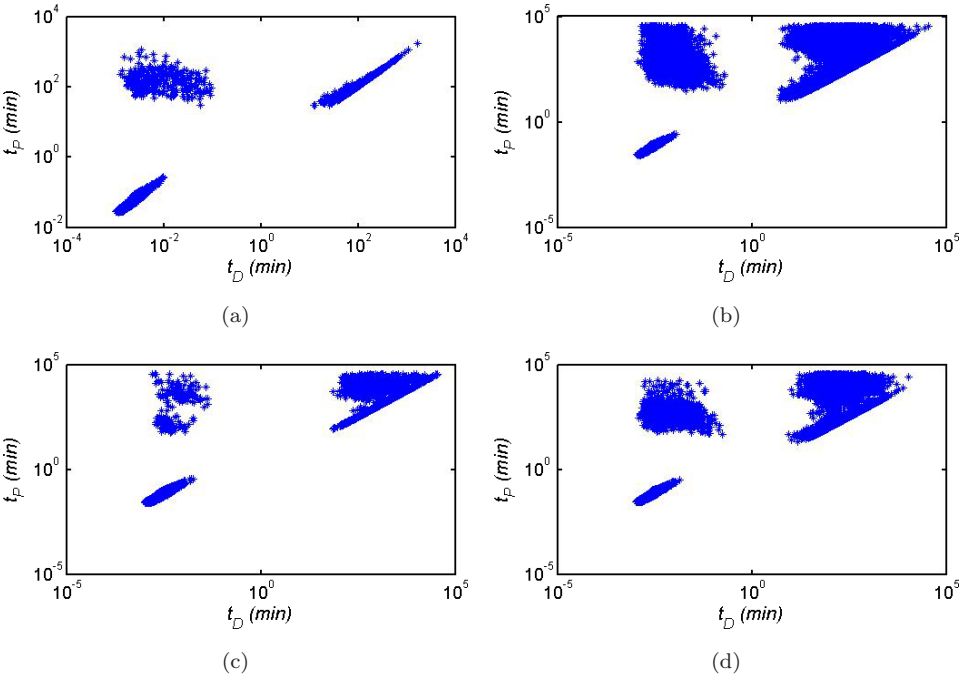

Fig. 5. Features of the responses of type 1 (panel a), type 2 with asymptotically stable *non-life* equilibrium (panel b) and type 3 models (panels c and d). For each model the pair t_P (time at which $[\mathrm{C3}^*]$ attains the maximum) — t_D (time at which the slope of the graph of $[\mathrm{C3}^*]$ attains the maximum) is plotted. The simulation interval is [0, 36,000] *min*. The initial perturbations are: type 1 models: $[\mathrm{C8}^*]_{\mathrm{IN}} = 10,000\, mol/cell$; type 2 models: $[\mathrm{C8}^*]_{\mathrm{IN}} = 1000\, mol/cell$; type 3 models (panel c): $[\mathrm{C8}^*]_{\mathrm{IN}} = 1000\, mol/cell$; type 3 models (panel d): $[\mathrm{C8}^*]_{\mathrm{IN}} = 10,000\, mol/cell$.

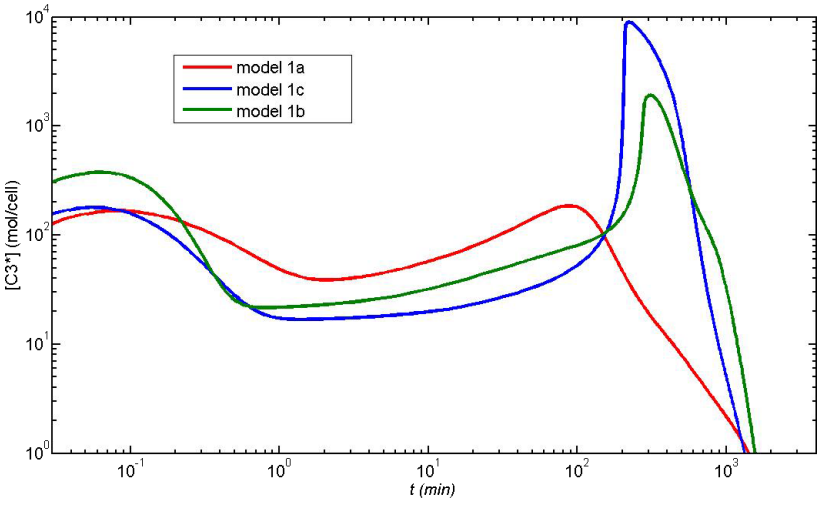

Fig. 6. Characteristic time evolutions of [C3*] in type 1 models.

- 307 models (type 1b) characterized by a very small delay ($< 10^{-3}$ *min*) and a large peak time (> 20 *min*); in these models $[C3^*]_M$ is almost uniformly distributed in the interval 50–8000 *mol/cell*;
- 1238 models (type 1c) characterized by a large delay (> 10 *min*) and a slightly larger peak time; in these models $[C3^*]_M$ ranges from 542 to 18,407 *mol/cell*, and 800 models (65% of the group) have $[C3^*]_M > 8000$ *mol/cell*.

Typical time responses of models in the three groups are shown in Fig. 6.

Type 2 models. Among the 50,566 models with unstable *life* equilibrium, 303 models have an unstable *non-life* equilibrium. As expected, such models have periodic evolutions: Fig. 7 shows a typical plot of [C3*], consisting of sequences of spikes. Experiments with several values of $[C8^*]_{IN}$ in the range 100–10,000 *mol/cell* have shown that the steady-state period and amplitude do not depend on the stimulus intensity. On the whole the amplitudes of [C3*] range from few tens to more than 10,000 *mol/cell* and periods from hours to days.

The vast majority of type 2 models has a stable *non-life* equilibrium: for these models the relation between t_D and t_P shown in Fig. 5b ($[C8^*]_{IN} = 1000$ *mol/cell*) suggests a partition of the models of $\mathcal{S}_2$ into four classes:

- type 2a models: $t_D < 0.02$ *min*, $t_P < 0.4$ *min*;
- type 2b models: $t_D < 0.3$ *min*, $t_P > 20$ *min*;
- type 2c models: $t_D > 5$ *min* and t_P slightly larger than t_D;
- type 2d models: $t_D > 5$ *min* and t_P much larger than t_D.

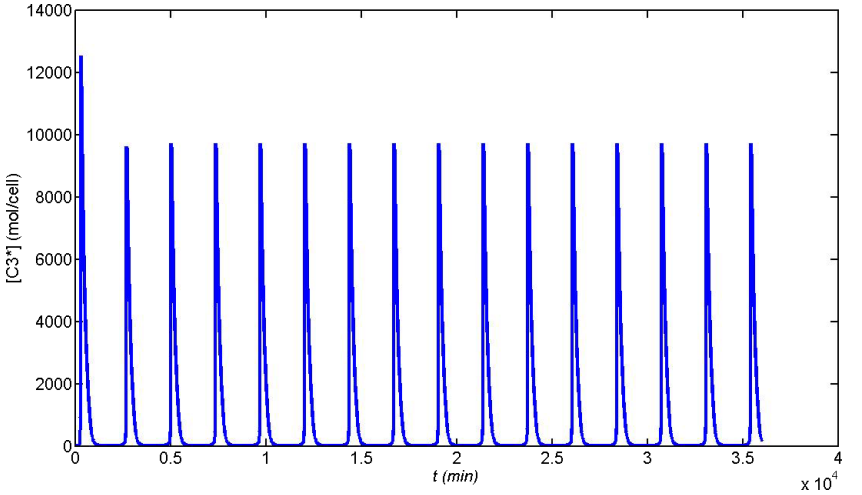

Fig. 7. Time evolution of [C3*] in a model with unstable *life* and *non-life* equilibria; the parameter vector is $\underline{k} = [2.80 \times 10^{-5}, 1.57 \times 10^{-5}, 2.12 \times 10^{-4}, 2.41 \times 10^{-4}, 9.58 \times 10^{-3}, 5.41 \times 10^{-3}, 1.66 \times 10^{-2}, 2.03 \times 10^{-2}, 4.63 \times 10^{-4}, 2.51 \times 10^{-3}, 7.31 \times 10^{-4}, 1.46 \times 10^{-3}, 9.96 \times 10^{-3}, 2.01 \times 10^{-1}, 8.13 \times 10^{+2}, 6.02 \times 10^{+1}, 5.26 \times 10^{+1}, 3.91 \times 10^{-1}, 5.85 \times 10^{+1}]$.

Table 5 reports some parameters of the responses of the various groups. We note that the substantial increase of [C3*] characteristic of an apoptotic phenotype occurs only in types 2c and 2d models. When the models are simulated with initial perturbation $[\text{C8}^*]_{\text{IN}} = 100\,mol/cell$, four groups with the same features as for $[\text{C8}^*]_{\text{IN}} = 1000\,mol/cell$ are again singled out. The change of the initial condition sensibly affects the level of [C3*] in models of types 2a and 2b; on the contrary it affects the length of the decision phase in models of types 2c and 2d, as already reported for bistable models. Figure 8 shows typical time evolutions of [C3*]: the graph of [C3*] has a fast rise time with overshoot in models of type 2c, while it is monotonically increasing to the *non-life* equilibrium value in models of type 2c.

Type 3 models. These models, with the exception of 97 cases that behave like type 1 models, show the typical pattern of bistability: we present here the main results of simulations with $[\text{C8}^*]_{\text{IN}} = 1000\,mol/cell$ and $[\text{C8}^*]_{\text{IN}} = 10{,}000\,mol/cell$, because now the intensity of initial stimulus is essential in triggering the activation phase. A fundamental point is that in both cases the models can be classified according to same criterion as for models of type 2 (see Figs. 5c and 5d). Table 5 shows the parameters of the time evolutions of [C3*]. The graphs are not reported for the sake of brevity, because they are very similar to those of Fig. 8. The increase (decrease) of the sizes of groups 3c and 3d (3a and 3b) with the increase of the initial perturbation means that more models attain the activation phase in the simulation interval, although a substantial fraction (about 50%) still does not commute.

Table 5. Parameters of the responses of types 2 and 3 models. Models are classified according to the values of t_D (time at which the graph of [C3*] has maximum slope) and of t_P (time at which [C3*] has maximum value). The table shows, for the responses belonging to each class, the median of t_D, the median of t_P, , the minimum (min), median, maximum (max) of the maximum value and of the final value of [C3*] ($[C3^*]_M$ and $[C3^*]_F$ respectively).

Type ($[C8^*]_{IN}$)	Number of models	Median t_D	Median t_P	Min-Median-Max $[C3^*]_M$ Min-Median-Max$[C3^*]_F$
2a (1000)	1534 (3.1%)	0.002	0.055	3.61-30.95-168.3 0.004-5.44-94.7
2b (1000)	2979 (5.9%)	0.008	545.13	5.63-91.09-1698 0.001-39.97-61.49
2c (1000)	33531 (66.7%)	177.54	196.19	27.9-14,841-36,525 0-5227-28,583
2d (1000)	12226 (24.3%)	173.07	9316.7	48.14-29,138-248,930 47.26-29,126-248,930
3a (1000)	30747 (88.5%)	0.002	0.046	1.22-14.74-161.6 0-0-25.25
3b (1000)	191 (0.5%)	0.006	1860	2.53-38.89-40.70 0-20.90-33.51
3c (1000)	2686 (7.7%)	89.90	91.36	87.20-15,219-24,918 0-6956-23,882
3d (1000)	1132 (3.4%)	817.8	9945.5	39.11-29,418-213,970 39.11-29,418-213,970
3a (10,000)	17199 (49.5%)	0.002	0.046	12.5-147.3-1211.4 0-0-448.8
3b (10,000)	889 (2.6%)	0.008	371.5	21.85-635.43-14,299 0-137.6-7213.5
3c (10,000)	11758 (33.8%)	129.2	142.9	508.8-14,251-27,089 0-6039-21,415
3d (10,000)	4909 (14.1%)	134.5	8859.8	1247-27,507-220,130 1247-27,446-220,130

Let us consider now a sample Σ consisting of 4471 bistable models with parameter vectors belonging to the region $R(0.5, \underline{k}^{nom})$ and characterized by $[C3^*]_{NLA} > 3607\, mol/cell$. Since each model may be regarded as representative of a cell, the set Σ may represent a rather homogeneous populations of cells that in normal conditions have the same concentrations of relevant proteins because the *life* equilibrium is the same for all models. The integration of the model equations over an interval $[0,\ t_F]$ for all parameter vectors in Σ, starting from the same initial condition $\underline{x}(0) = [x_{L1}\, x_{02}\, x_{L3}\, 0 x_{L5}\, 0\, x_{L7} 0]^T$ is representative of a laboratory experiment in which the population is uniformly exposed to a suitable stimulus, and is monitored in the subsequent t_F minutes to measure the time evolution of active caspases and the number of dead cells. Note that Eissing *et al.* represent the randomness of the population by randomness in the perturbations acting on the same basic model[14,15]: our approach is complementary because we applied the same perturbation to a number of models with randomly chosen parameters.

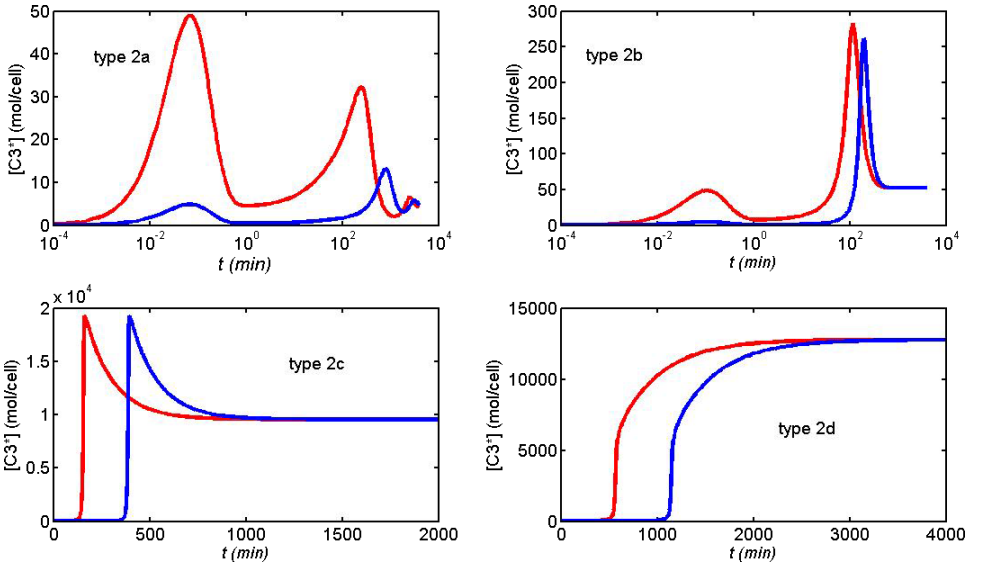

Fig. 8. Characteristic time evolutions of [C3*] in type 2 models, for $[C8^*]_{IN} = 100$ *mol/cell* (blue) and $[C8^*]_{IN} = 1000$ *mol/cell* (red).

The time evolutions of the models in Σ were computed over an interval of 3600 minutes, for initial perturbations in the range $[C8^*]_{IN} = 1000$–7000 *mol/cell*. The shape of the histograms of the peak values of [C3*] does not depend sensibly on the intensity of the perturbation, thus confirming the result of the *single cell* experiment. On the contrary, the distribution of the delay times t_D strongly depends on the intensity of the perturbation. Rather than showing the frequency distribution of the delay times we provide an equivalent representation in terms of survival functions of the cell population. If we assume that t_D well approximates the time when the activation of caspase-3 decides the death of the cell, then the number of models for which $t_D \leq T$, say $N(T)$, represents the number of cells in the population which entered the final phase of apoptosis in a time interval less than or equal to T. The survival function $S(T)$ of the cell population is the fraction of the initial population still surviving T minutes after the application of the external stimulus, and is given by $S(T) = 1 - N(T)/N(0)$. The survival functions of Σ corresponding to the different initial perturbations are shown in Fig. 9.

4. Discussion and Conclusions

In this paper a dynamical model of the extrinsic pathway to caspase activation in apoptosis is analyzed from several points of view. In comparison with the results reported in the literature,[14,15] essentially based on numerical experiments, we believe it is important (1) to have proved formally that either one, two or three equilibrium states can occur (Proposition 1), (2) to have deduced the criterion for

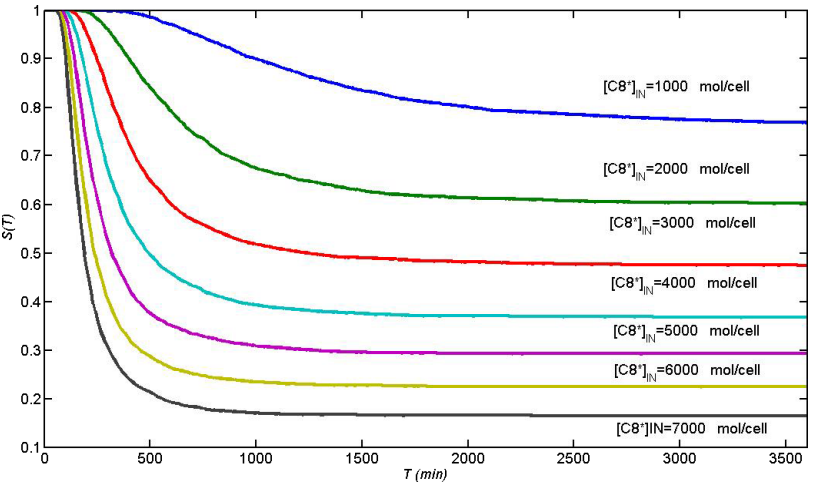

Fig. 9. Survival functions $S(T)$ of a virtual population of cells, for several intensities of the initial perturbation. The population is represented by a sample Σ consisting of 4471 bistable models with parameter vectors belonging to the restricted region $R(0.5, \underline{k}^{nom})$ and characterized by $[\mathrm{C3}^*]_{\mathrm{NL2}} > 3607$ *mol/cell*. $S(T)$ is the fraction of the initial population that has not undergone the transition to apoptosis within T minutes after the application of the external stimulus.

asymptotic stability/instability of the *life* equilibrium state (Proposition 2), (3) to have established a connection between number of equilibrium states and stability/instability of the *life* equilibrium (Proposition 3). Although such model properties might be foreseen on the basis of the numerical experiments, their formal proof was not available. On this theoretical basis we have performed numerical experiments: a region in the parameter space has been explored by analyzing equilibria, stability properties, time evolutions of randomly generated models. The attention has been focused not only on the standard classification of the models as *life-monostable*, *bistable*, *death-monostable*, but on exceptions to such a pattern, on the equilibrium concentration of active caspase-3, on quantitative features of the time response such as the peak value of active caspase-3. Our strategy does not overlap with previous work[14,15] on the model, which mainly addressed the "size" of the bistability region and the response of a model with given parameters to randomly chosen perturbations.

The classification of models according to the paradigm: *life-monostable*, *bistable*, *death-monostable* suggests a parallelism between a region in the parameter space and a cell population. In such population we may find normal cells, which undergo apoptosis if the stimulus is sufficiently strong, refractory cells, whose models have a unique equilibrium, the *life*, which is asymptotically stable, and hypersensitive cells, whose models have an unstable *life* equilibrium. Exceptions with respect to this pattern are models with two unstable *non-life* equilibria: the time evolutions of these models behave like those of models with the unique asymptotically stable *life* equilibrium. Another, more interesting exception are models with unstable *life*

and the *non-life* equilibria: the time evolutions of [C3*] consist, after a transient, of periodic sequences of pulses whose periods and amplitudes depend on the specific parameter vector. But the wealth of possible behaviors is not limited to equilibrium patterns. In the region of parameter space under examination the steady-state value of [C3*] at the asymptotically stable *non-life* equilibrium, as well as the peak value during the response to the stimulus, vary of five orders of magnitude. Also the duration of the decision phase for a given initial perturbation may vary from dozens of minutes to days.

The variety of behaviors found in a set of models whose parameters may vary at most by a factor of 20, and the wide variability of relevant features of the model response, also within a class of models which exhibit the same equilibrium and stability pattern, suggest to critically evaluate the role of the standard classification.

If we assume that a level of some thousands molecules per cell of C3* (for instance[15] 8000 *mol/cell*) attained for a time interval of few minutes is necessary and sufficient to irreversibly start up the cleavage of downstream proteins and DNA fragmentation, then some important remarks arise from the results of the simulations in Sec. 3.1:

(1) instability of the *life* equilibrium of a model does not imply that a cell corresponding to that model is appointed to apoptosis, because the concentration of active caspase-3 may not reach the threshold: out of 50,263 type 2 models with asymptotically stable *non-life* equilibrium (Sec. 2.4.2), 11,230 models (22.3%) have responses to $[C8^*]_{IN} = 1000\,mol/cell$ with peak values $[C3^*]_M < 8000\,mol/cell$;
(2) a model with the sole, asymptotically stable *life* equilibrium may represent a cell in which the caspase-activation cascade takes place over meaningful time intervals, provided that the external stimulus is sufficiently high: 800 models of type 1 (5.5% of $\mathcal{S}_1$) have responses with peak values $[C3^*]_M > 8000\,mol/cell$ (initial perturbation $[C8^*]_{IN} = 10,000\,mol/cell$);
(3) in the sub-sample of $\mathcal{S}_{nom}$ consisting of the bistable models only 48% of the responses to the initial perturbation $[C8^*]_{IN} = 10,000\,mol/cell$ attain the activation phase within 36,000 *min* from the application of the stimulus, and 10% of these responses show peak values lower than 8000 *mol/cell*.

The sensitivity of equilibrium patterns to parameter changes indicates that the reactions involving the inhibitors BAR and IAP play a fundamental role in determining the patterns. Likewise a comparison between models with "high" and "low" [C3*] peak response shows that "high" [C3*] is associated to high values of k_{-3}, k_{-11} (dissociation of complexes), k_4 (cleavage of IAP), k_1, k_2 (positive feedback loop parameters), and low values of k_3, k_{11} (formation of complexes), k_7, k_{13} (decay of complexes), k_{-8}, k_8 (production and decay of IAP).

Next steps in the study will be to check the qualitative agreement between model response and biological phenomena, and to calibrate the model with laboratory

data. Indeed, the analysis of the model and the numerical simulations have provided as a first consequence the guidelines for designing *in vitro* experiments which are now in progress. In these experiments populations of osteosarcoma cells 143B.TK$^-$ are firstly synchronized (arrested in G°/G1 phase of the cell cycle) by suitably culturing. Then the synchronized cells are treated with recombinant Apo2L/TRAIL protein which acts as extrinsic apoptotic stimulus. The response of the real cells to increasing concentration of Apo2L/TRAIL (100, 250, 500, 1000 *ng/ml*) and different times of treatment (15, 30, 60, 120, 240, 360, 720 *min*) is being tested. The tests involve the measurement at different times of cells viability and of the concentrations of C3* , C8*, IAP, and BAR. Further investigations on the role of BAR and IAP in the apoptosis pathway will be carried out by selective silencing of IAP and BAR genes.

The realization of such a complementary effort between mathematical modeling and experimental analyses may get insights on one of the most complex and crucial biological processes.

Supplementary Material

Appendices can be found at the site http://biologia.unical.it/apopt/jbs07.

Acknowledgments

This work was partially supported by Fondo Sociale Europeo — FSE (PhD course in Molecular Biopathology, University of Calabria, Italy).

The authors are grateful to Dr. Thomas Eissing for his valuable comments and suggestions in improving the paper.

References

1. Hengartner MO, The biochemistry of apoptosis, *Nature* **407**:770–776, 2000.
2. Riedl SJ, Shi Y, Molecular mechanisms of caspase regulation during apoptosis, *Nat Rev Mol Cell Biol* **5**:897–907, 2004.
3. Adams JM, Ways of dying: multiple pathways to apoptosis, *Genes Dev* **17**:2481–2495, 2003.
4. Bredesen ED, Rao RV, Mehlen P, Cell death in the nervous system, *Nature* **443**:796–802, 2006.
5. Shi Y, Caspase activation, inhibition and reactivation: a mechanistic view, *Protein Sci* **13**:1979–1987, 2004.
6. Krammer PH, CD95's deadly mission in the immune system, *Nature* **407**:789–795, 2000.
7. Green DR, Kroemer G, The pathophysiology of mitochondrial cell death, *Science* **305**:626–629, 2004.
8. Deveraux QL, Reed JC, IAP family proteins-suppressors of apoptosis, *Genes Dev* **13**:239–252, 1999.
9. Salvesen GS, Duckett CS, IAP proteins: blocking the road to death's door, *Nat Rev Mol Cell Biol* **3**:401–410, 2002.

10. Yang Y, Yu X, Regulation of apoptosis: the ubiquitous way, *FASEB J* **17**:790–799, 2003.
11. Zhang H, Xu Q, Krajewski S, Krajewska M, Xie Z, Fuess S, Kitada S, Pawlowski K, Godzik A, Reed JC, BAR: an apoptosis regulator at the intersection of caspases and Bcl-2 family proteins, *Proc Nat Acad Sci* **97**:2597–2602, 2000.
12. Fussenegger M, Bailey JE, Varner JA, Mathematical model of caspase function in apoptosis, *Nat Biotechnol* **18**:768–774, 2000.
13. Stucki JW, Simon HU, Mathematical modeling of the regulation of caspase-3 activation and degradation, *J Theor Biol* **23**:123–131, 2005.
14. Eissing T, Colzemann H, Gilles ED, Allgower F, Bullinger E, Scheurich P, Bistability analyses of a caspase activation model for receptor-induced apoptosis, *J Biol Chem* **279**:36892–36897, 2004.
15. Eissing T, Allgower F, Bullinger E, Robustness properties of apoptosis models with respect to parameter variations and intrinsic noise, *IEE Proc-Syst Biol* **12**:221–228, 2005.
16. Bagci EZ, Vodovotz Y, Billiar TR, Ermentrout GB, Bahar I, Bistability in apoptosis: roles of Bax, Bcl-2 and mitochondrial permeability transition pores, *Biophys J* **90**:1546-1559, 2006.
17. Bentele M, Lavrik I, Ulrich M, Stosser S, Heermann DH, Kalthoff H, Krammer PH, Eils R, Mathematical modeling reveals threshold mechanism in CD95-induced apoptosis, *J Cell Biol* **166**:839–851, 2004.
18. Rehm M, Huber HJ, Dussmann H, Prehn JHM, Systems analysis of effector caspase activation and its control by X-linked inhibitor of apoptosis protein, *EMBO J.* **25**:4338–4349, 2006.
19. Willems JL, *Stability Analysis of Dynamical Systems*, Nelson, New York, NY, USA, 1970.
20. Ogata K, *Modern Control Engineering*, 4th edn., Prentice Hall, Upper Saddle River, NJ, USA, 2002.
21. Tyson JJ, Othmer HG, The dynamics of feedback control circuits in biochemical pathways, in Rosen R, Snell FM (eds.), *Progress in Theoretical Biology*, Vol. 5, pp. 1–62, 1978.
22. Vidyasagar M, A tutorial introduction to randomized algorithms for robust controller synthesis using statistical learning theory, *Eur J Control* **5–6**:283–310, 2001.
23. Sokal RR, Rohlf FJ, *Biometry*, WH Freeman, New York, NY, USA, 1994.